

## **Supporting Information**

### **Accessing Two-Stage Regioselective Photoisomerization in Unsymmetrical N,C-Chelate Organoboron Compounds: Reactivity of B(ppz)(Mes)Ar**

Cally Li, Soren K. Mellerup, Xiang Wang, Suning Wang\*

Department of Chemistry, Queen's University, Kingston, Ontario K7L 3N6, Canada

#### **Table of Contents**

**S1. Experimental Methods and Synthetic Details**

**S2. NMR Characterization Data of 1 – 7**

**S3. NMR Photoisomerization Data of 1 – 7**

**S4. Photophysical Properties of 1 – 7**

**S5. UV/Vis Photoisomerization Data of 1 – 7**

**S6. TD-DFT Calculation Data of 1 – 6**

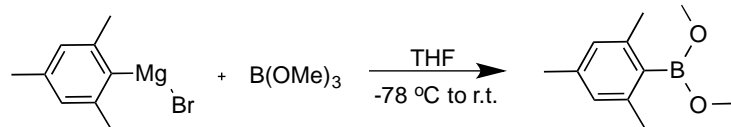
**S7. X-Ray Crystal Structure Data of 4 and 6**

**S8. References**

## **S1: Experimental Methods and Synthetic Details**

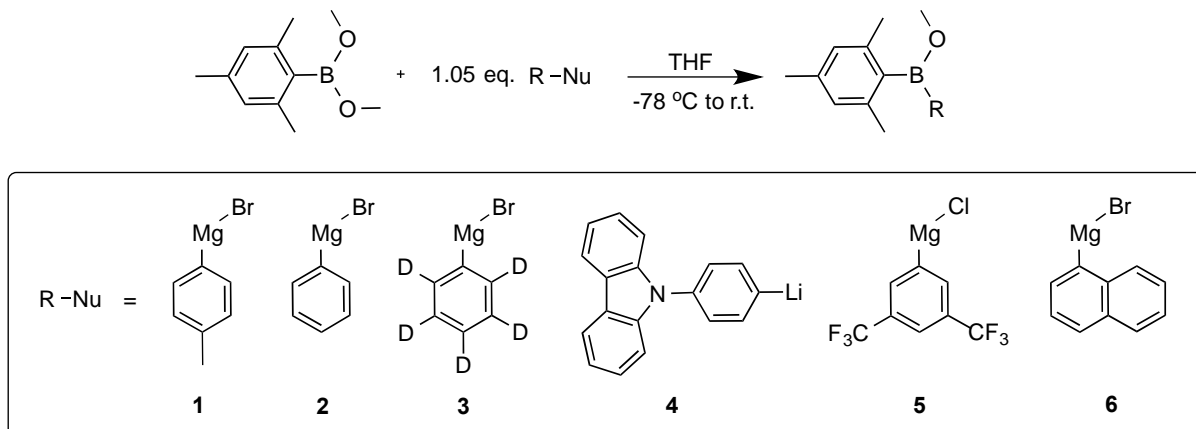
All experiments were carried out under an inert atmosphere of N<sub>2</sub>. All starting materials were purchased from Sigma-Aldrich and used without further purification. 1-(2-bromophenyl)-1*H*-pyrazole<sup>[1]</sup> and 9-(4-bromophenyl)-9*H*-carbazole<sup>[2]</sup> were prepared according to literature procedures. All solvents were dried over Na and degassed. <sup>1</sup>H, <sup>11</sup>B, and <sup>13</sup>C NMR spectra were recorded on a Bruker Avance 400, 600, or 700 MHZ spectrometer. Deuterated solvents were purchased from Cambridge Isotopes and dried/degassed prior to use. Photochemical reactions were performed in J-Young NMR tubes and photochemical reactions were carried out using a Rayonet Photochemical Reactor. High resolution mass spectra (HRMS) were obtained using a Micromass GCT TOF-EI Mass spectrometer. Excitation and emission spectra were recorded using a Photon Technologies International QuantaMaster Model 2 spectrometer. UV-Visible spectra were recorded on a Varian Cary 50 spectrometer. Photoluminescent quantum yields were measured using a Hamamatsu QY spectrometer (C11347-11). DFT and TD-DFT calculations were performed using the Gaussian 09 suite of programs<sup>[3]</sup> on the High Performance Computing Virtual Laboratory (HPCVL) at Queen's University. Geometry optimizations and vertical excitations of all compounds were obtained at the cam-B3LYP<sup>[4]</sup>/SVP<sup>[5]</sup> level of theory, with the resulting structures confirmed to be stationary points through vibrational frequency analysis.

### **Synthesis of B(OMe)<sub>2</sub>(Mes):**



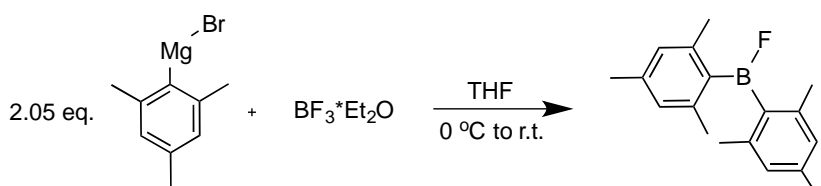
B(OMe)<sub>2</sub>(Mes) was prepared according to literature procedures.<sup>[6]</sup> Mesityl magnesium bromide was prepared from 2-bromomesitylene (10.0 g, 50.3 mmol), magnesium turnings (1.22 g, 50.3 mmol), and a small iodine crystal in 100 mL of dry/degassed THF. The mixture was refluxed for 2 hours at 80 °C until all the magnesium disappeared, and slowly cooled to -78 °C for 30 minutes using a dry ice/acetone bath. B(OMe)<sub>3</sub> (~5.59 mL, 50.3 mmol) was added quickly and the solution was slowly warmed to room temperature overnight. The solvent was removed *in vacuo* and the residue was extracted with dry/degassed hexanes (200 mL). The crude mixture was filtered through Celite under N<sub>2</sub> and concentrated under reduced pressure to afford B(OMe)<sub>2</sub>(Mes) as a cloudy oil (5.19 g, 52% yield). The <sup>1</sup>H NMR of B(OMe)<sub>2</sub>(Mes) agreed with that reported in the literature.<sup>[7]</sup>

### **Synthesis of B(OMe)(Mes)(R) Reagents:**



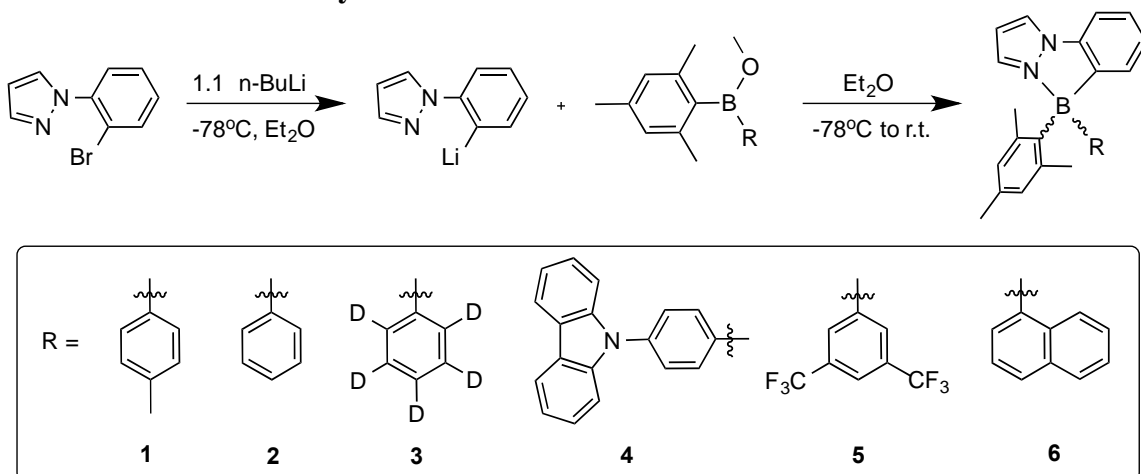
In a 50 mL oven dried Schlenk flask under N<sub>2</sub>, the appropriate Grignard reagent (1.05 eq; 5.3 mmol in 15 mL THF) was prepared using the method described above (*i.e.* bromobenzene, 4-bromotoluene, bromobenzene-d<sub>5</sub>, and 1-bromonaphthalene) or with the low-temperature halogen-magnesium exchange described by Knochel (*i.e.* 1,3- bis(trifluoromethyl)-5-bromobenzene).<sup>[8]</sup> To prepare the (4-(9H-carbazol-9-yl)phenyl)lithium solution, 9-(4-bromophenyl)-9H-carbazole (1.61 g, 5 mmol) was dissolved in THF (~15 mL) and cooled to -78 °C using a dry ice/acetone bath. After 30 minutes, n-BuLi (2.3 mL, 5.8 mmol, 2.5 M in hexanes) was added dropwise and the mixture was stirred for 1 hour to afford the lithiated reagent. A separate 50 mL oven dried Schlenk flask under N<sub>2</sub> was charged with B(OMe)<sub>2</sub>(Mes) (0.96 g, 5 mmol) and THF (~10 mL). Both the B(OMe)<sub>2</sub>(Mes) solution and the appropriate R-Nu reagent were then cooled to -78 °C simultaneously, after which the R-Nu mixture was cannula transferred to the borate solution. The resulting B(OMe)(Mes)(R) solution was warmed to ambient temperature overnight and used as is in the preparation of **1 – 6**.

### Synthesis of B(F)(Mes)<sub>2</sub> Reagent:



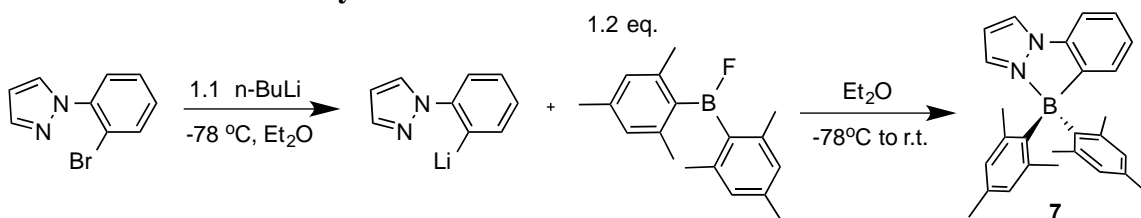
In a 50 mL oven dried Schlenk flask under N<sub>2</sub>, mesyl magnesium bromide (35.1 mmol, 2.05 eq.) was prepared using the method described above. The Grignard reagent was then cooled to 0 °C using an ice bath, after which BF<sub>3</sub>\*Et<sub>2</sub>O (~2.11 mL, 17.1 mmol, 1 eq.) was added in one portion and the mixture allowed to warm to room temperature overnight. The following day, the THF was removed *in vacuo* and the residue was extracted with dry/degassed hexanes (200 mL). The extract was then filtered through Celite under inert atmosphere. The crude mixture was filtered through Celite under N<sub>2</sub> and concentrated under reduced pressure to afford B(F)(Mes)<sub>2</sub> as an off-white solid (4.142 g, 15.4 mmol, 90% yield). The <sup>1</sup>H NMR of B(F)(Mes)<sub>2</sub> agreed with that reported in the literature<sup>[9]</sup> and the product was used as is in the preparation of **7**.

### General Procedure for the Synthesis of 1 – 6.



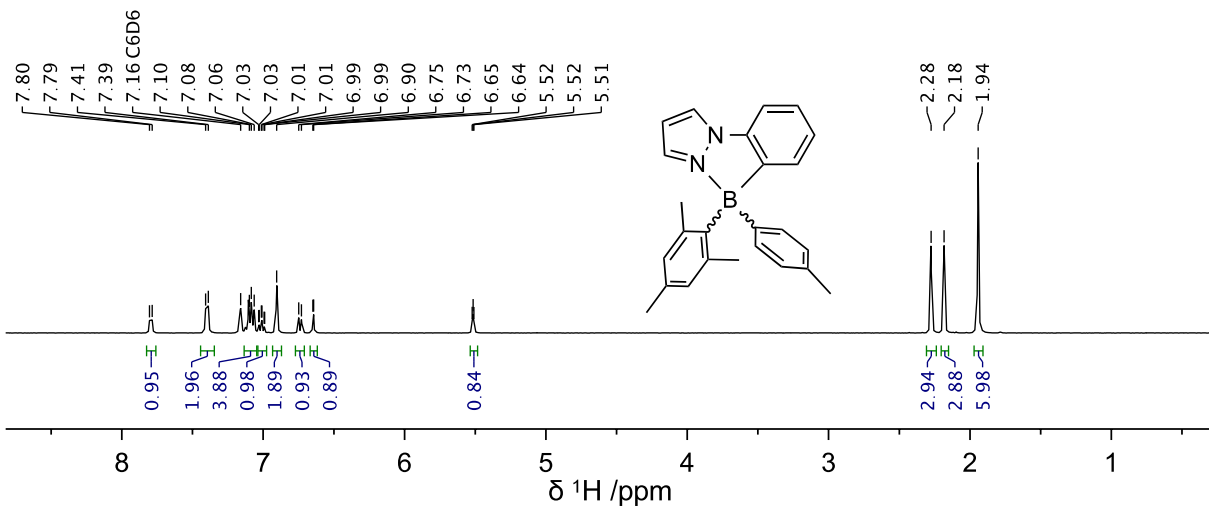
In an oven dried 50 mL Schlenk flask under  $\text{N}_2$ , 1-(2-bromophenyl)-1*H*-pyrazole (0.74 g, 3.3 mmol) was dissolved in 15 mL of dry/degassed  $\text{Et}_2\text{O}$ . The solution was cooled to  $-78^\circ\text{C}$  for 30 minutes, after which n-BuLi (1.5 mL, 3.63 mmol, 2.5 M in hexanes) was added dropwise. As the lithiated ligand solution was allowed to stir for 1 hour, the  $\text{B}(\text{OMe})(\text{Mes})(\text{R})$  mixture was cooled to the same temperature. After the allotted hour of stirring, the borate mixture was cannula transferred into the lithiation flask and the completed reaction mixture was slowly warmed to room temperature overnight. The products were extracted with  $\text{CH}_2\text{Cl}_2$ , washed with  $\text{H}_2\text{O}$ , and dried with  $\text{MgSO}_4$ . Flash column chromatography using a gradient elution (10:1  $\rightarrow$  4:1 hexanes: ethyl acetate) was used to purify the desired products. **1 – 6** were obtained in low to moderate yields (5–50%).

### General Procedure for the Synthesis of 7.

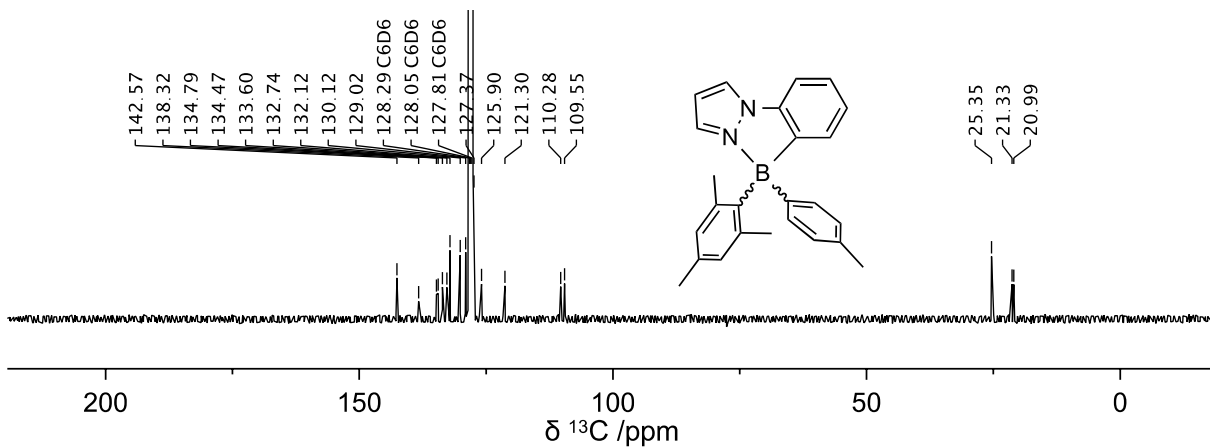


In an oven dried 50 mL Schlenk flask under  $\text{N}_2$ , 1-(2-bromophenyl)-1*H*-pyrazole (0.38 g, 1.7 mmol) was dissolved in 15 mL of dry/degassed  $\text{Et}_2\text{O}$ . The solution was cooled to  $-78^\circ\text{C}$  for 30 minutes, after which n-BuLi (0.72 mL, 1.8 mmol, 2.5 M in hexanes) was added dropwise. The lithiated ligand solution was allowed to stir for 1 hour at  $78^\circ\text{C}$ . After the allotted hour,  $\text{B}(\text{F})(\text{Mes})_2$  (0.53 g, 2.0 mmol, 1.2 eq.) was added to the flask and the mixture was allowed to stir overnight. The products were extracted with  $\text{CH}_2\text{Cl}_2$ , washed with  $\text{H}_2\text{O}$ , and dried with  $\text{MgSO}_4$ . Purification by flash column chromatography using a gradient elution (10:1  $\rightarrow$  4:1 hexanes:  $\text{CH}_2\text{Cl}_2$ ) afforded **7** as a pale-yellow solid (0.44 g, 69%).

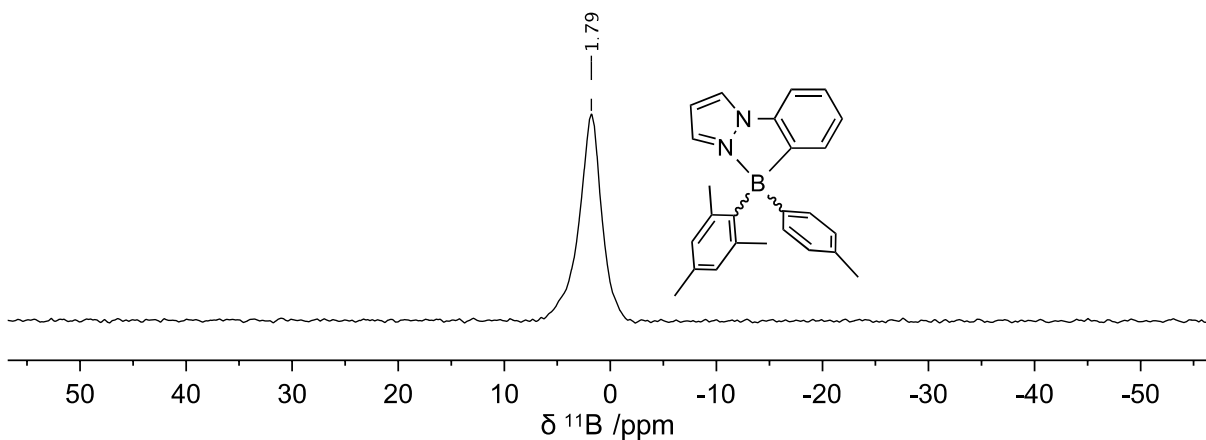
### S2: NMR Characterization Data of 1 – 7



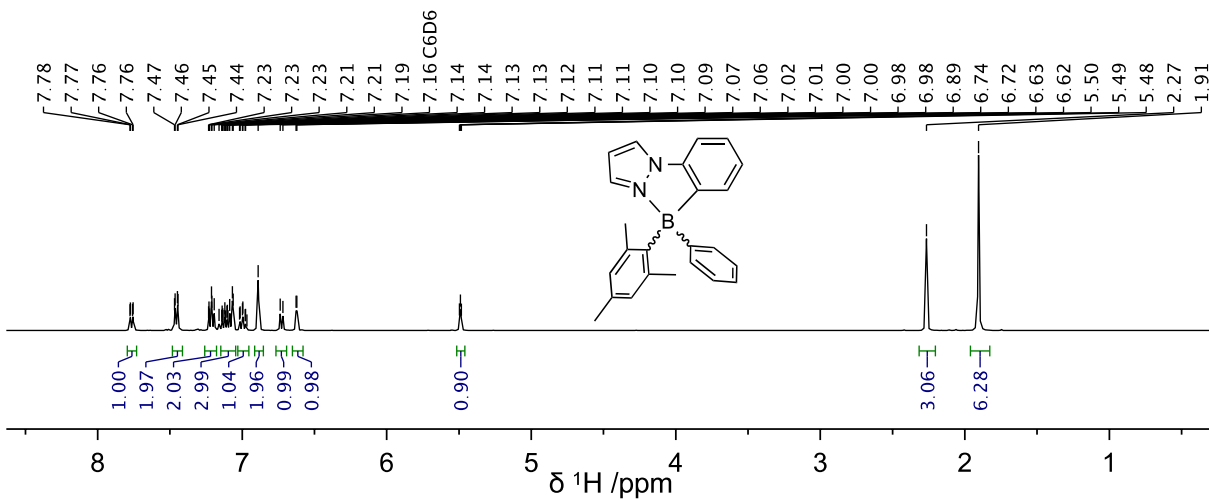
**Figure S1.**  $^1\text{H}$  NMR spectrum of **1** in  $\text{C}_6\text{D}_6$ .



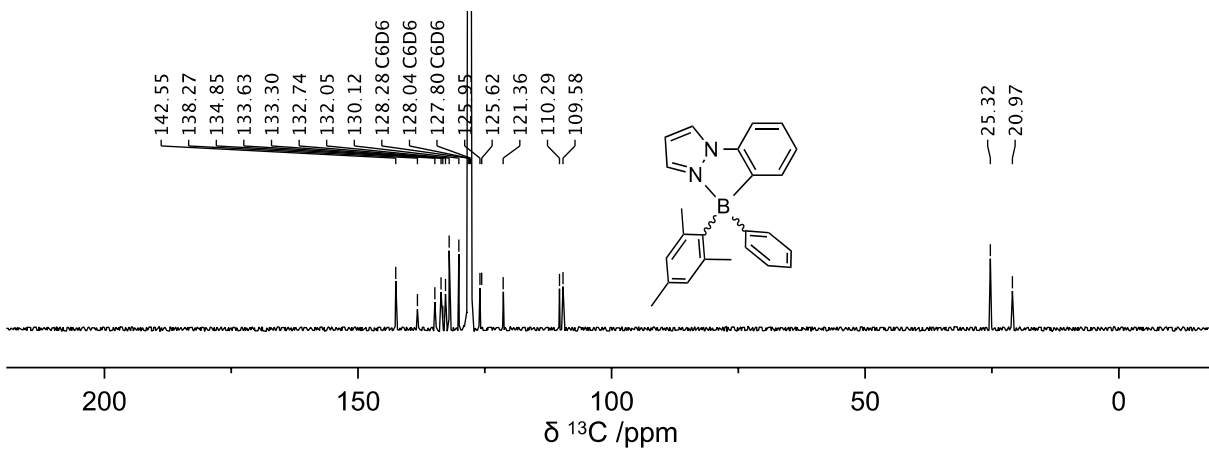
**Figure S2.**  $^{13}\text{C}$  NMR spectrum of **1** in  $\text{C}_6\text{D}_6$ .



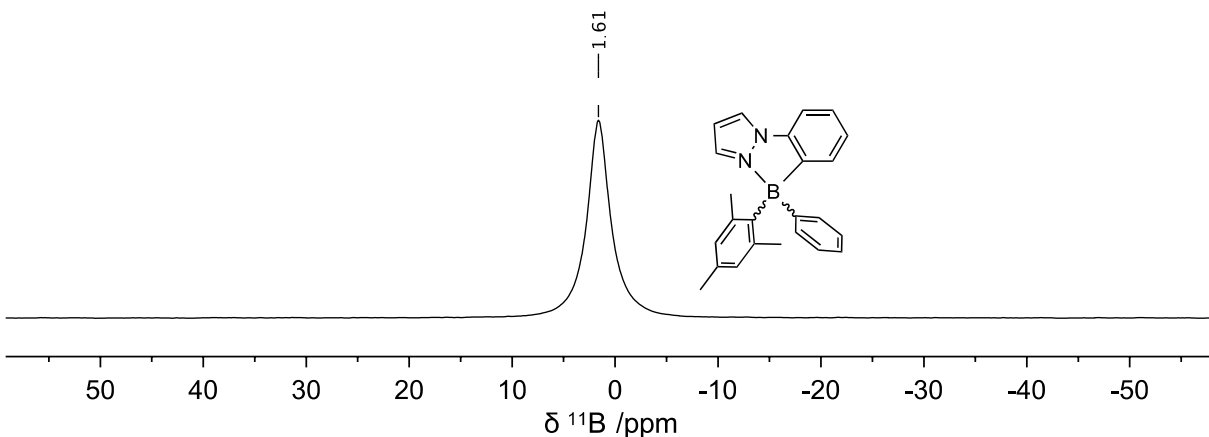
**Figure S3.**  $^{11}\text{B}$  NMR spectrum of **1** in  $\text{C}_6\text{D}_6$ .



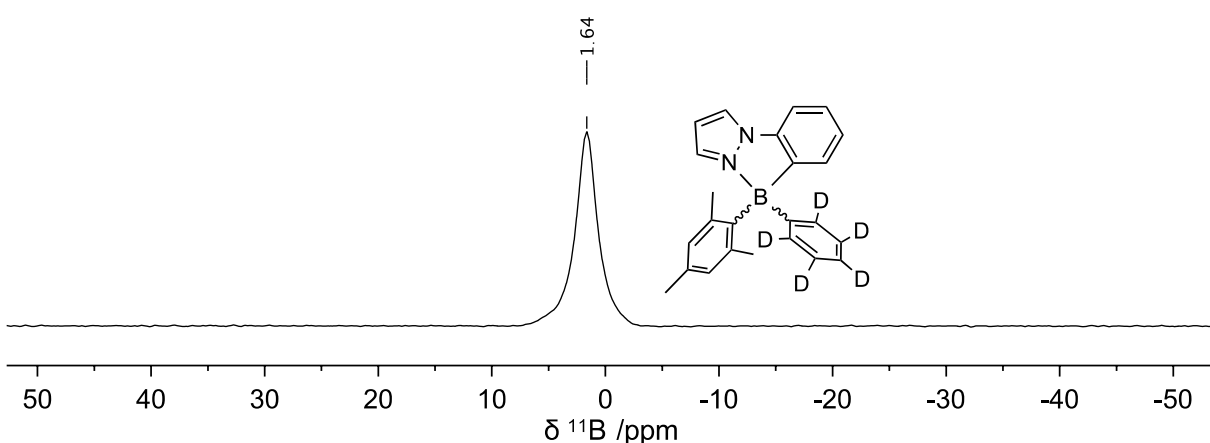
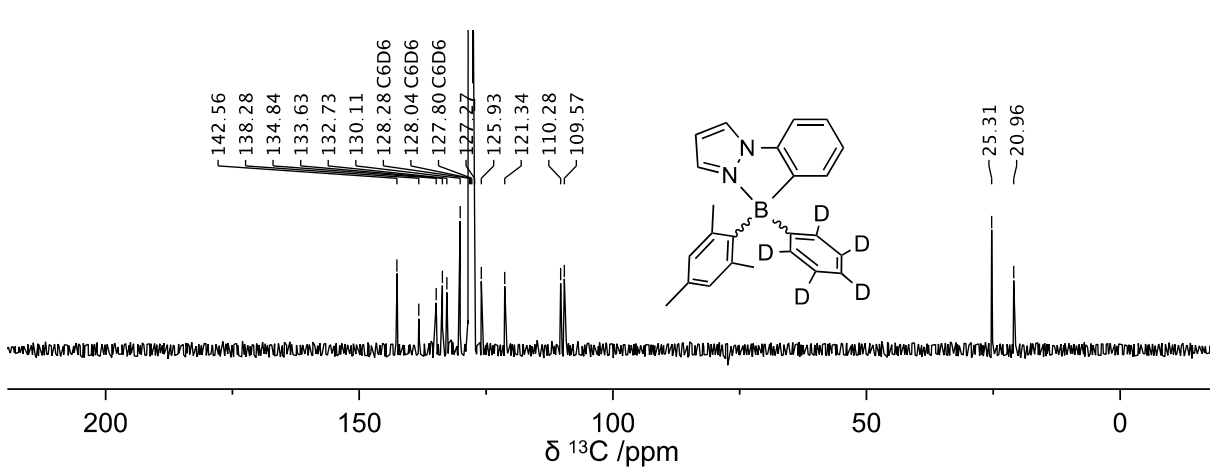
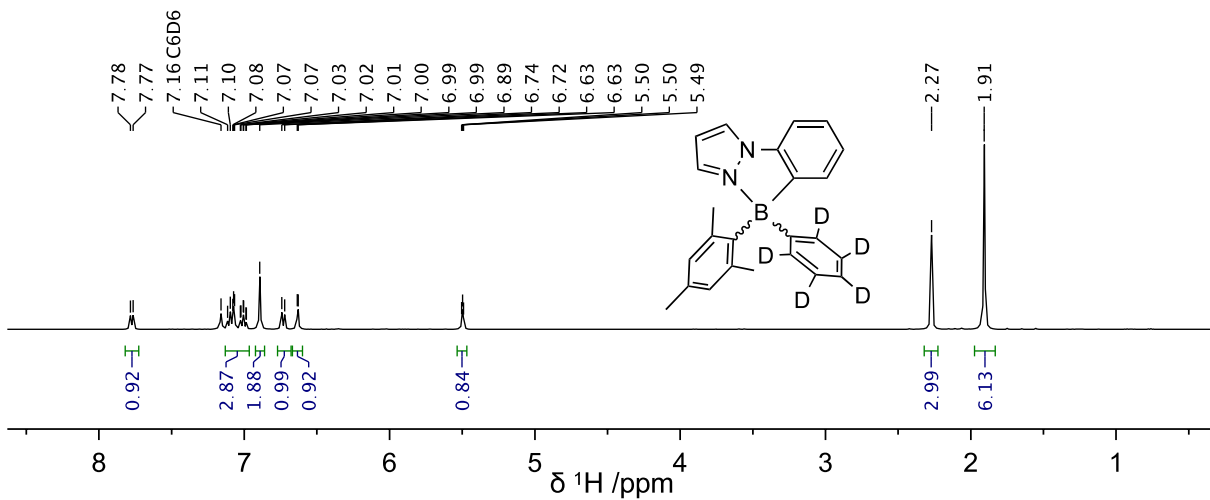
**Figure S4.**  $^1\text{H}$  NMR spectrum of **2** in  $\text{C}_6\text{D}_6$ .

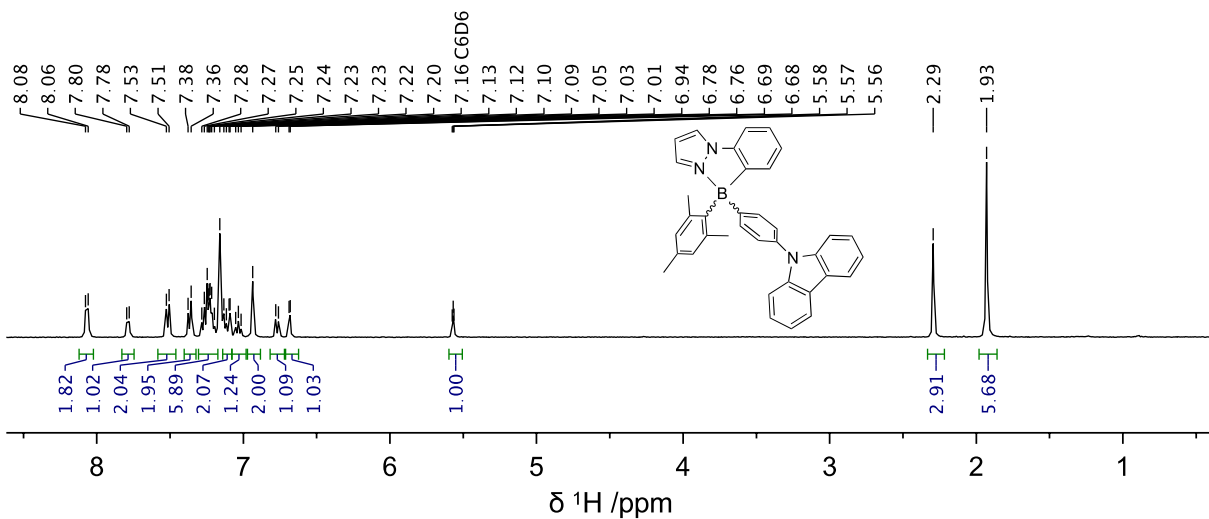


**Figure S5.**  $^{13}\text{C}$  NMR spectrum of **2** in  $\text{C}_6\text{D}_6$ .

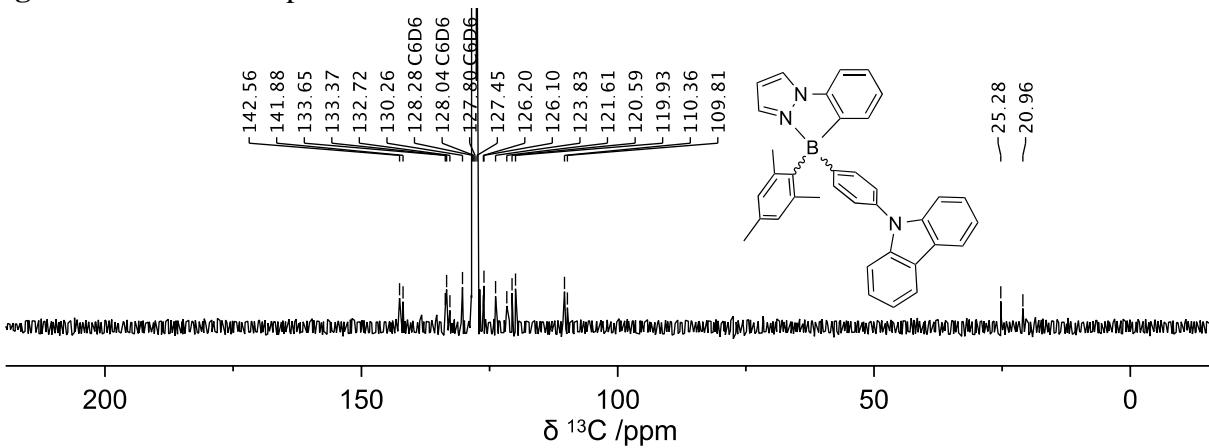


**Figure S6.**  $^{11}\text{B}$  NMR spectrum of **2** in  $\text{C}_6\text{D}_6$ .

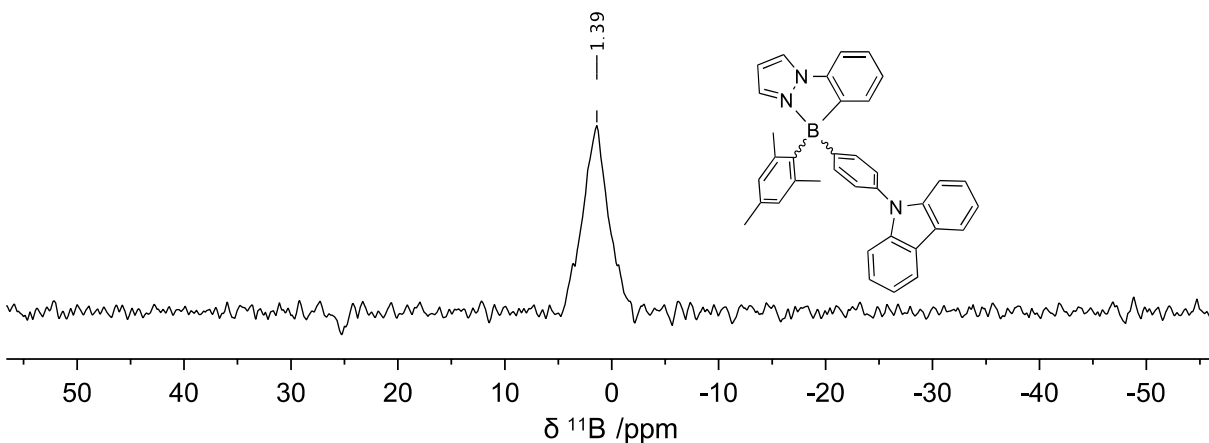




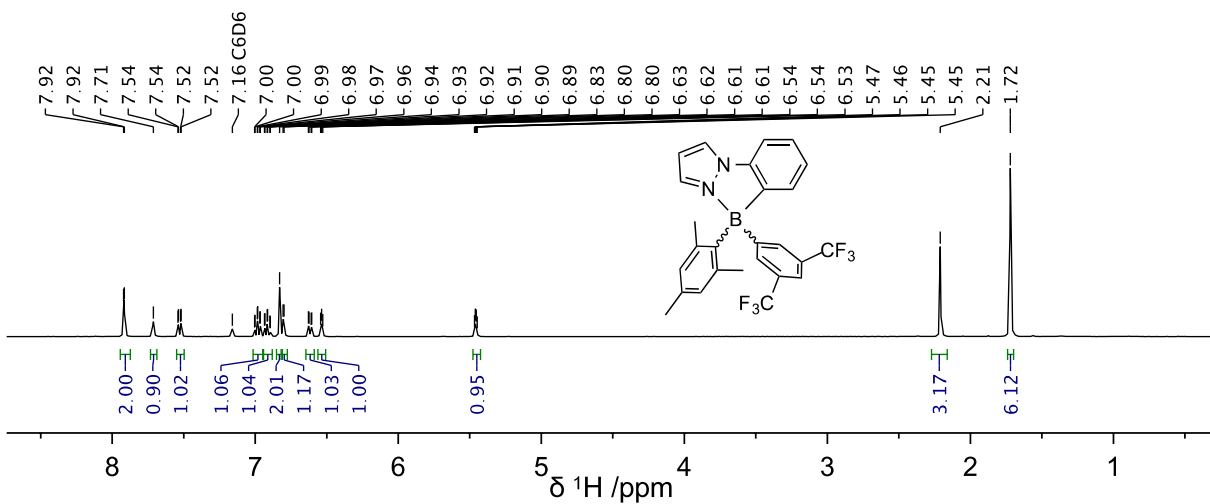
**Figure S10.**  $^1\text{H}$  NMR spectrum of **4** in  $\text{C}_6\text{D}_6$ .



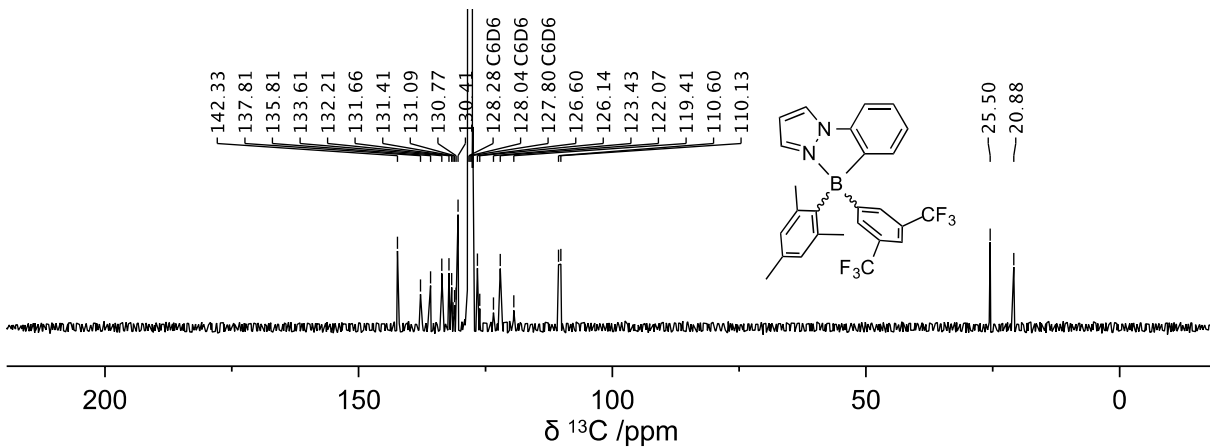
**Figure S11.**  $^{13}\text{C}$  NMR spectrum of **4** in  $\text{C}_6\text{D}_6$ .



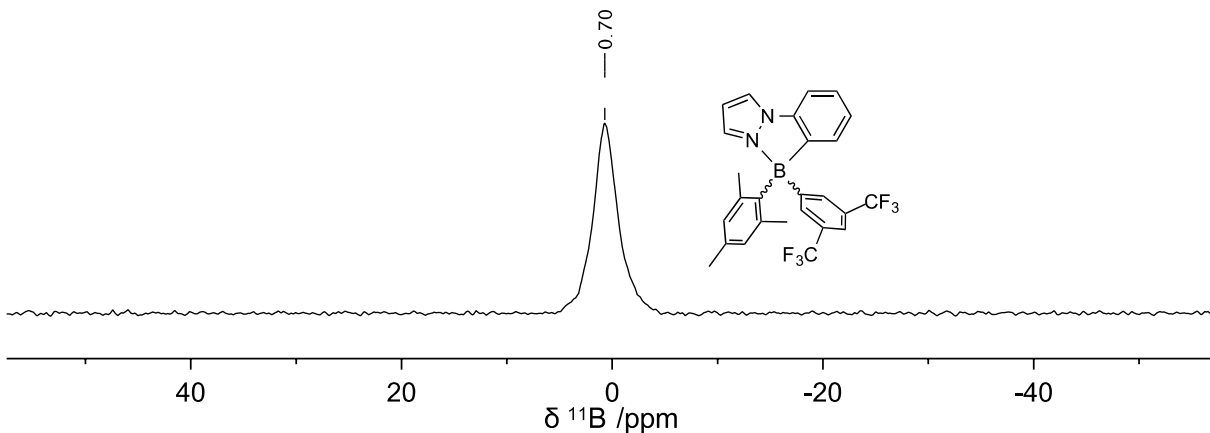
**Figure S12.**  $^{11}\text{B}$  NMR spectrum of **4** in  $\text{C}_6\text{D}_6$ .



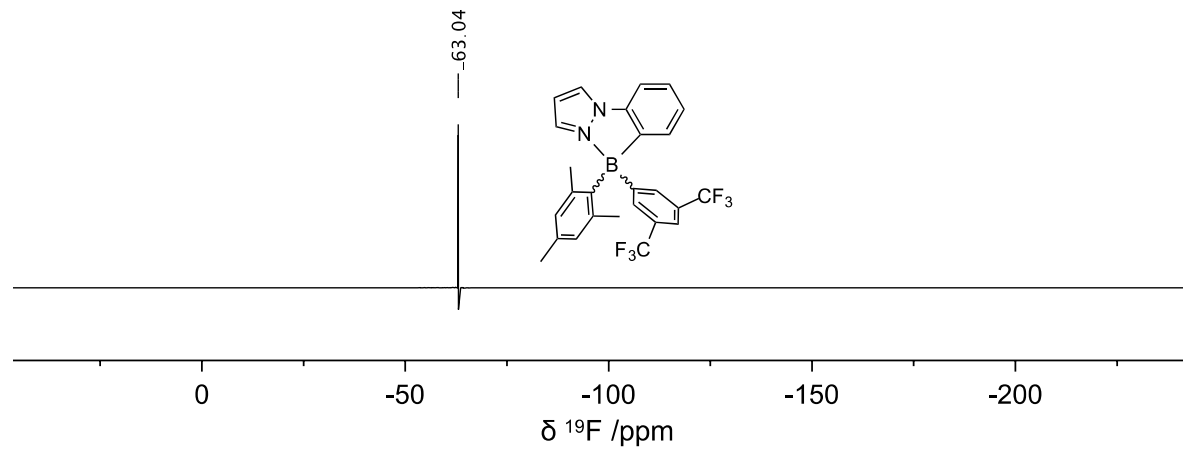
**Figure S13.**  $^1\text{H}$  NMR spectrum of **5** in  $\text{C}_6\text{D}_6$ .



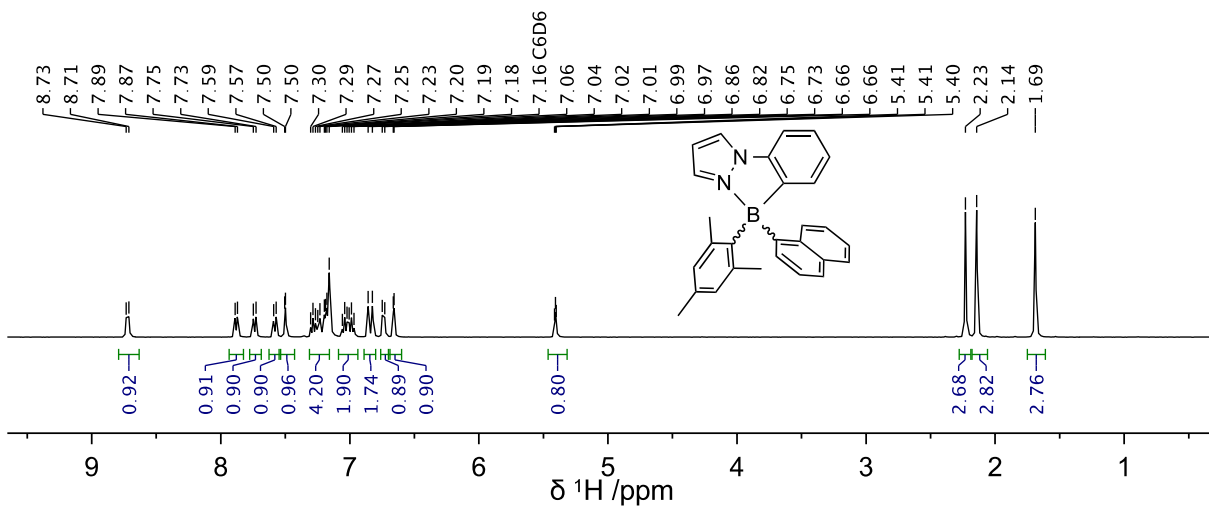
**Figure S14.**  $^{13}\text{C}$  NMR spectrum of **5** in  $\text{C}_6\text{D}_6$ .



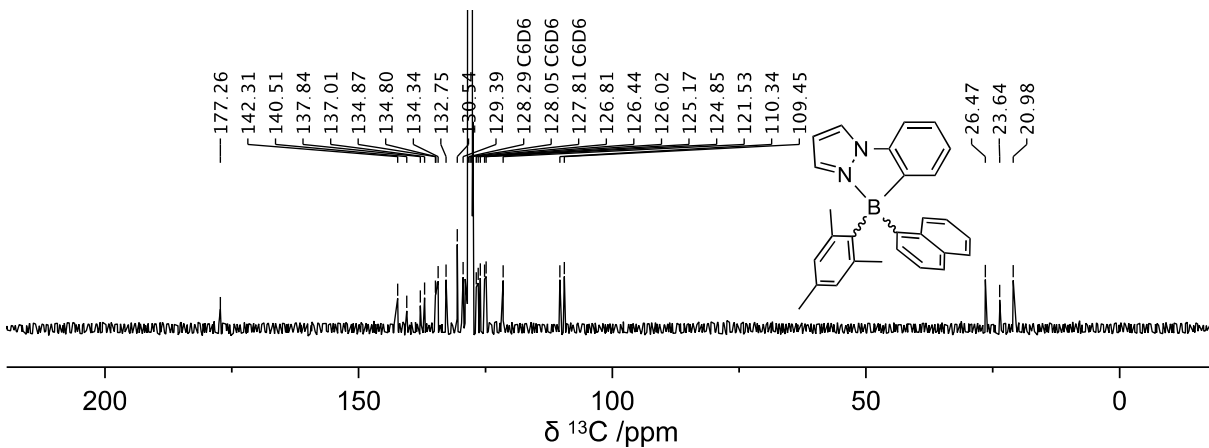
**Figure S15.**  $^{11}\text{B}$  NMR spectrum of **5** in  $\text{C}_6\text{D}_6$ .



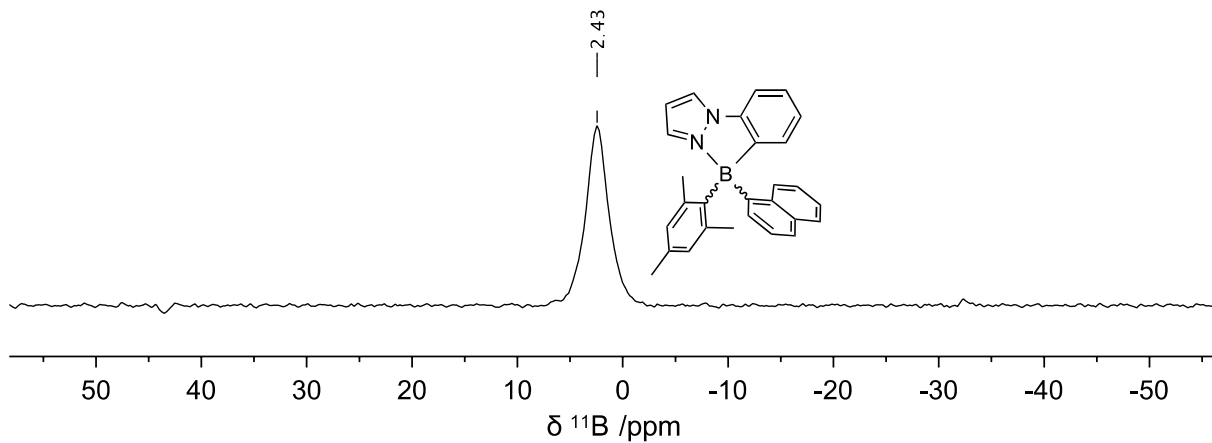
**Figure S16.**  $^{19}\text{F}$  NMR spectrum of **5** in  $\text{C}_6\text{D}_6$ .



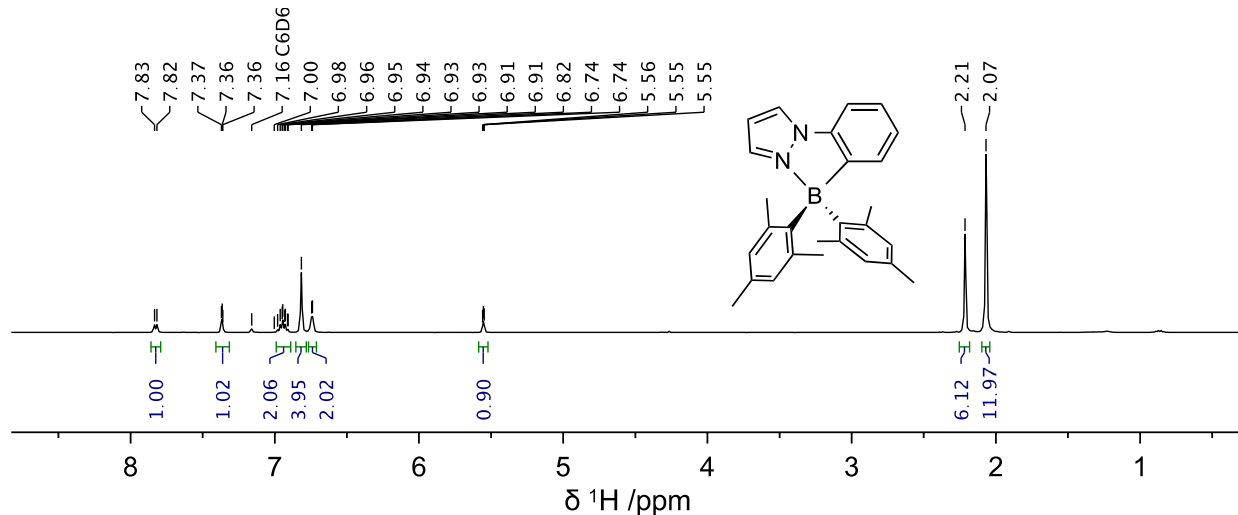
**Figure S17.**  $^1\text{H}$  NMR spectrum of **6** in  $\text{C}_6\text{D}_6$ .



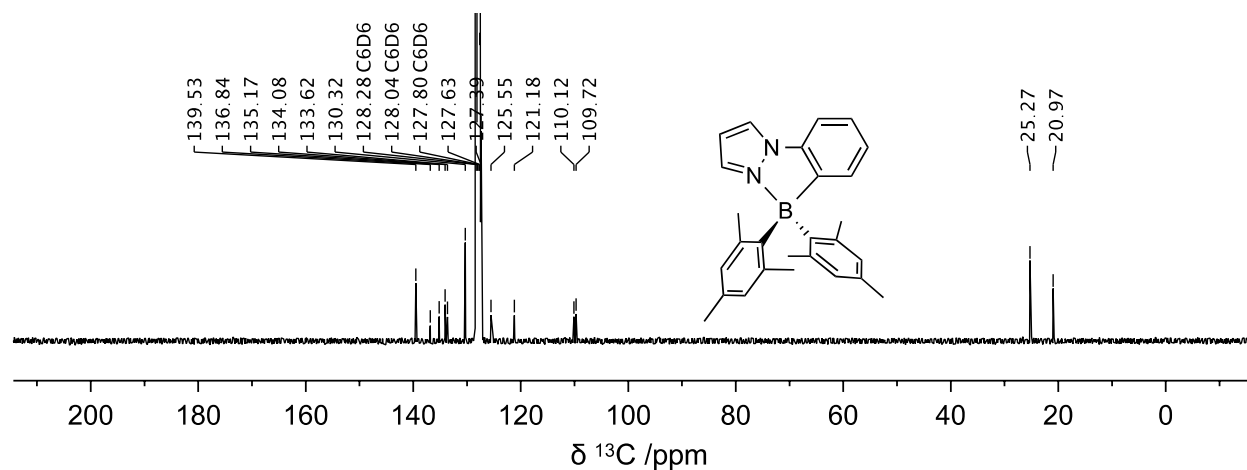
**Figure S18.**  $^{13}\text{C}$  NMR spectrum of **6** in  $\text{C}_6\text{D}_6$ .



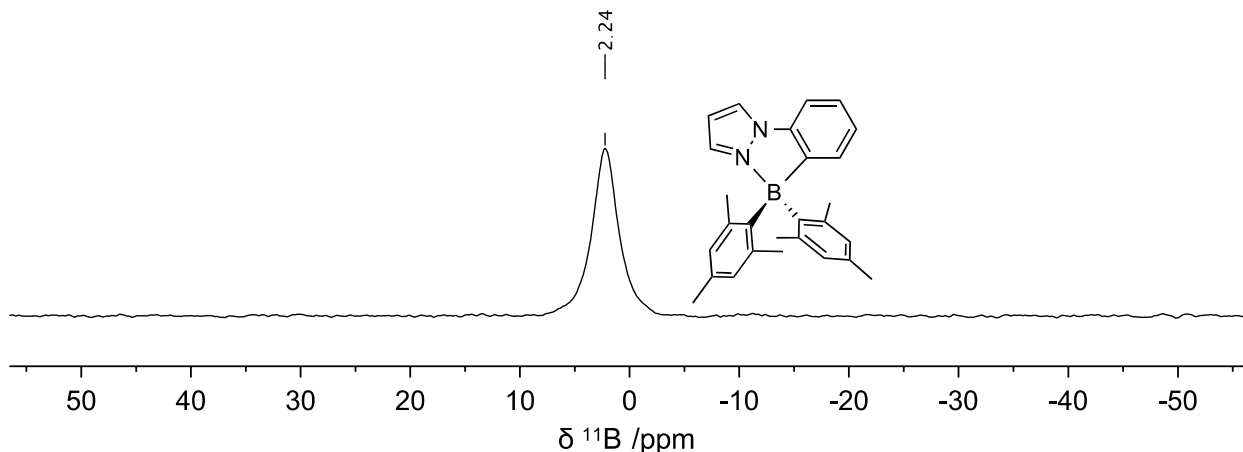
**Figure S19.**  $^{11}\text{B}$  NMR spectrum of **6** in  $\text{C}_6\text{D}_6$ .



**Figure S20.**  $^1\text{H}$  NMR spectrum of **7** in  $\text{C}_6\text{D}_6$ .



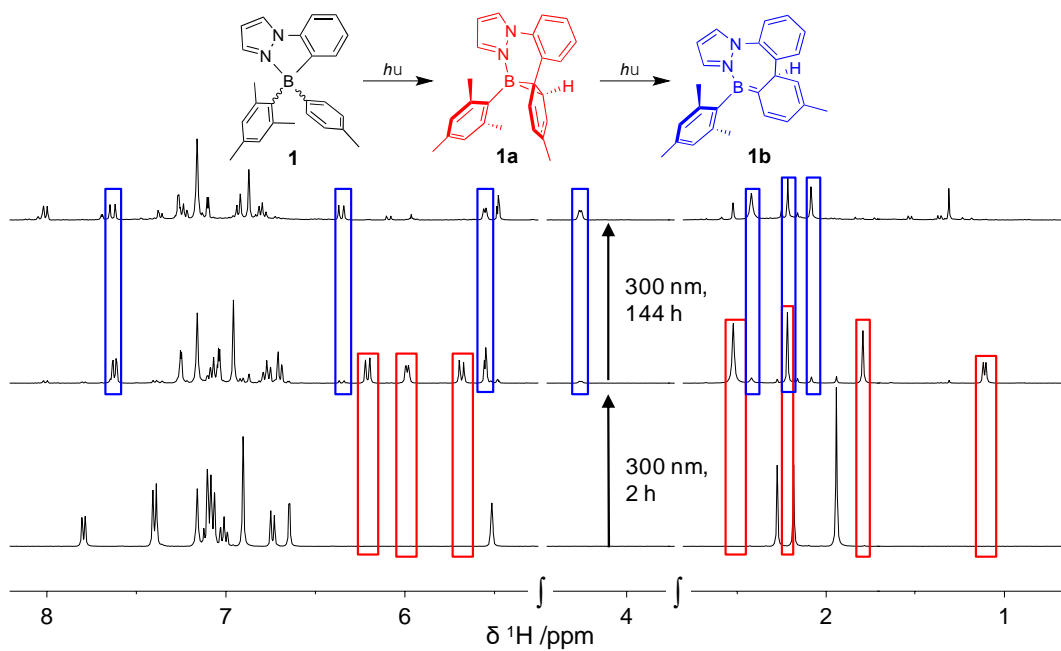
**Figure S21.**  $^{13}\text{C}$  NMR spectrum of **7** in  $\text{C}_6\text{D}_6$ .



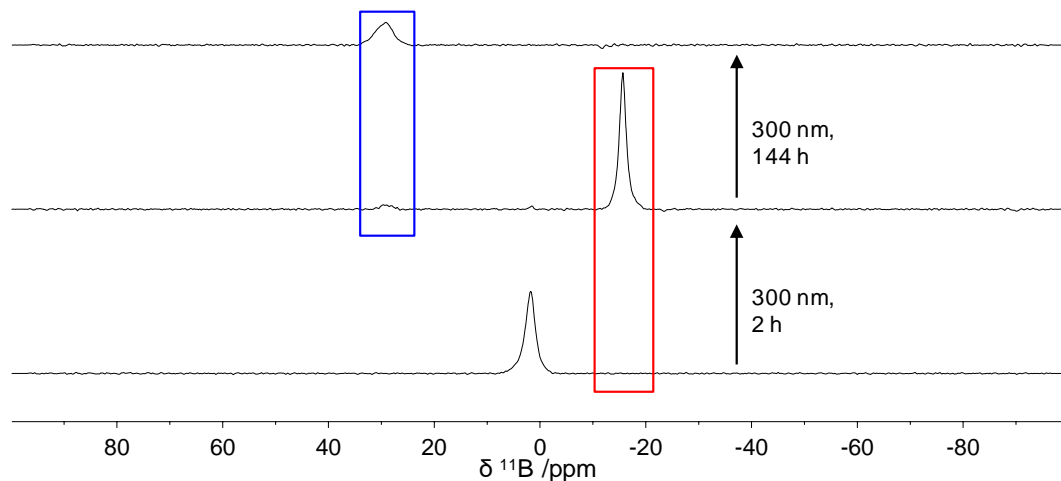
**Figure S22.**  $^{11}\text{B}$  NMR spectrum of 7 in  $\text{C}_6\text{D}_6$ .

### **S3: NMR Photoisomerization Data of 1 – 7**

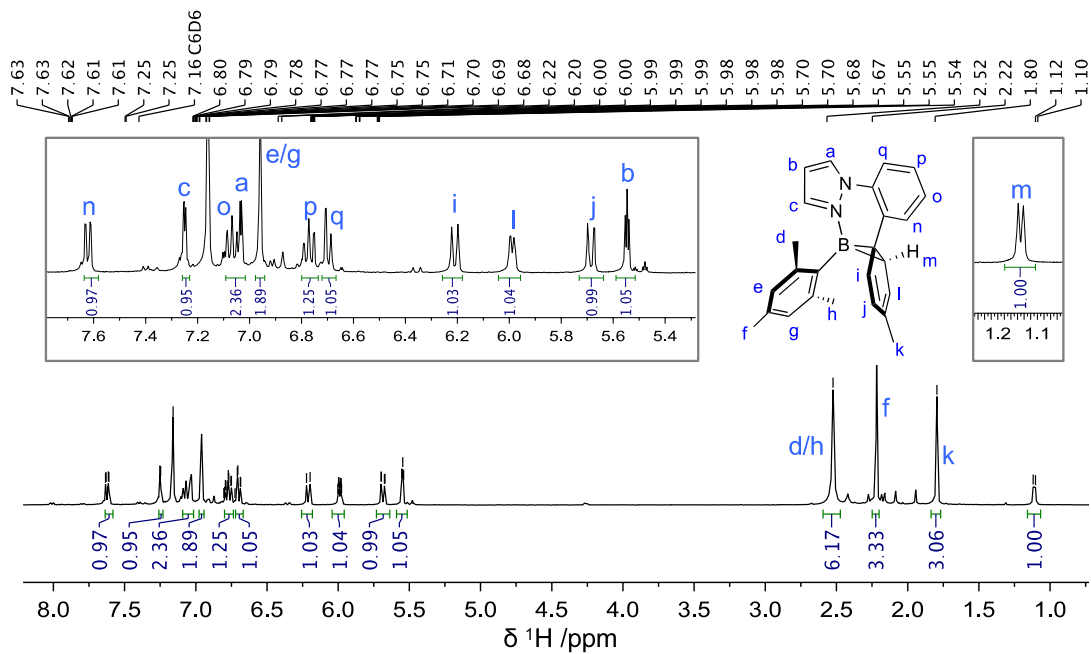
In a  $\text{N}_2$  filled glovebox, **1 – 7** were added to J-Young NMR tubes to obtain concentrations of  $10^{-2}$  M in  $\text{C}_6\text{D}_6$  (~0.4 mL). The NMR tubes were sealed with their teflon caps and removed from the glove box. Photochemical experiments were carried out using a Rayonet Photochemical Reactor (300 nm) and the photoisomerization processes of **1 – 7** were monitored periodically by  $^1\text{H}$ ,  $^{11}\text{B}$ , and  $^{19}\text{F}$  NMR (where applicable) until all compounds were converted to their diazaborepin isomers (**1b – 4b**) or no additional spectral change was observed. The resulting photochemical transformations of compounds **2** and **3** yielded mixtures of products (**2b + 2b'** and **3b + 3b'**), from which the identities of **2b'** and **3b'** could not be confirmed by NMR due to overlap with the chemical shifts of **2b** and **3b**.



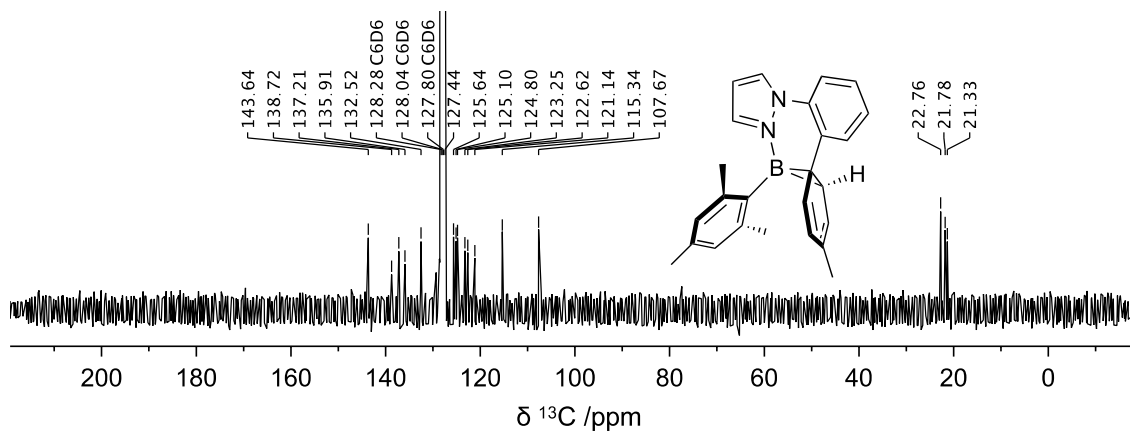
**Figure S23.** Stacked <sup>1</sup>H-NMR spectra showing the conversion of **1** → **1a** → **1b** under  $\text{N}_2$  in  $\text{C}_6\text{D}_6$  (300 nm irradiation) with diagnostic chemical shifts highlighted in red (**1a**) or blue (**1b**).



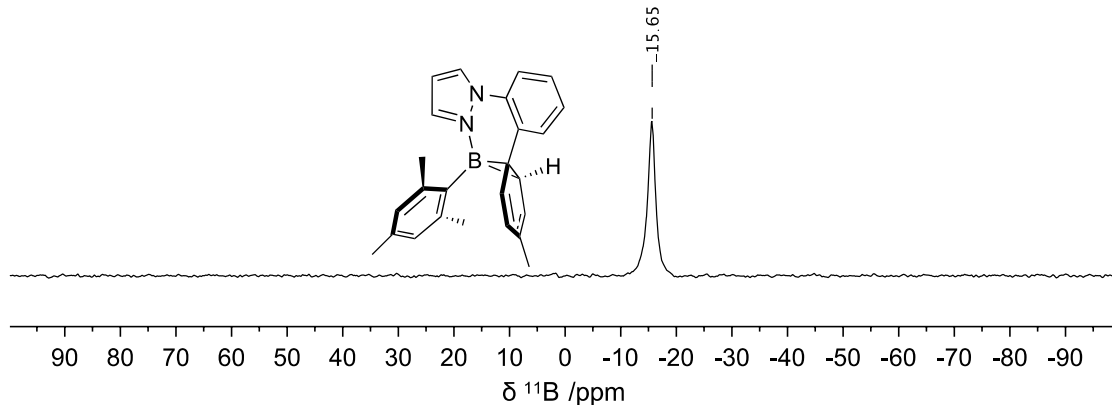
**Figure S24.** Stacked <sup>11</sup>B-NMR spectra showing the conversion of **1** → **1a** → **1b** under  $\text{N}_2$  in  $\text{C}_6\text{D}_6$  (300 nm irradiation) with diagnostic chemical shifts highlighted in red (**1a**) or blue (**1b**).



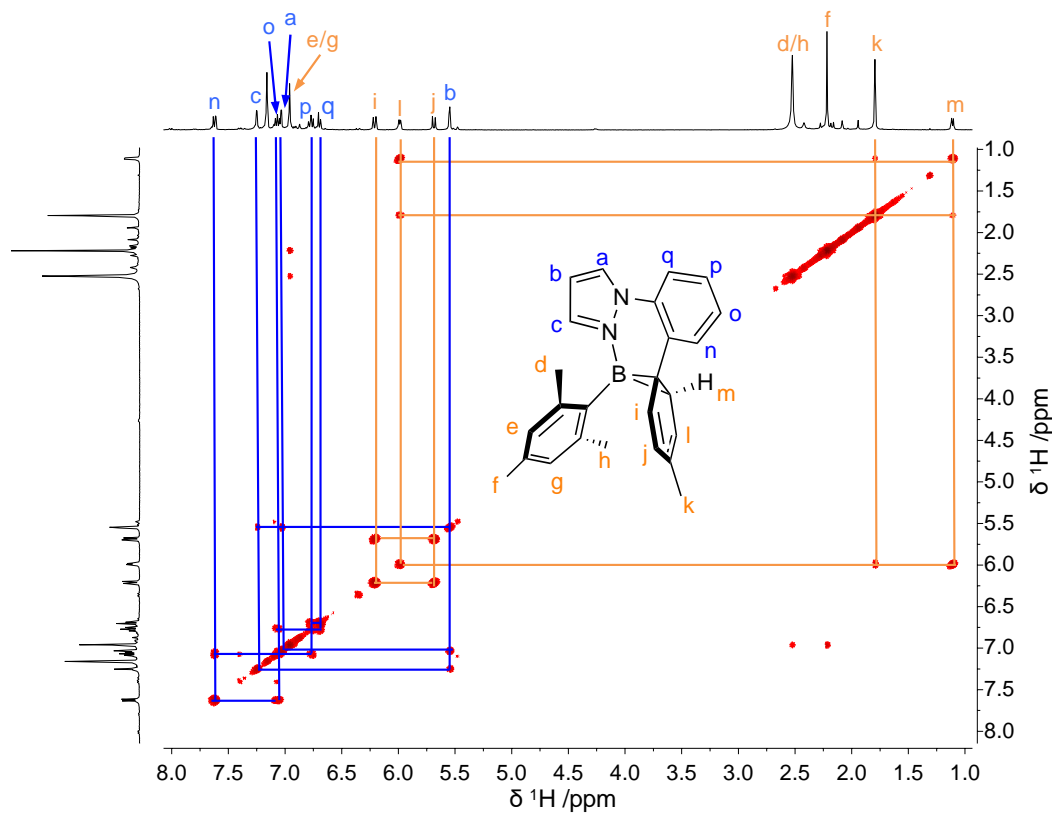
**Figure S25.**  $^1\text{H}$  NMR spectrum of **1a** in  $\text{C}_6\text{D}_6$ .



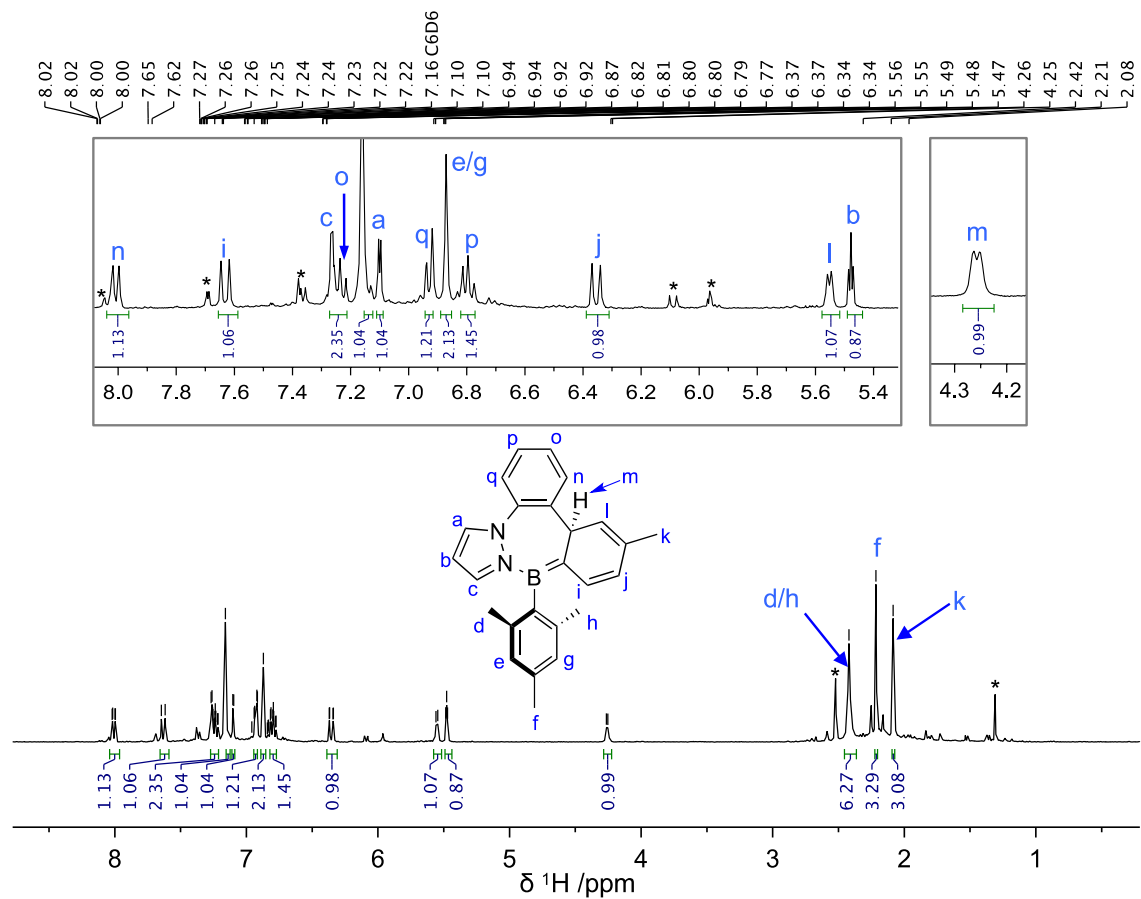
**Figure S26.**  $^{13}\text{C}$  NMR spectrum of **1a** in  $\text{C}_6\text{D}_6$ .



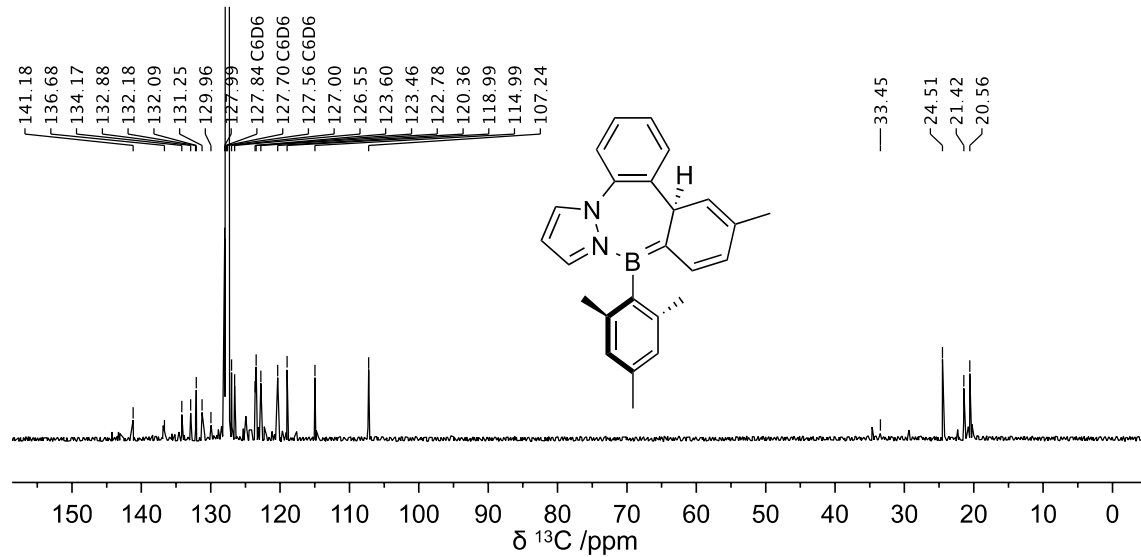
**Figure S27.**  $^{11}\text{B}$  NMR spectrum of **1a** in  $\text{C}_6\text{D}_6$ .



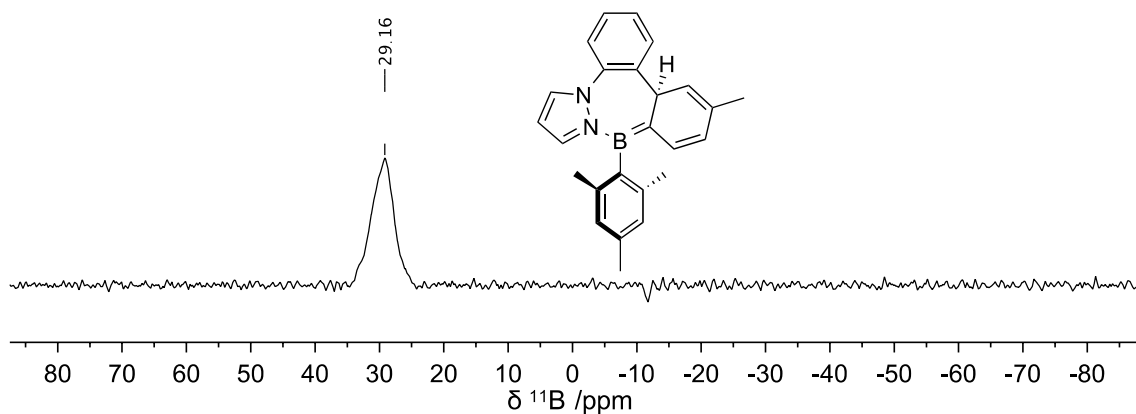
**Figure S28.**  $^1\text{H}$ - $^1\text{H}$  COSY NMR spectrum of **1a** in  $\text{C}_6\text{D}_6$  with diagnostic correlations.



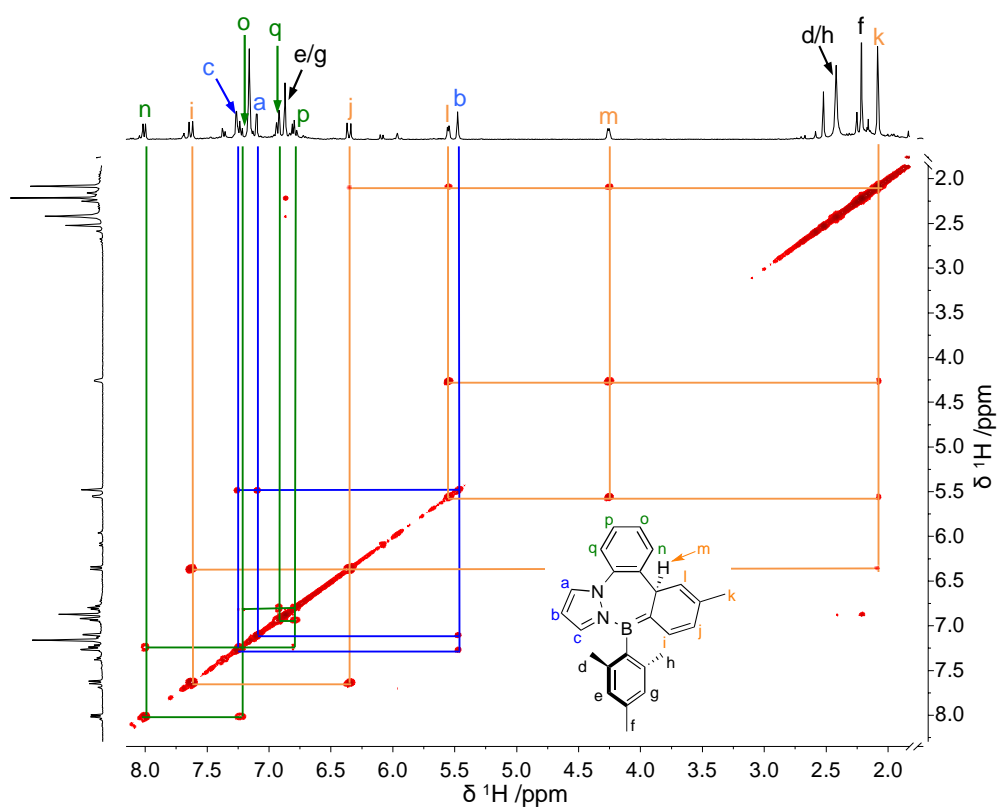
**Figure S29.**  $^1\text{H}$  NMR spectrum of **1b** in  $\text{C}_6\text{D}_6$ . \*Unknown impurities.



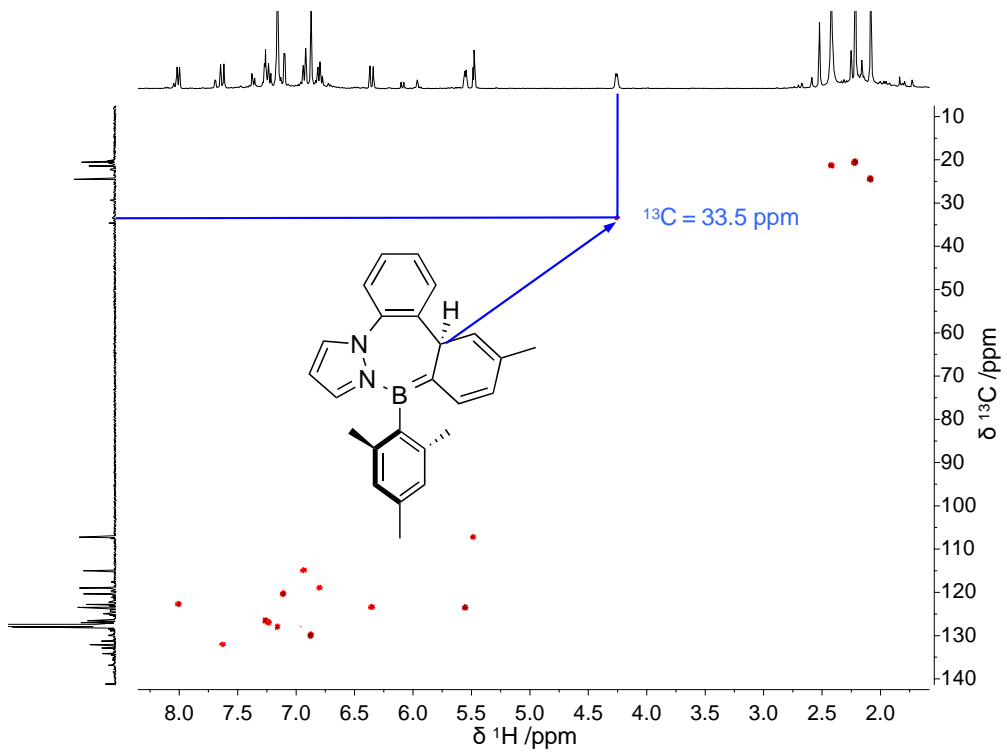
**Figure S30.**  $^{13}\text{C}$  NMR spectrum of **1b** in  $\text{C}_6\text{D}_6$ .



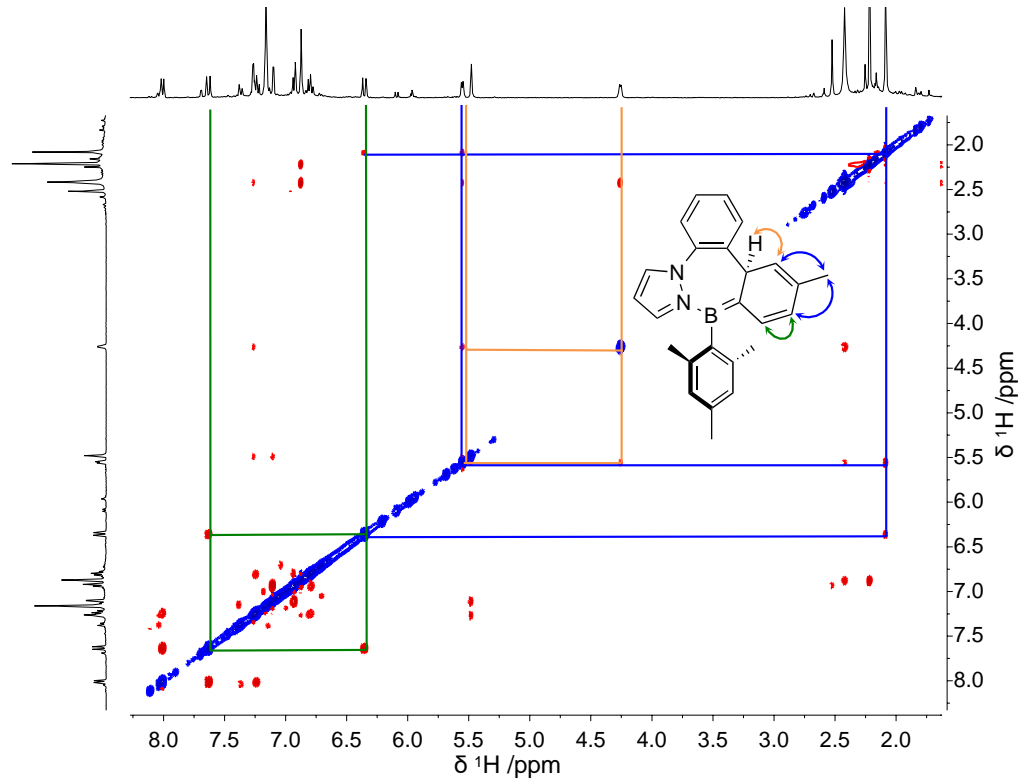
**Figure S31.**  $^{11}\text{B}$  NMR spectrum of **1b** in  $\text{C}_6\text{D}_6$ .



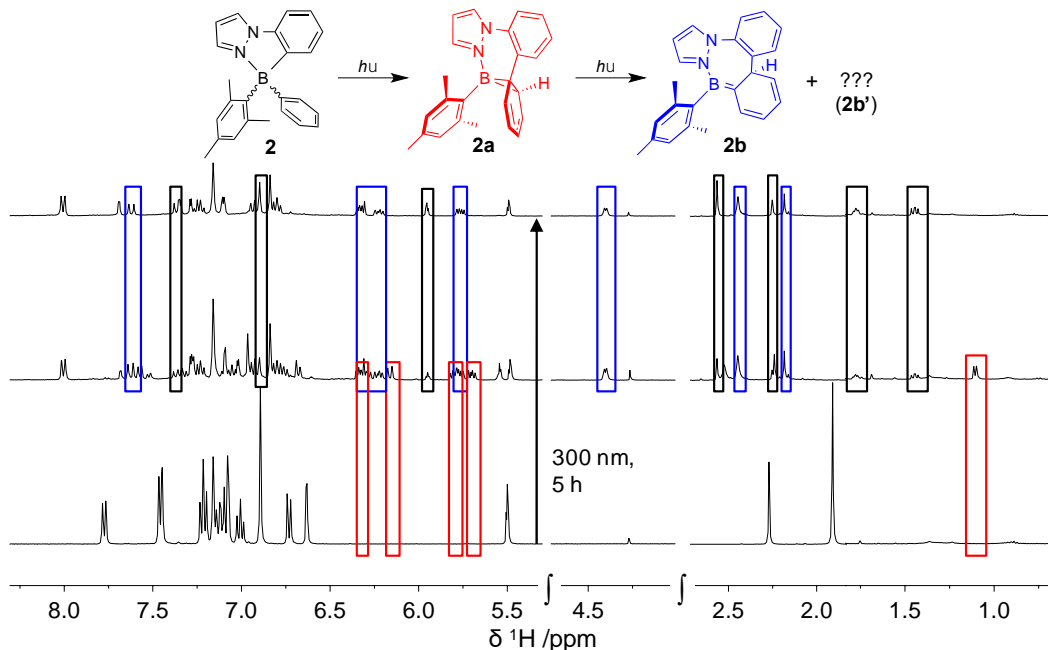
**Figure S32.**  $^1\text{H}$ - $^1\text{H}$  COSY NMR spectrum of **1b** in  $\text{C}_6\text{D}_6$  with diagnostic correlations.



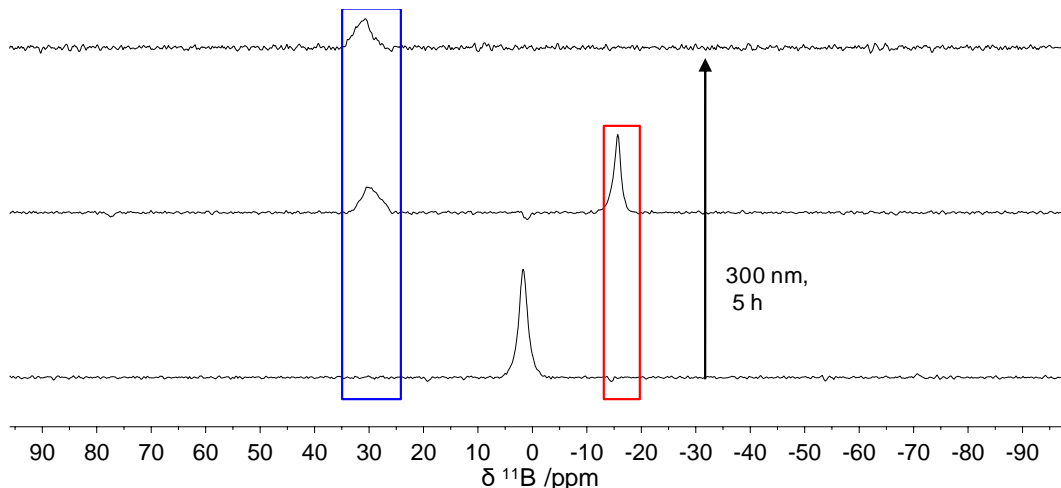
**Figure S33.**  $^1\text{H}$ - $^{13}\text{C}$  HSQC NMR spectrum of **1b** in  $\text{C}_6\text{D}_6$  showing the diagnostic chemical shift of the chiral carbon atom.



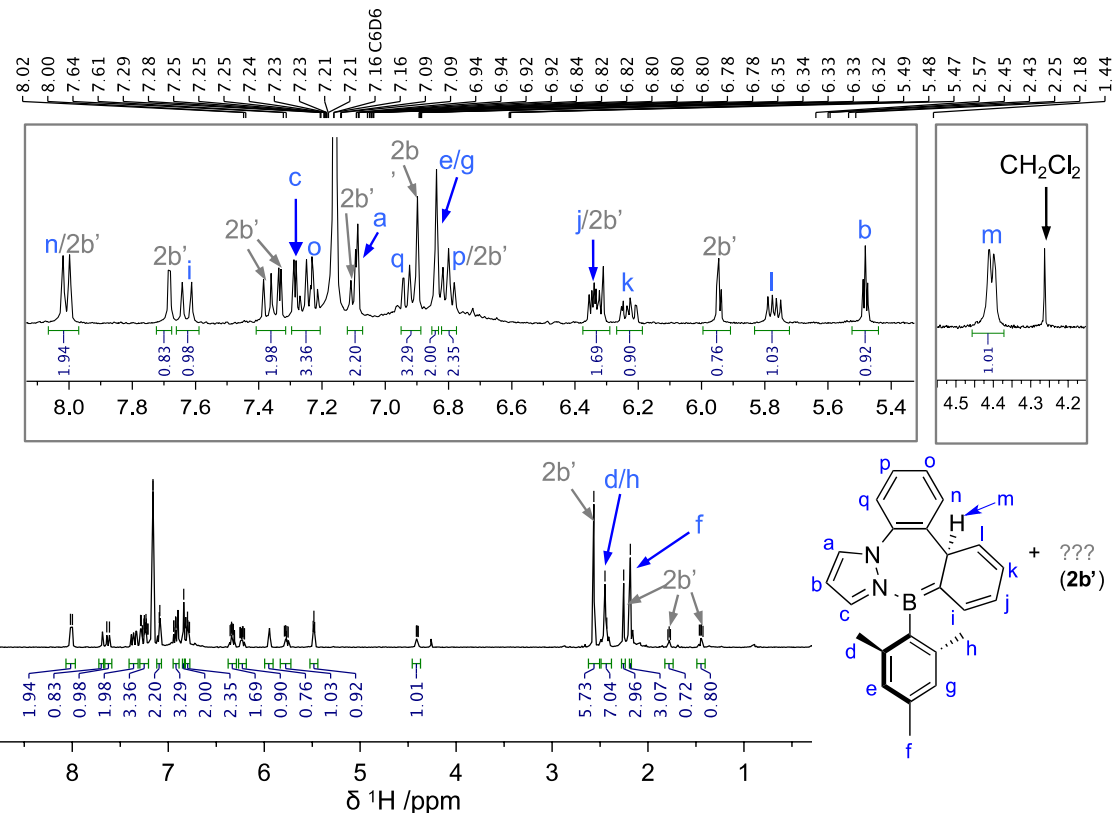
**Figure S34.**  $^1\text{H}$ - $^1\text{H}$  NOESY NMR spectrum of **1b** in  $\text{C}_6\text{D}_6$  with diagnostic correlations.



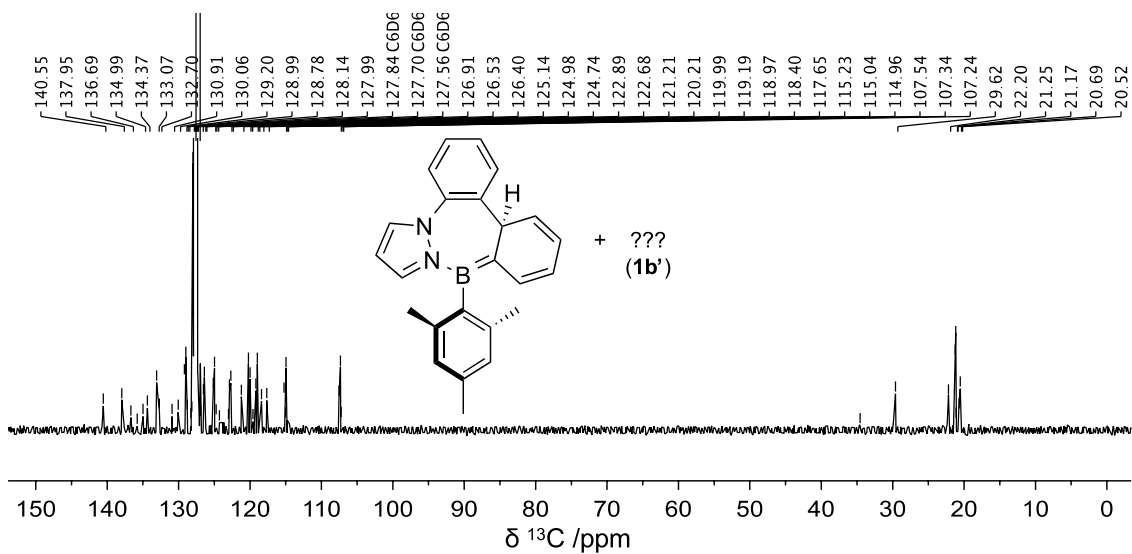
**Figure S35.** Stacked  $^1\text{H}$ -NMR spectra showing the conversion of **2**  $\rightarrow$  **2a** + **2b**  $\rightarrow$  **2b** + **2b'** under  $\text{N}_2$  in  $\text{C}_6\text{D}_6$  (300 nm irradiation) with diagnostic chemical shifts highlighted in red (**2a**), blue (**2b**), or black (**2b'**).



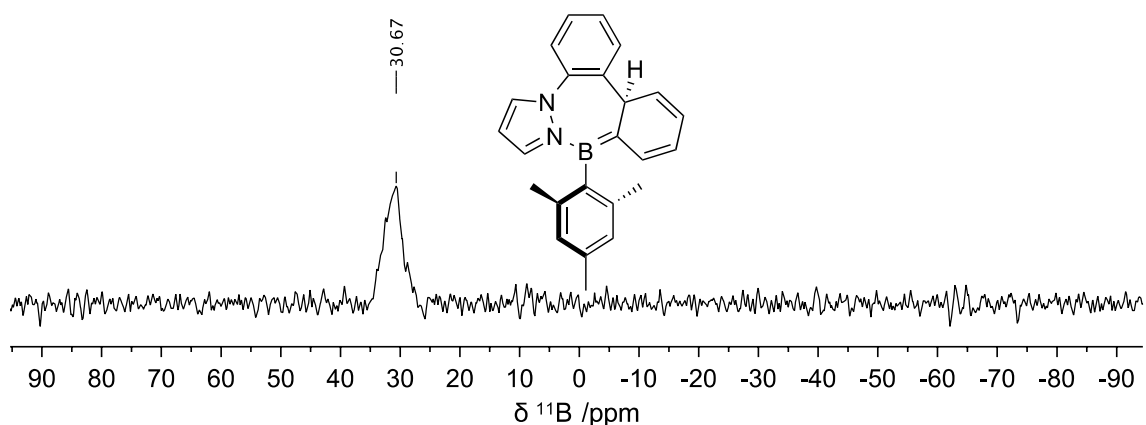
**Figure S36.** Stacked  $^{11}\text{B}$ -NMR spectra showing the conversion of **2**  $\rightarrow$  **2a** + **2b**  $\rightarrow$  **2b** under  $\text{N}_2$  in  $\text{C}_6\text{D}_6$  (300 nm irradiation) with diagnostic chemical shifts highlighted in red (**2a**) or blue (**2b**).



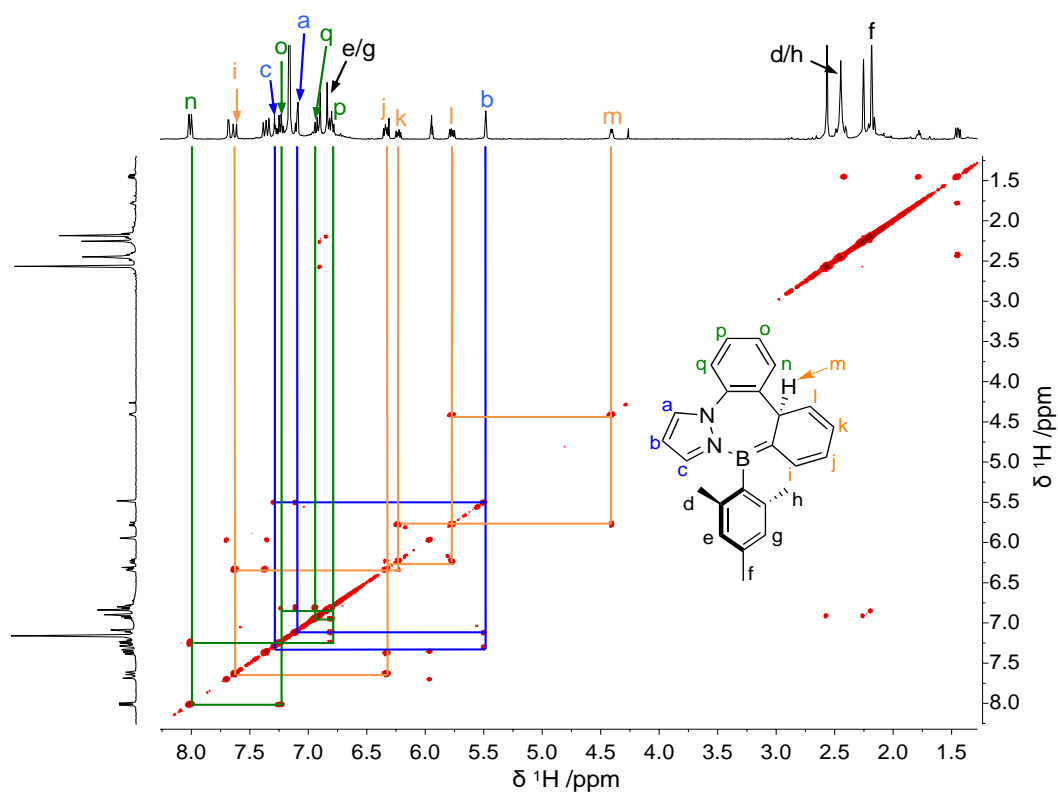
**Figure S37.**  $^1\text{H}$  NMR spectrum of **2b** and **2b'** (unidentified product) in  $\text{C}_6\text{D}_6$ .



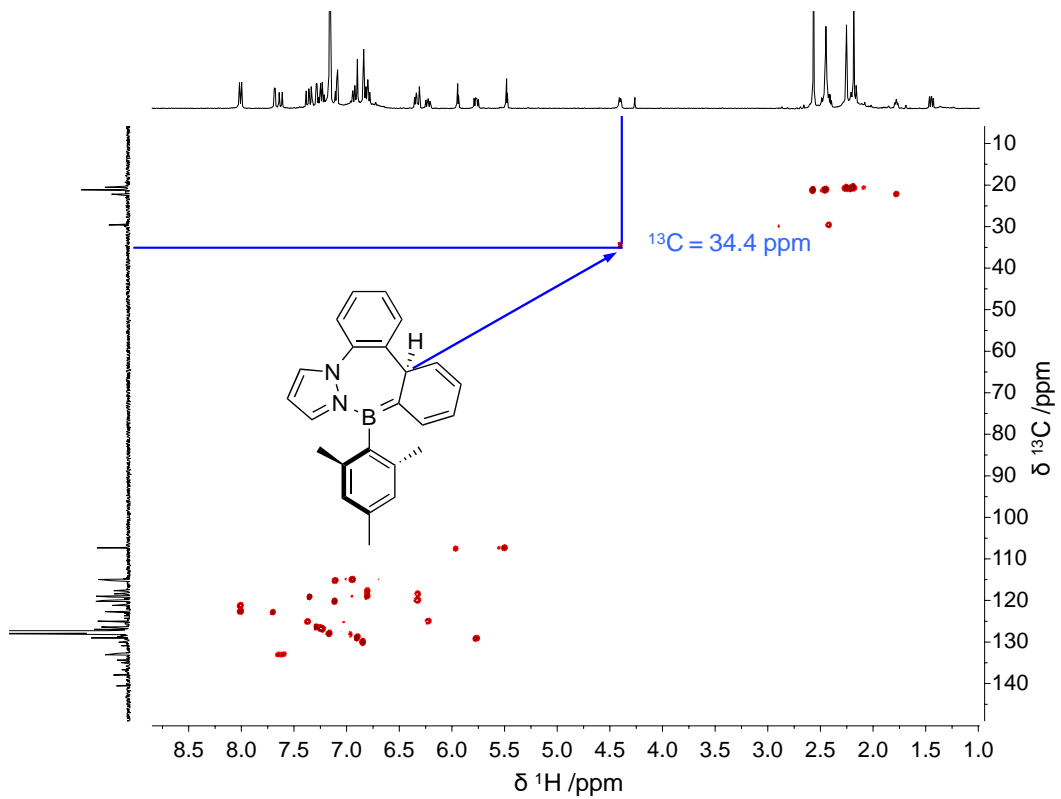
**Figure S38.**  $^{13}\text{C}$  NMR spectrum of **2b** and **2b'** (unidentified product) in  $\text{C}_6\text{D}_6$ .



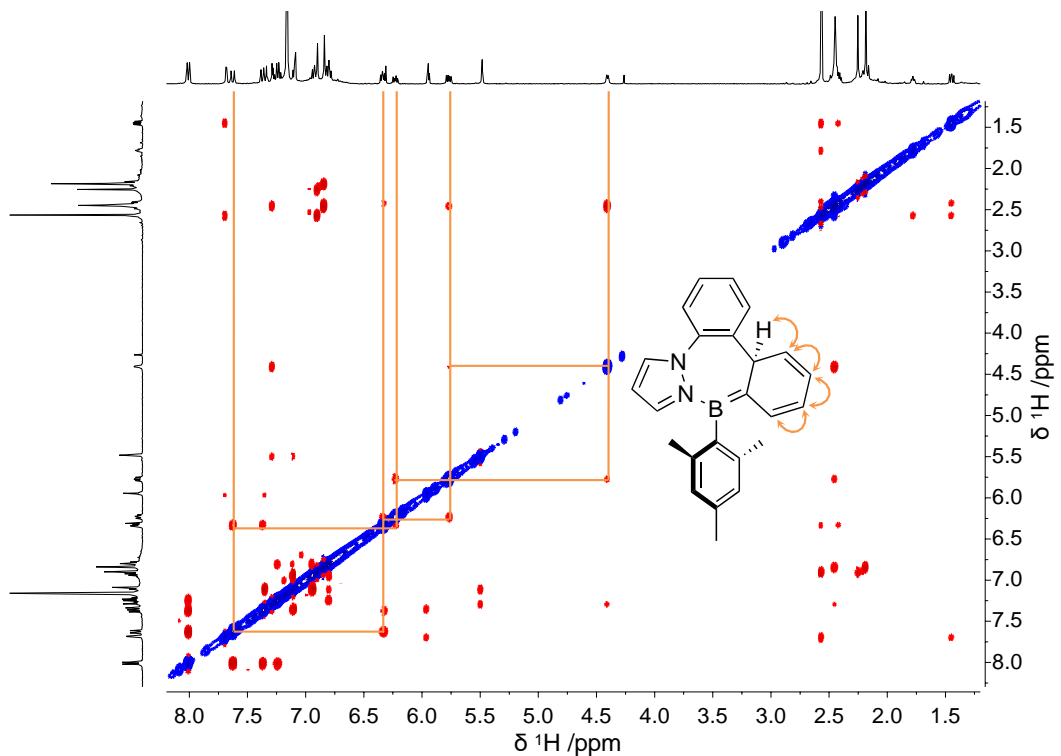
**Figure S39.**  $^{11}\text{B}$  NMR spectrum of **2b** in  $\text{C}_6\text{D}_6$ .



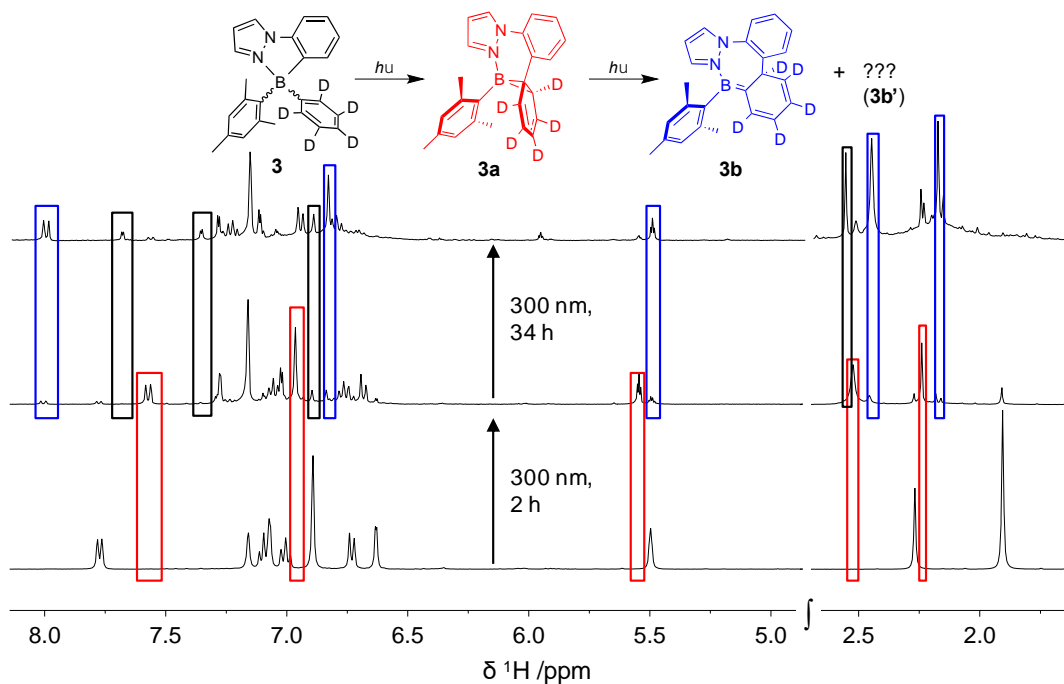
**Figure S40.**  $^1\text{H}$ - $^1\text{H}$  COSY NMR spectrum of **2b** + **2b'** in  $\text{C}_6\text{D}_6$  with diagnostic correlations.



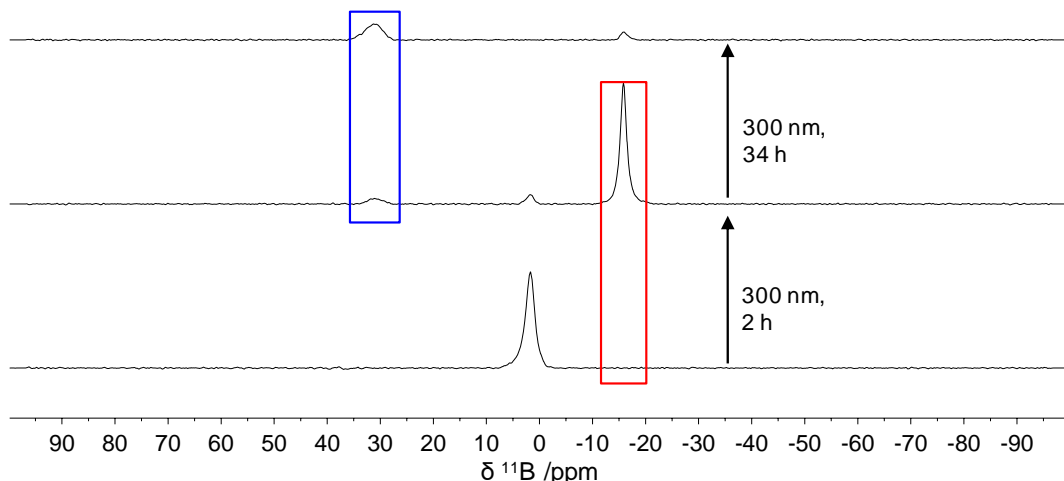
**Figure S41.**  $^1\text{H}$ - $^{13}\text{C}$  HSQC NMR spectrum of **2b** + **2b'** in  $\text{C}_6\text{D}_6$  showing the diagnostic chemical shift of the chiral carbon atom in **2b**.



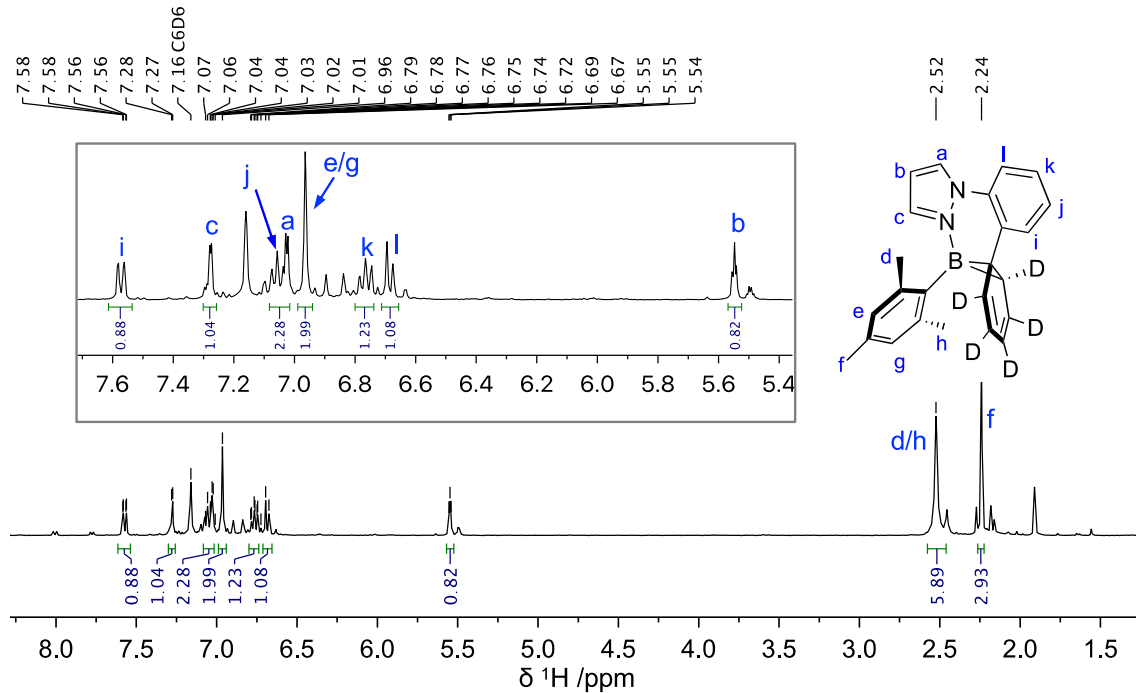
**Figure S42.**  $^1\text{H}$ - $^1\text{H}$  NOESY NMR spectrum of **2b** + **2b'** in  $\text{C}_6\text{D}_6$  with diagnostic correlations.



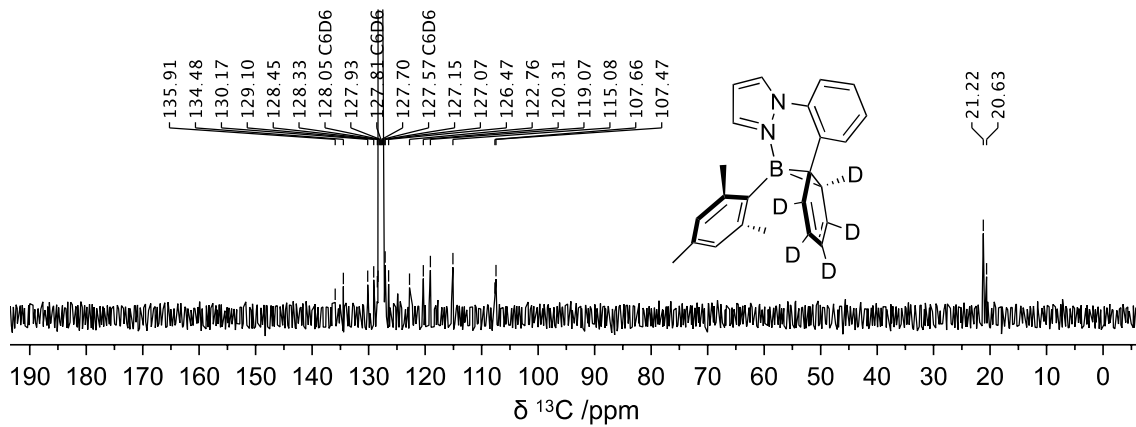
**Figure S43.** Stacked  $^1\text{H}$ -NMR spectra showing the conversion of **3**  $\rightarrow$  **3a**  $\rightarrow$  **3b** + **3b'** under  $\text{N}_2$  in  $\text{C}_6\text{D}_6$  (300 nm irradiation) with diagnostic chemical shifts highlighted in red (**3a**), blue (**3a**), or black (**3b'**).



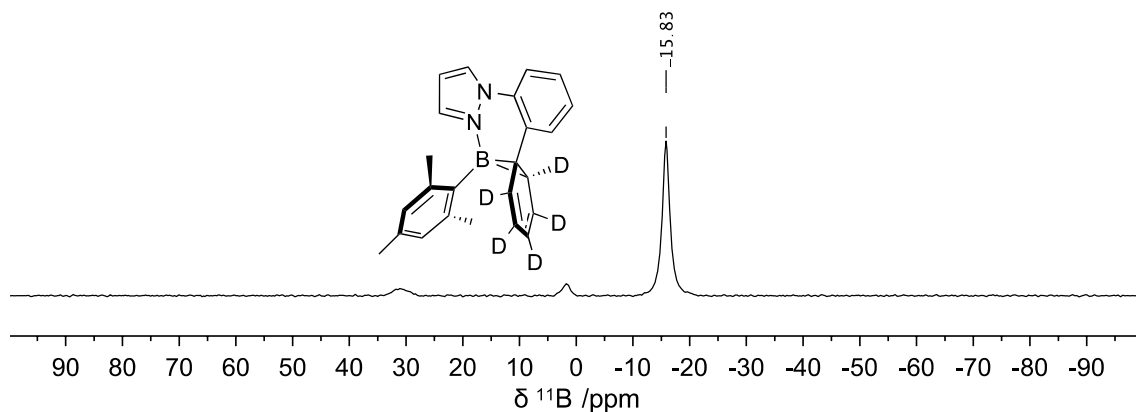
**Figure S44.** Stacked  $^{11}\text{B}$ -NMR spectra showing the conversion of **3**  $\rightarrow$  **3a**  $\rightarrow$  **3b** + **3b'** under  $\text{N}_2$  in  $\text{C}_6\text{D}_6$  (300 nm irradiation) with diagnostic chemical shifts highlighted in red (**3a**) or blue (**3a**).



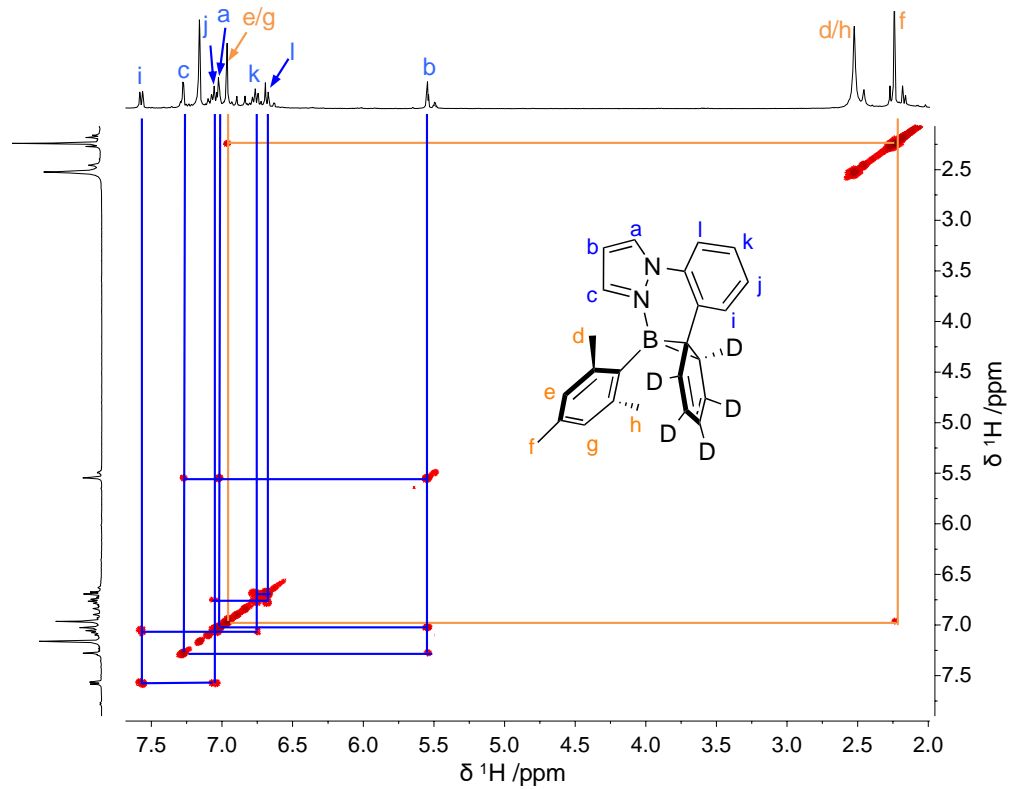
**Figure S45.**  $^1\text{H}$  NMR spectrum of **3a** in  $\text{C}_6\text{D}_6$ .



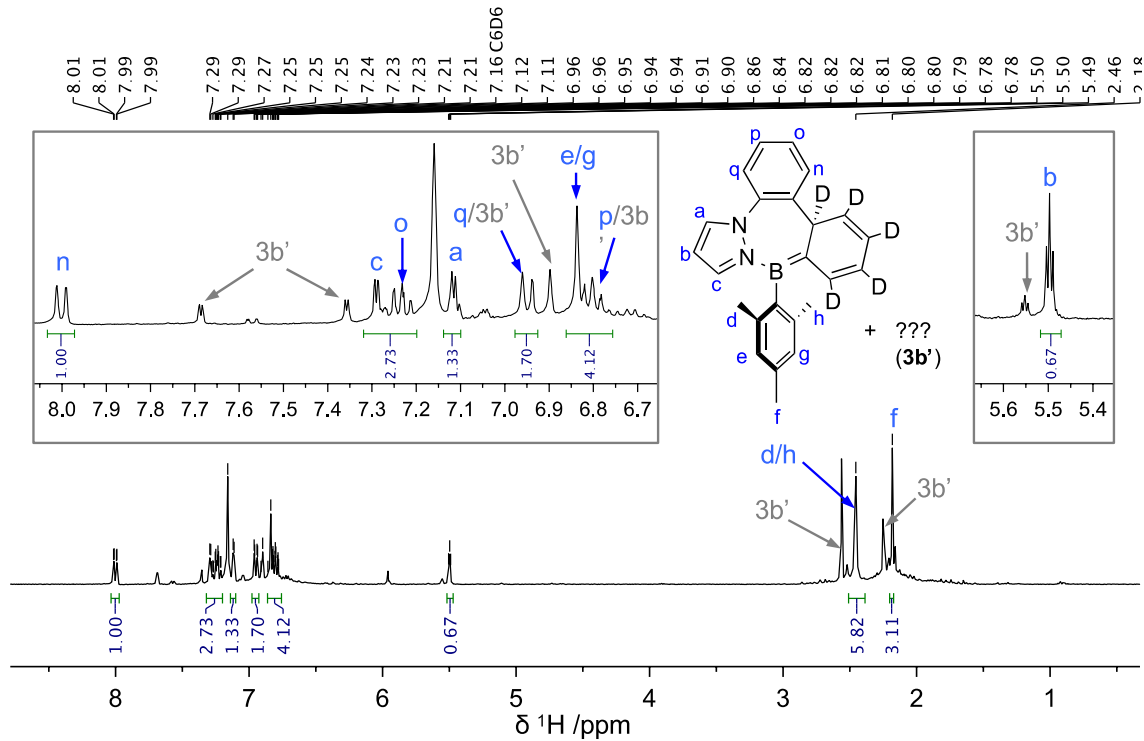
**Figure S46.**  $^{13}\text{C}$  NMR spectrum of **3a** in  $\text{C}_6\text{D}_6$ .



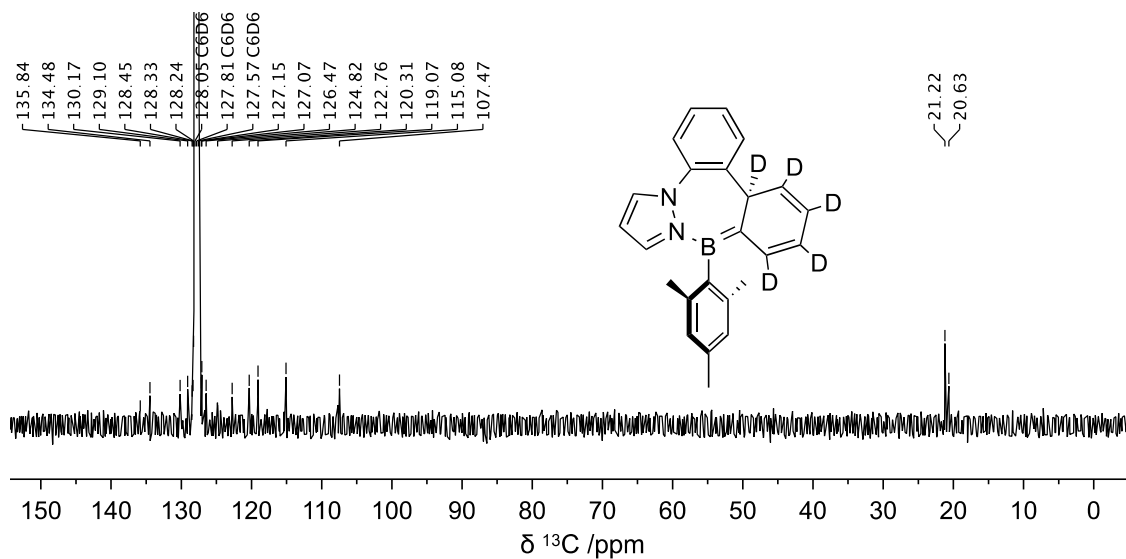
**Figure S47.**  $^{11}\text{B}$  NMR spectrum of **3a** in  $\text{C}_6\text{D}_6$ .



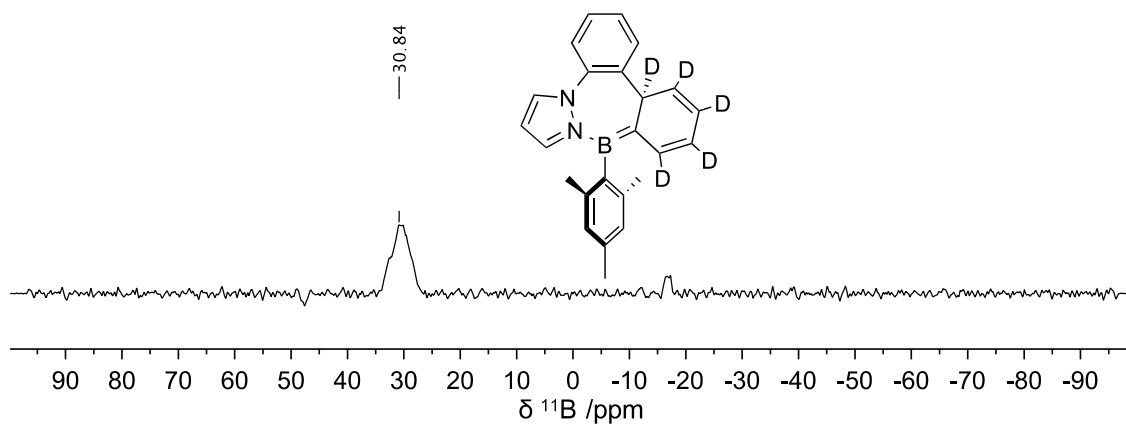
**Figure S48.**  $^1\text{H}$ - $^1\text{H}$  COSY NMR spectrum of **3a** in  $\text{C}_6\text{D}_6$  with diagnostic correlations.



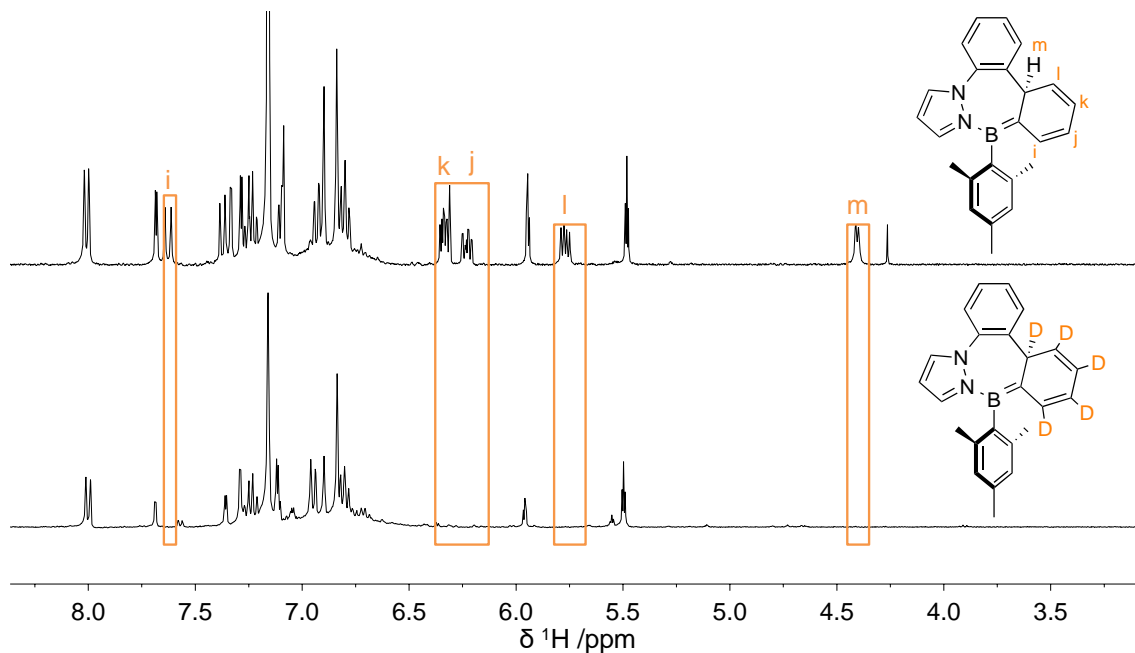
**Figure S49.**  $^1\text{H}$  NMR spectrum of **3b** and **3b'** (unidentified product) in  $\text{C}_6\text{D}_6$ .



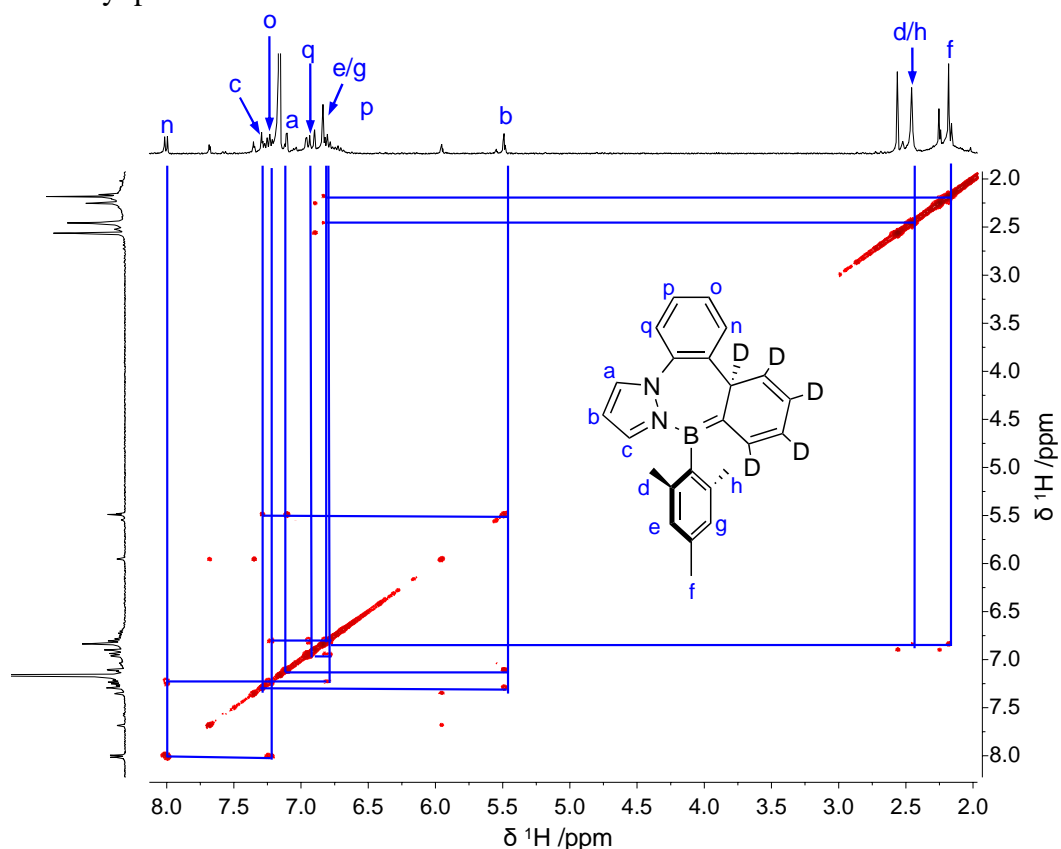
**Figure S50.**  $^{13}\text{C}$  NMR spectrum of **3b** and **3b'** (unidentified product) in  $\text{C}_6\text{D}_6$ .



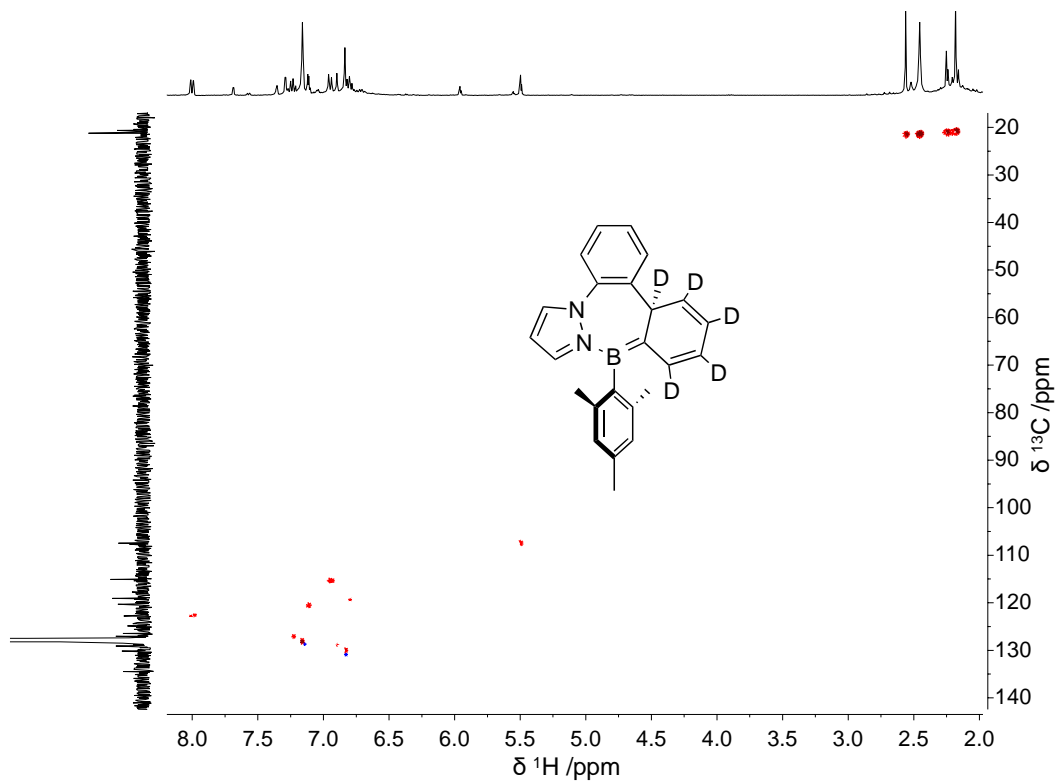
**Figure S51.**  $^{11}\text{B}$  NMR spectrum of **3b** in  $\text{C}_6\text{D}_6$ .



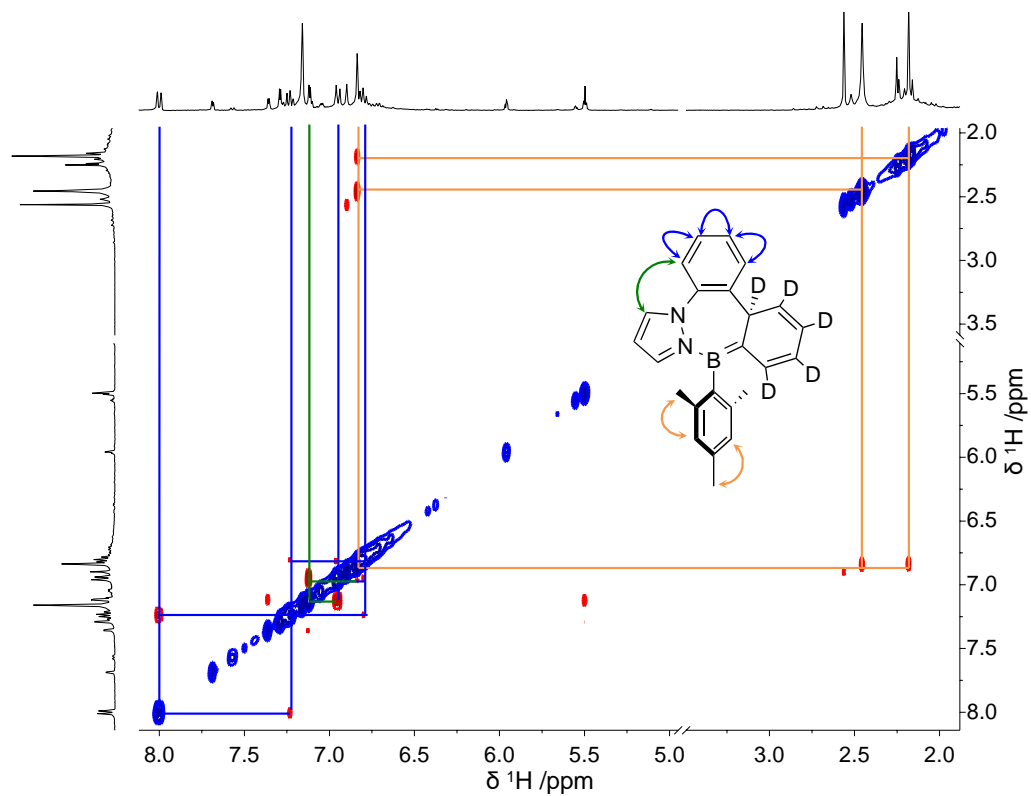
**Figure S52.** Stacked  $^1\text{H}$ -NMR spectra comparing **1b** (top) and **3b** (bottom) highlighting the absent chemical shifts of the deuterium atoms in **3b** relative to the chemical shifts of the cyclohexadienyl protons in **1b**.



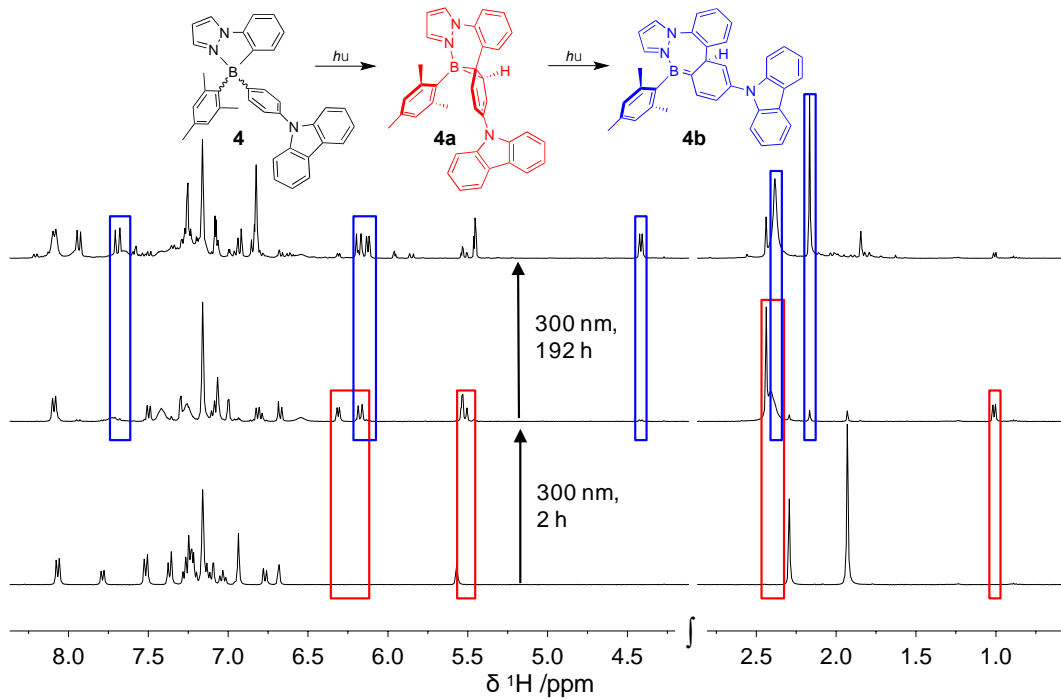
**Figure S53.**  $^1\text{H}$ - $^1\text{H}$  COSY NMR spectrum of **3b** + **3b'** in  $\text{C}_6\text{D}_6$  with diagnostic correlations.



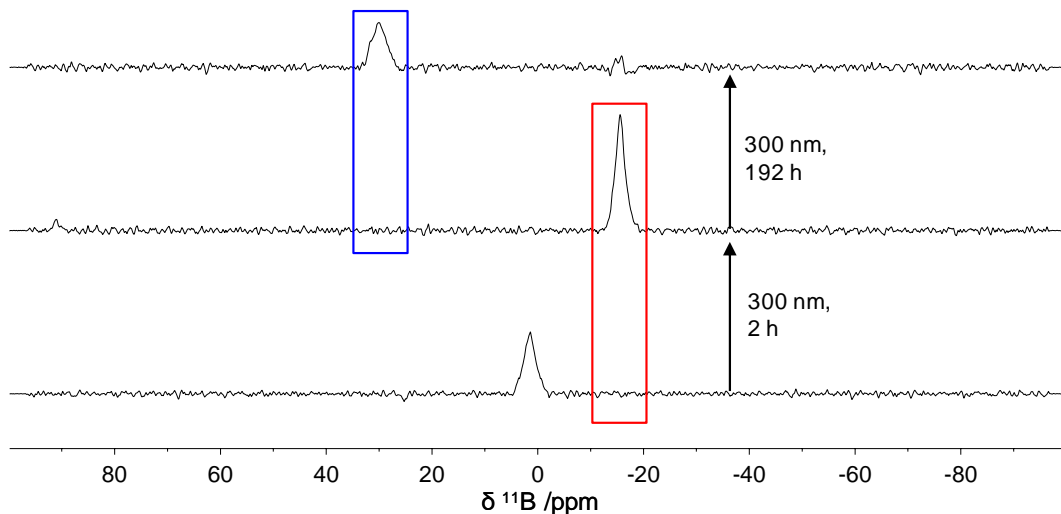
**Figure S54.**  $^1\text{H}$ - $^{13}\text{C}$  HSQC NMR spectrum of **3b** + **3b'** in  $\text{C}_6\text{D}_6$ .



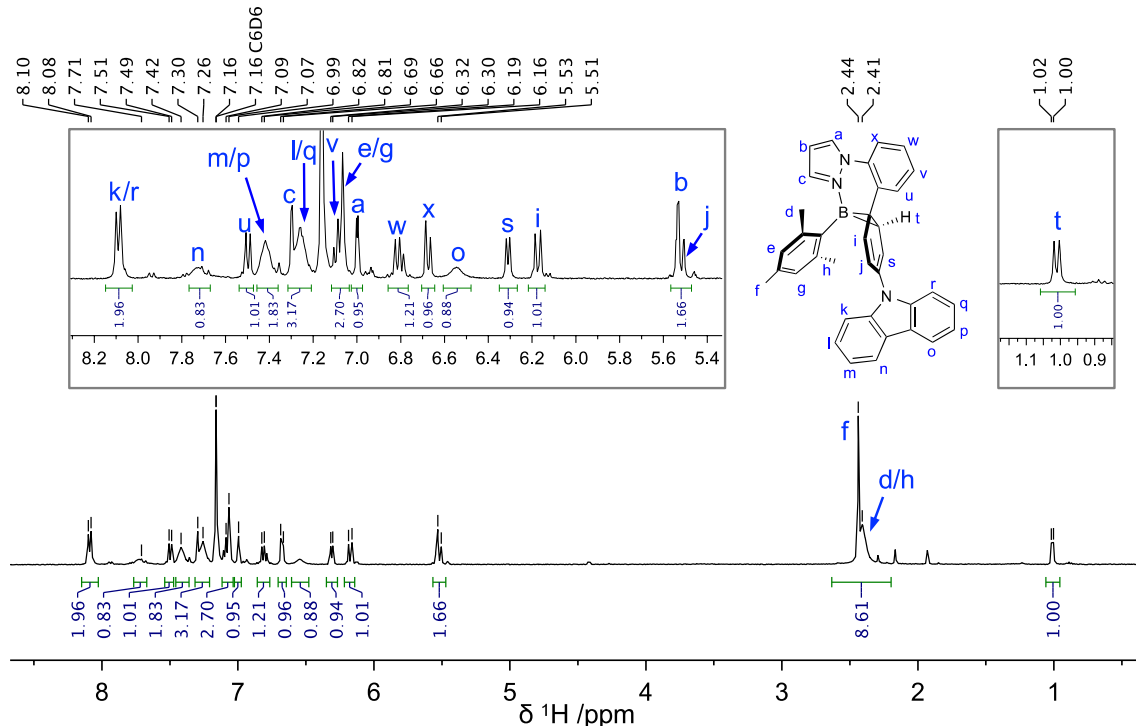
**Figure S55.**  $^1\text{H}$ - $^1\text{H}$  NOESY NMR spectrum of **3b** + **3b'** in  $\text{C}_6\text{D}_6$  with diagnostic correlations.



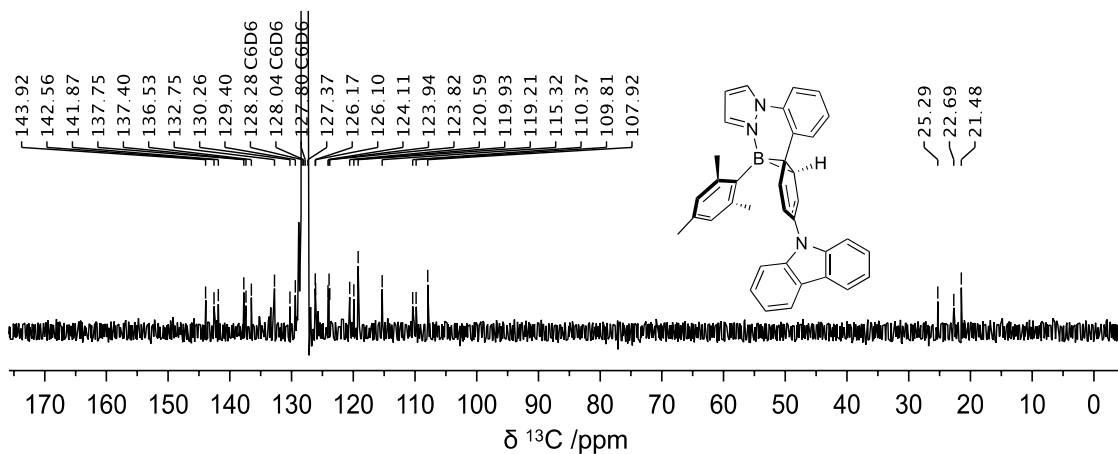
**Figure S56.** Stacked  $^1\text{H}$ -NMR spectra showing the conversion of **4**  $\rightarrow$  **4a**  $\rightarrow$  **4b** under  $\text{N}_2$  in  $\text{C}_6\text{D}_6$  (300 nm irradiation) with diagnostic chemical shifts highlighted in red (**4a**) or blue (**4a**).



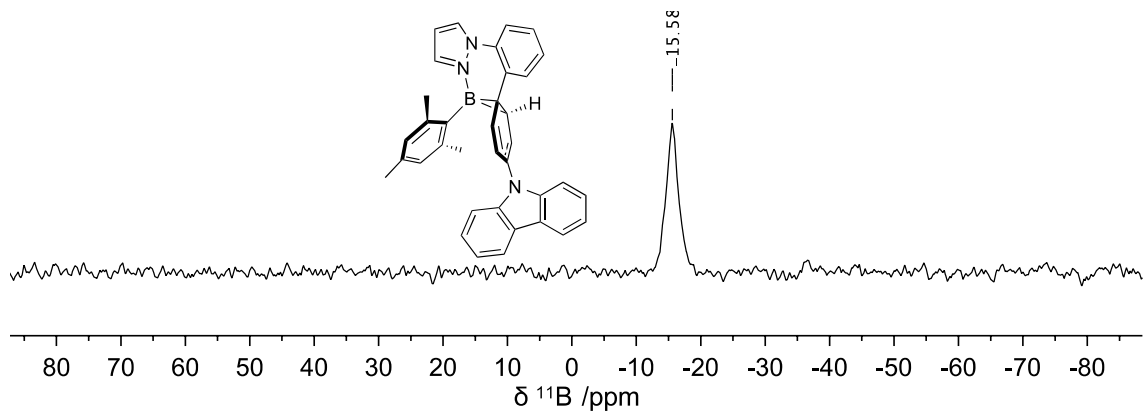
**Figure S57.** Stacked  $^{11}\text{B}$ -NMR spectra showing the conversion of **4**  $\rightarrow$  **4a**  $\rightarrow$  **4b** under  $\text{N}_2$  in  $\text{C}_6\text{D}_6$  (300 nm irradiation) with diagnostic chemical shifts highlighted in red (**4a**) or blue (**4a**).



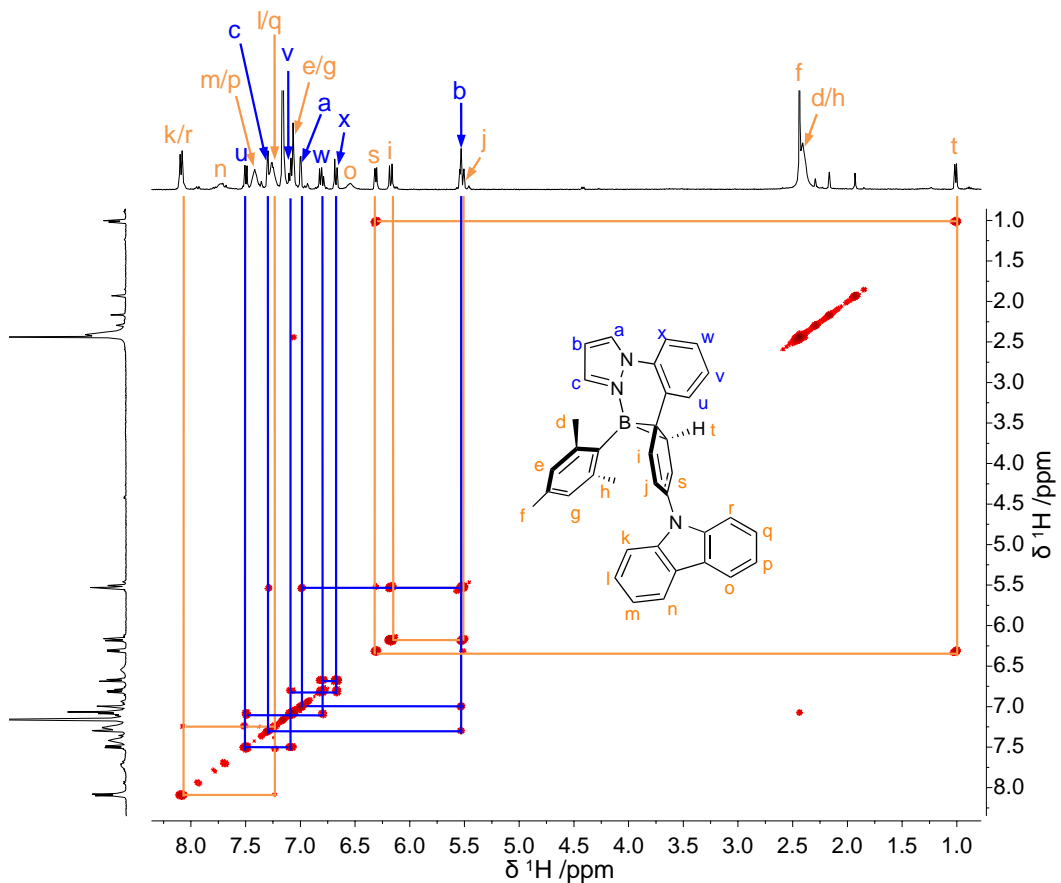
**Figure S58.**  $^1\text{H}$  NMR spectrum of **4a** in  $\text{C}_6\text{D}_6$ .



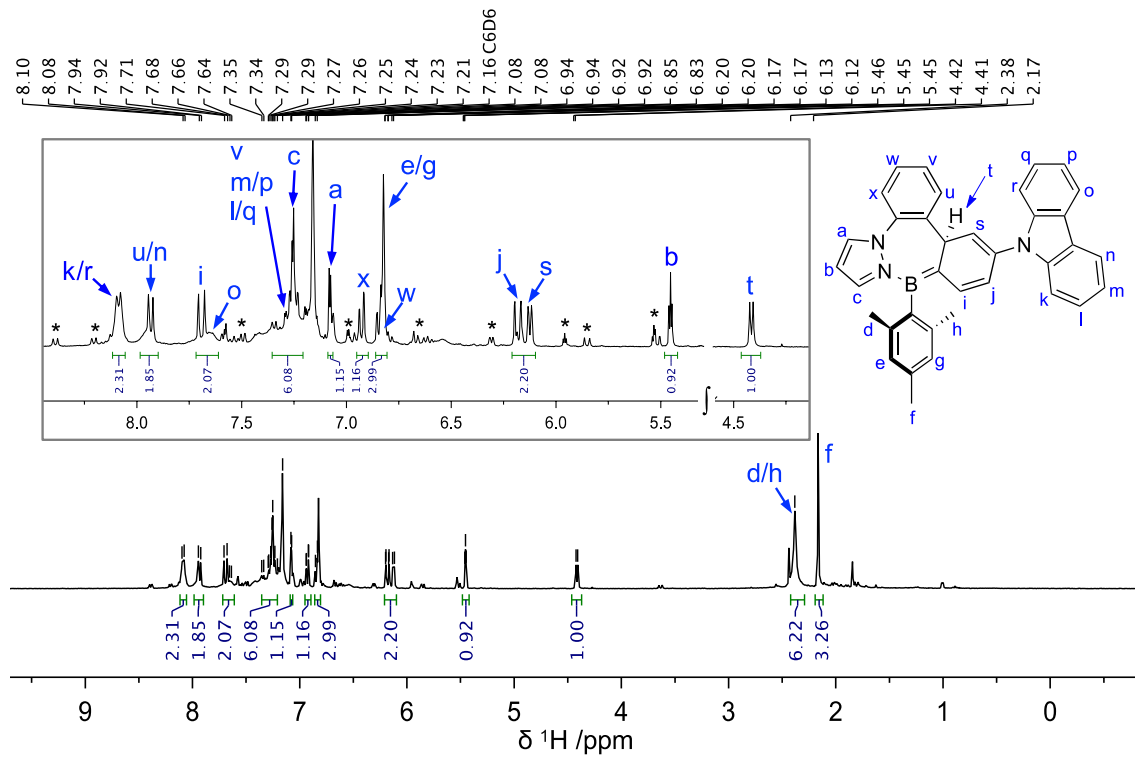
**Figure S59.**  $^{13}\text{C}$  NMR spectrum of **4a** in  $\text{C}_6\text{D}_6$ .



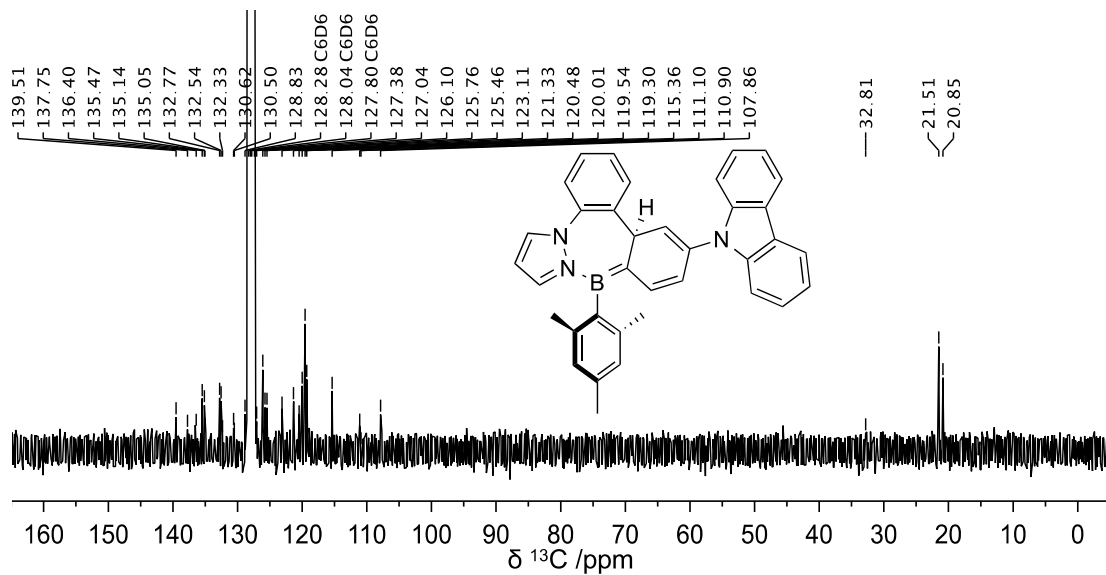
**Figure S60.**  $^{11}\text{B}$  NMR spectrum of **4a** in  $\text{C}_6\text{D}_6$ .



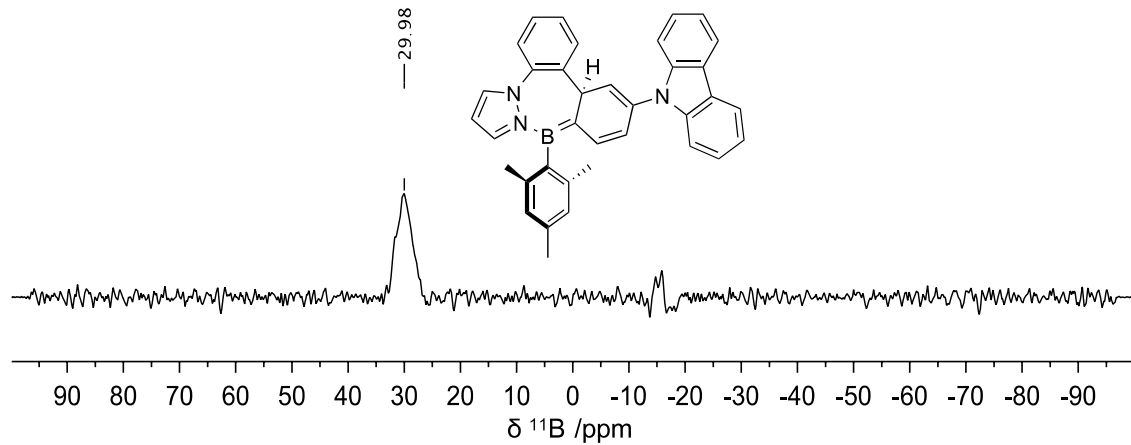
**Figure S61.**  $^1\text{H}$ - $^1\text{H}$  COSY NMR spectrum of **4a** in  $\text{C}_6\text{D}_6$  with diagnostic correlations.



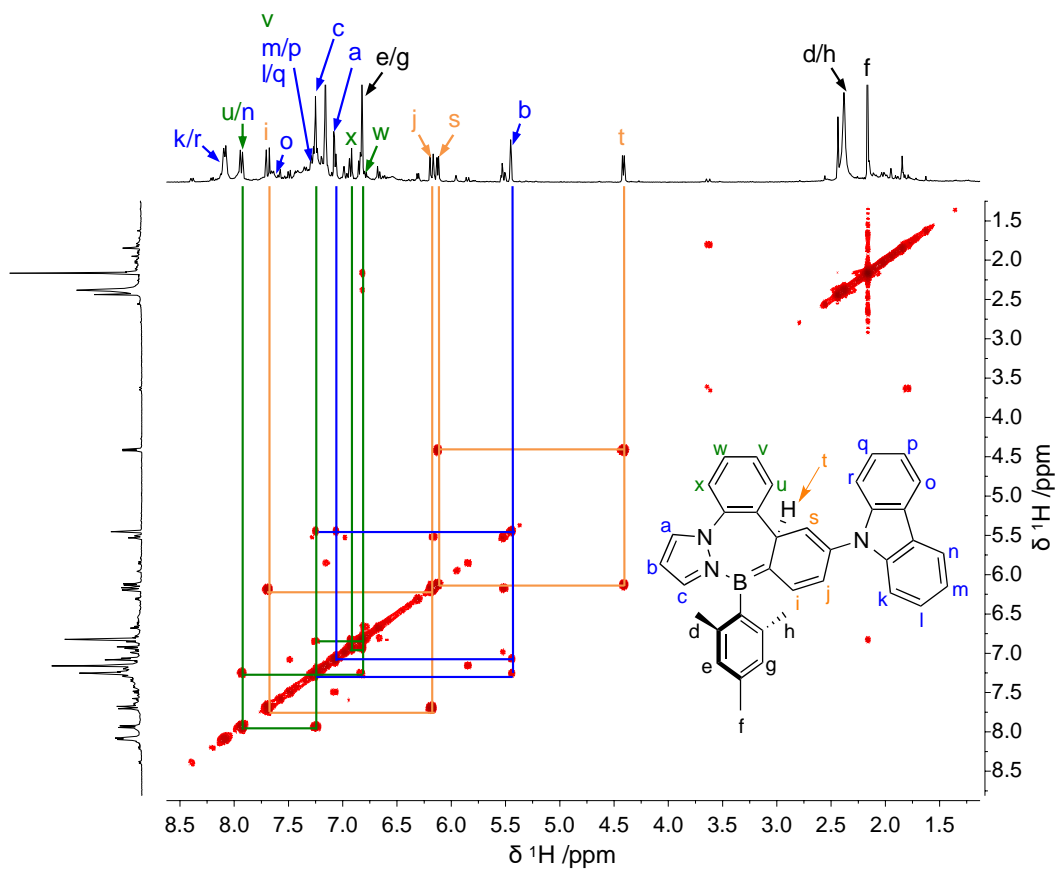
**Figure S62.**  $^1\text{H}$  NMR spectrum of **4b** in  $\text{C}_6\text{D}_6$ . \*Unknown impurities.



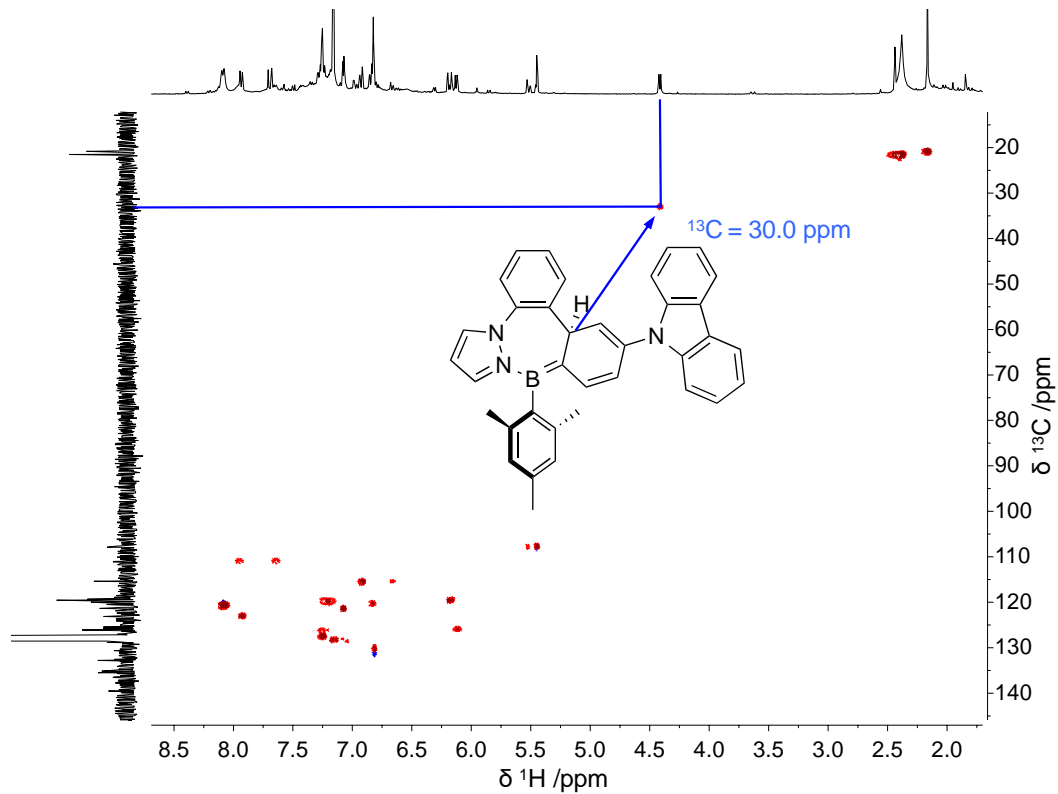
**Figure S63.**  $^{13}\text{C}$  NMR spectrum of **4b** in  $\text{C}_6\text{D}_6$ .



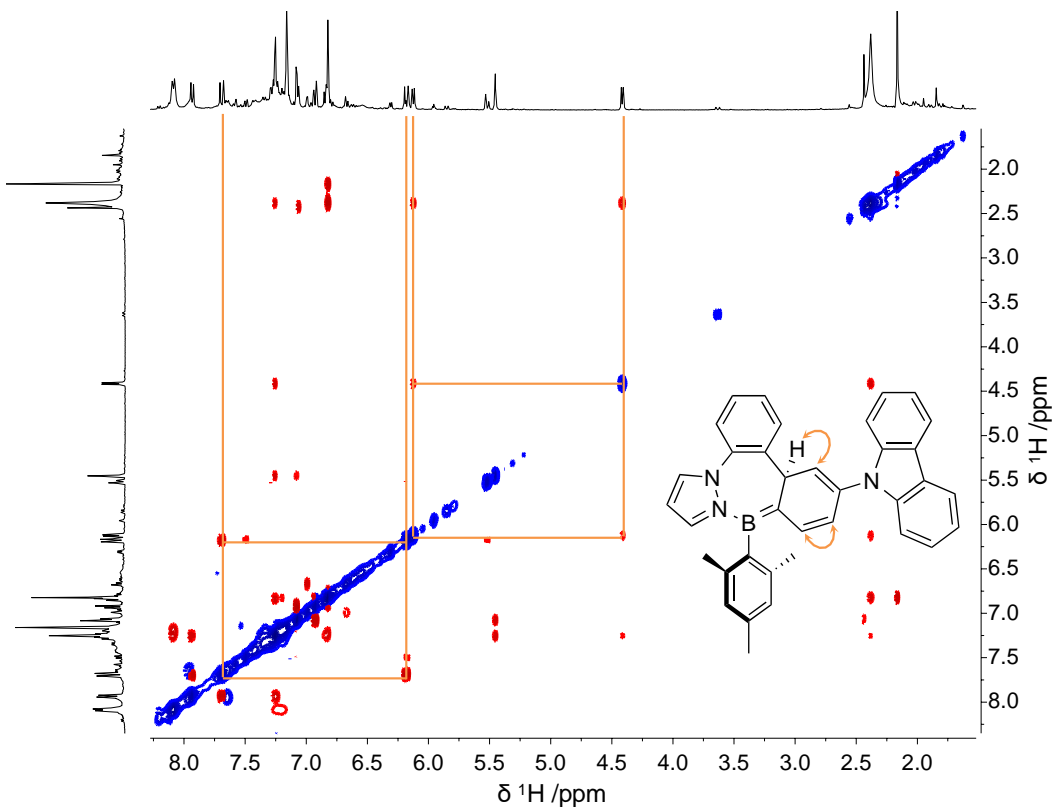
**Figure S64.**  $^{11}\text{B}$  NMR spectrum of **4b** in  $\text{C}_6\text{D}_6$ .



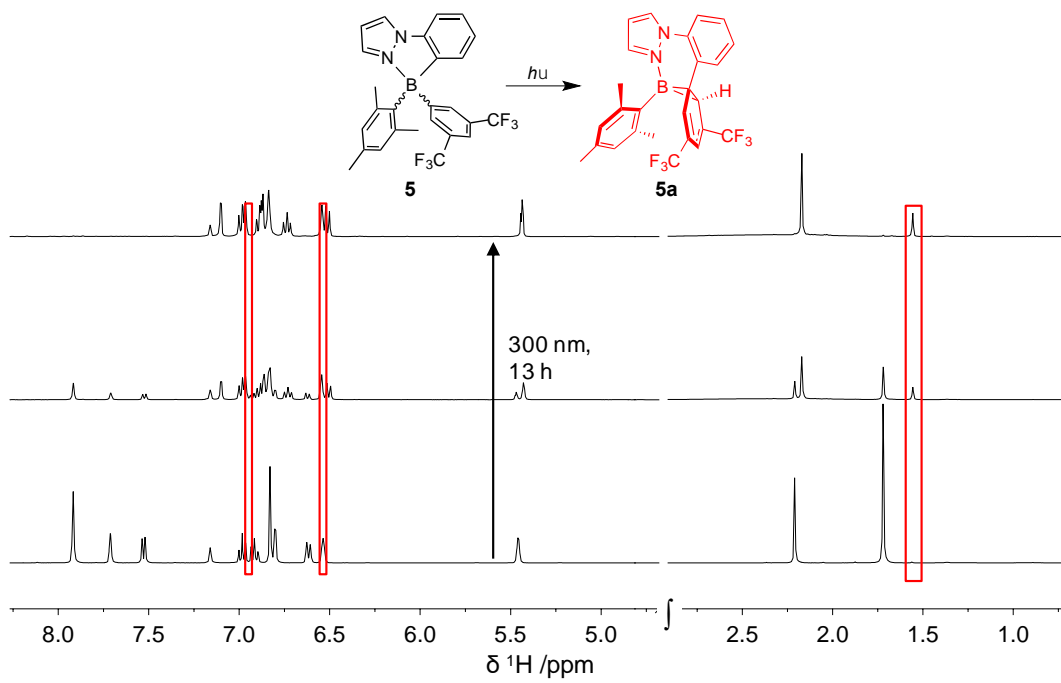
**Figure S65.**  $^1\text{H}$ - $^1\text{H}$  COSY NMR spectrum of **4b** in  $\text{C}_6\text{D}_6$  with diagnostic correlations.



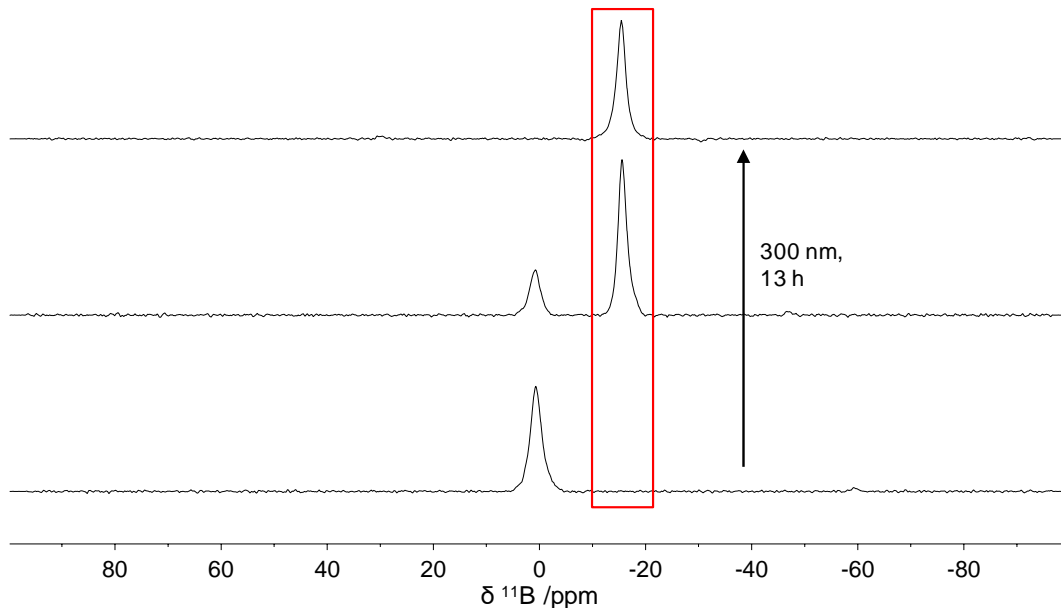
**Figure S66.**  $^1\text{H}$ - $^{13}\text{C}$  HSQC NMR spectrum of **4b** in  $\text{C}_6\text{D}_6$ .



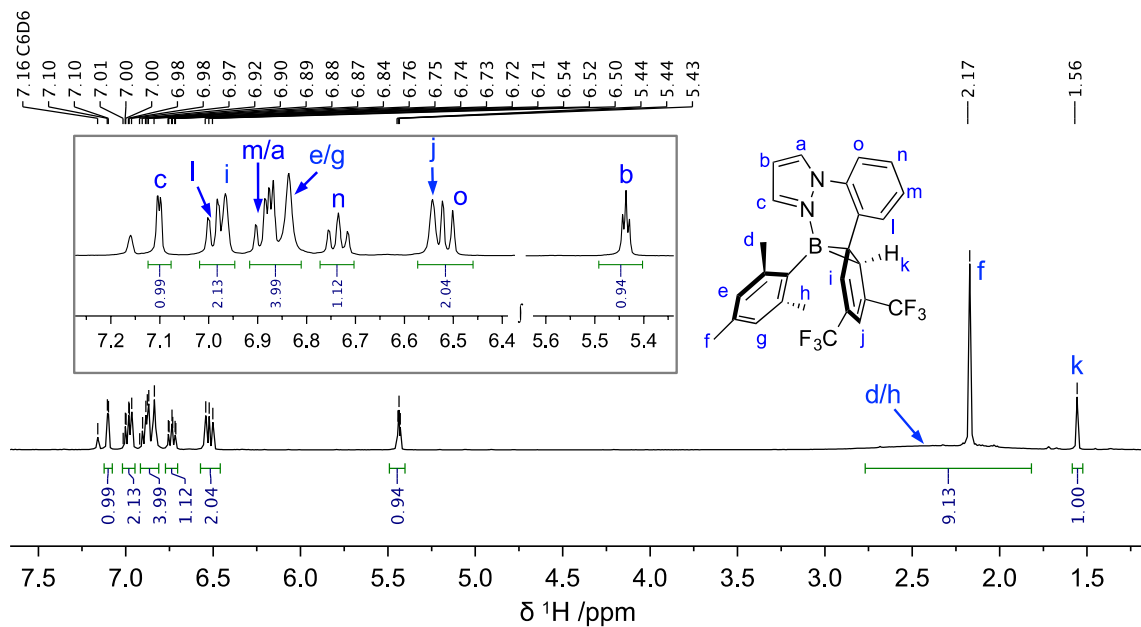
**Figure S67.**  $^1\text{H}$ - $^1\text{H}$  NOESY NMR spectrum of **4b** + **4b'** in  $\text{C}_6\text{D}_6$  with diagnostic correlations.



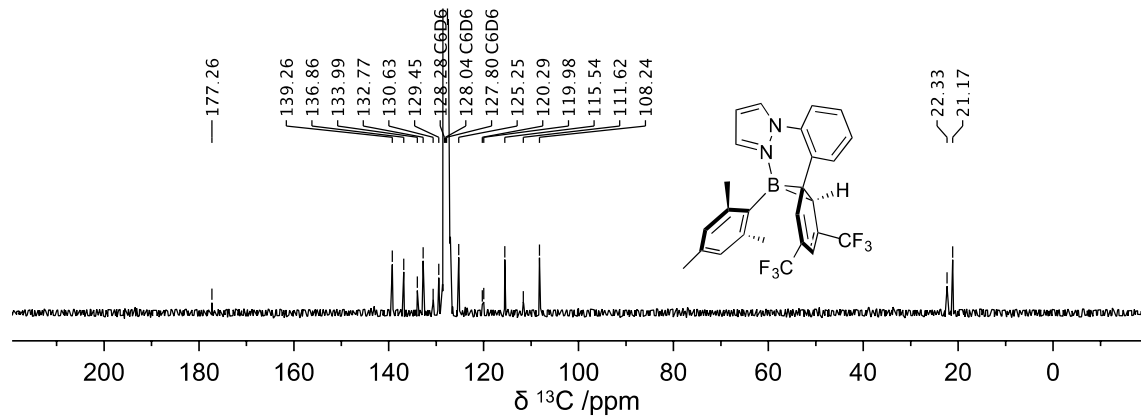
**Figure S68.** Stacked  $^1\text{H}$ -NMR spectra showing the conversion of **5**  $\rightarrow$  **5** + **5a**  $\rightarrow$  **5a** under  $\text{N}_2$  in  $\text{C}_6\text{D}_6$  (300 nm irradiation) with diagnostic chemical shifts highlighted in red (**5a**).



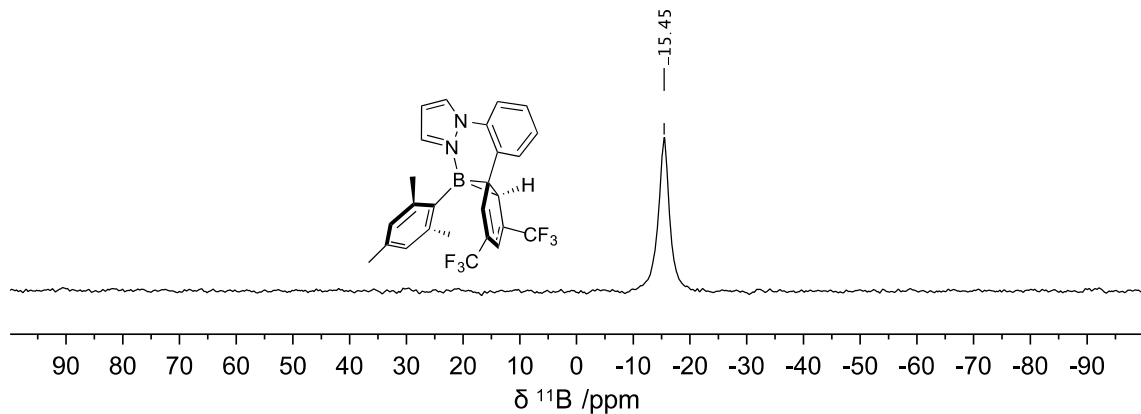
**Figure S69.** Stacked  $^{11}\text{B}$ -NMR spectra showing the conversion of **5**  $\rightarrow$  **5** + **5a**  $\rightarrow$  **5a** under  $\text{N}_2$  in  $\text{C}_6\text{D}_6$  (300 nm irradiation) with diagnostic chemical shifts highlighted in red (**5a**).



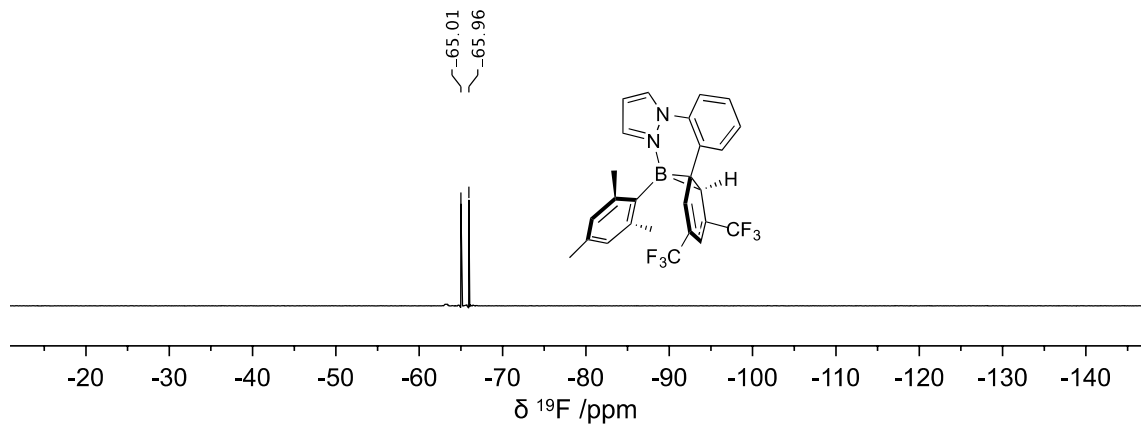
**Figure S70.**  $^1\text{H}$  NMR spectrum of **5a** in  $\text{C}_6\text{D}_6$ .



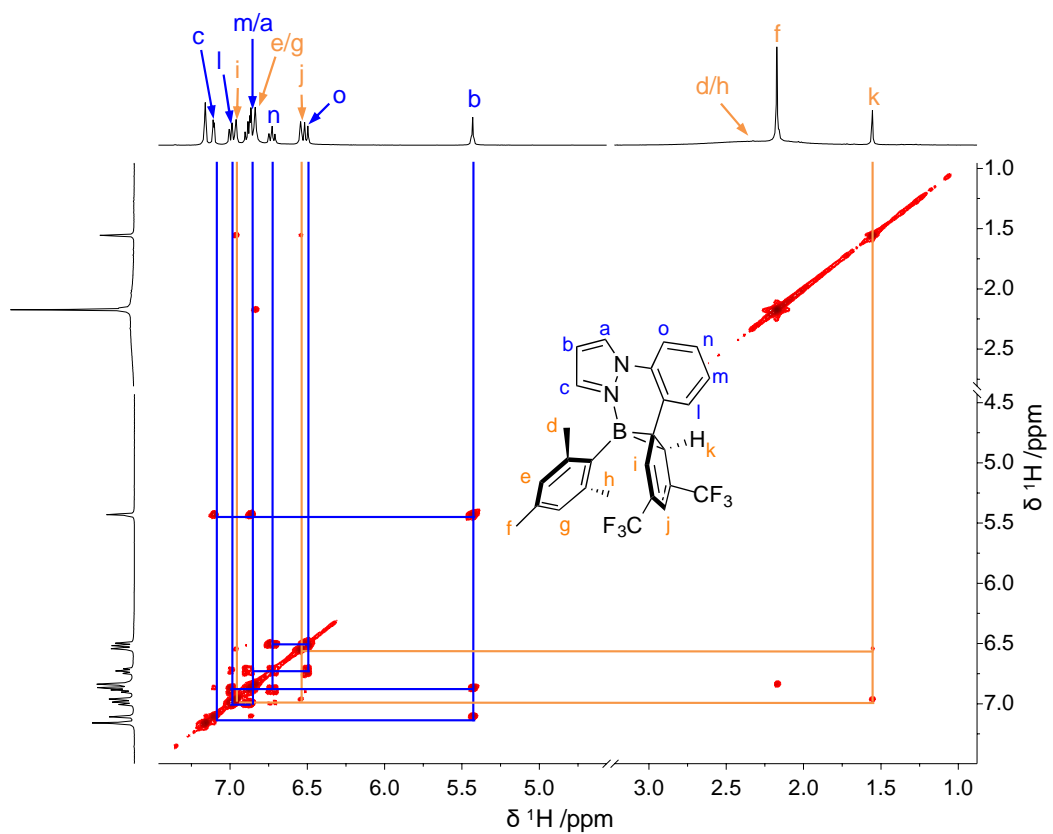
**Figure S71.**  $^{13}\text{C}$  NMR spectrum of **5a** in  $\text{C}_6\text{D}_6$ .



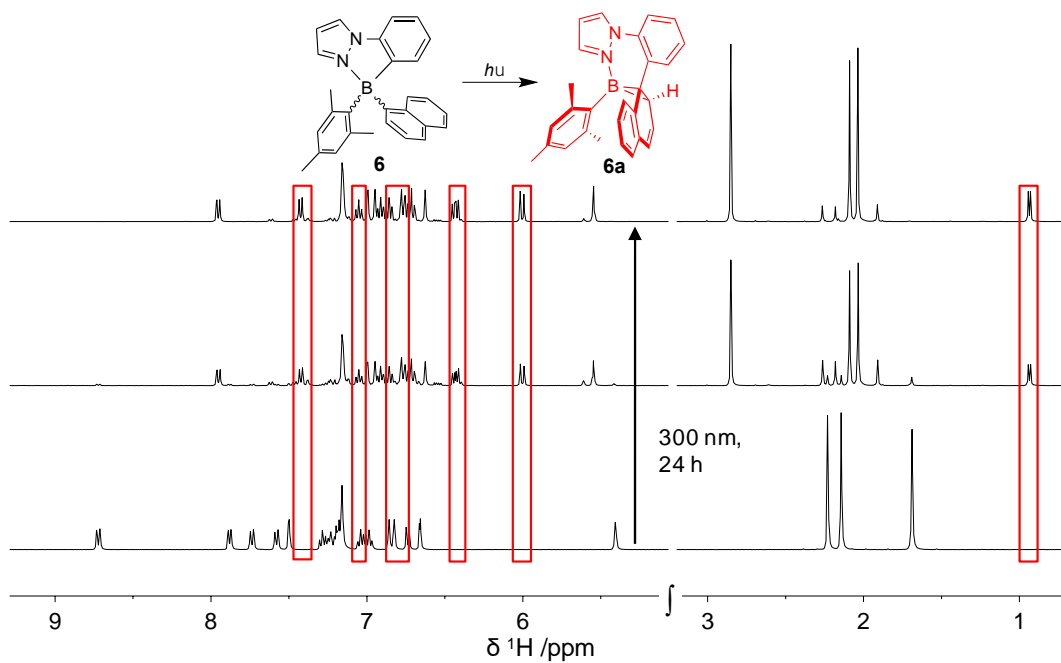
**Figure S72.**  $^{11}\text{B}$  NMR spectrum of **5a** in  $\text{C}_6\text{D}_6$ .



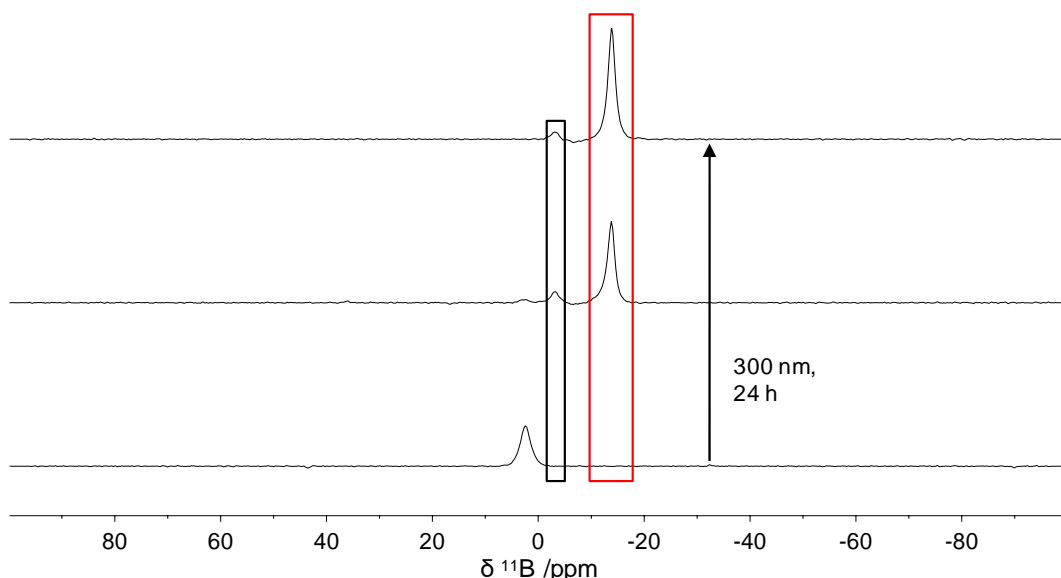
**Figure S73.**  ${}^{19}\text{F}$  NMR spectrum of **5a** in  $\text{C}_6\text{D}_6$ .



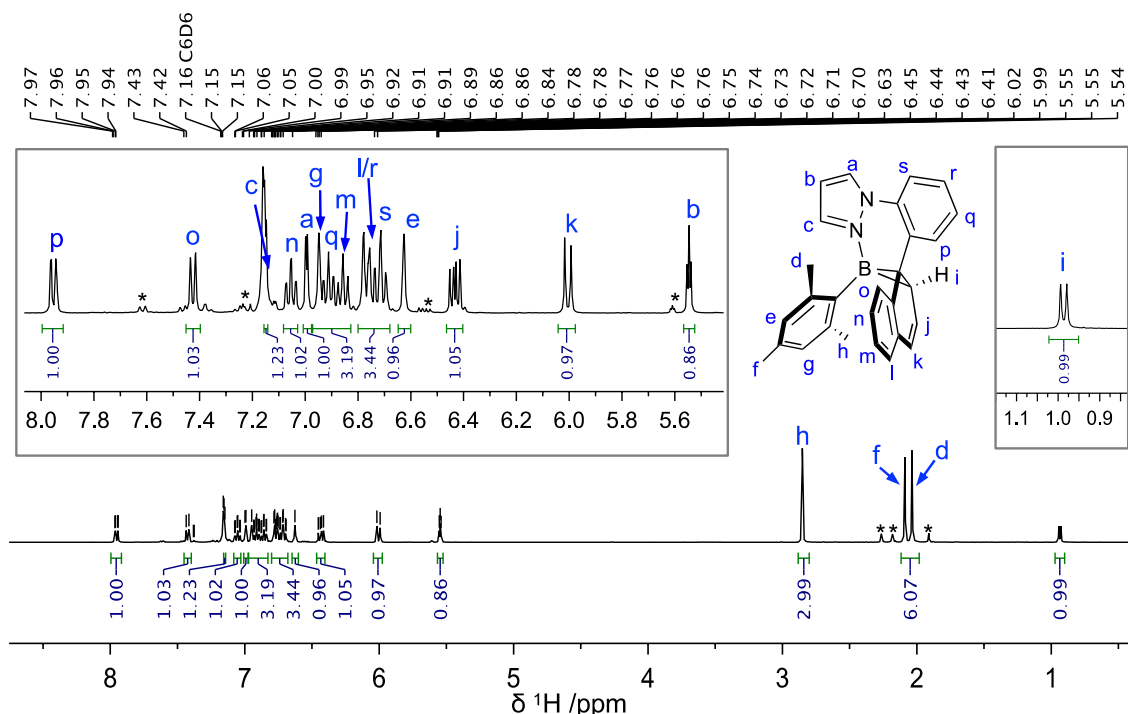
**Figure S74.**  ${}^1\text{H}$ - ${}^1\text{H}$  COSY NMR spectrum of **5a** in  $\text{C}_6\text{D}_6$  with diagnostic correlations.



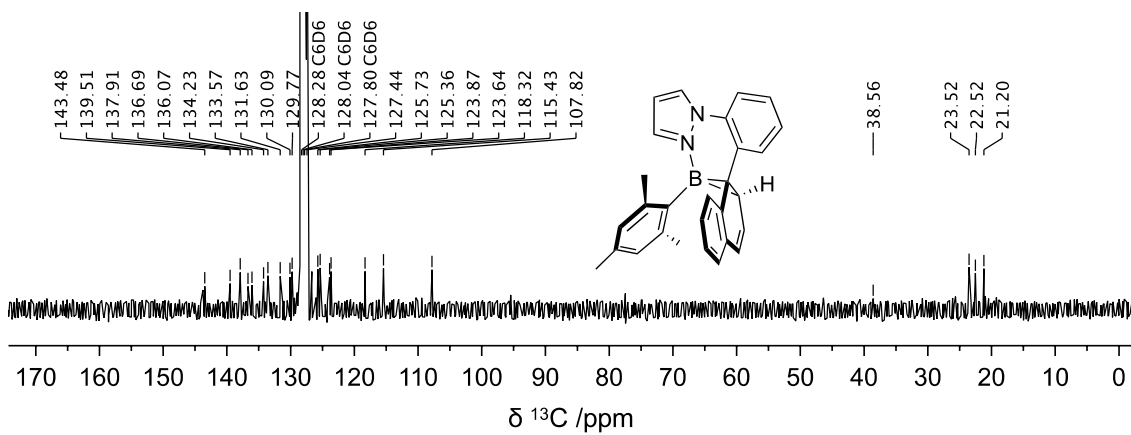
**Figure S75.** Stacked <sup>1</sup>H-NMR spectra showing the conversion of **6** → **6** + **6a** → **6a** under N<sub>2</sub> in C<sub>6</sub>D<sub>6</sub> (300 nm irradiation) with diagnostic chemical shifts highlighted in red (**6a**).



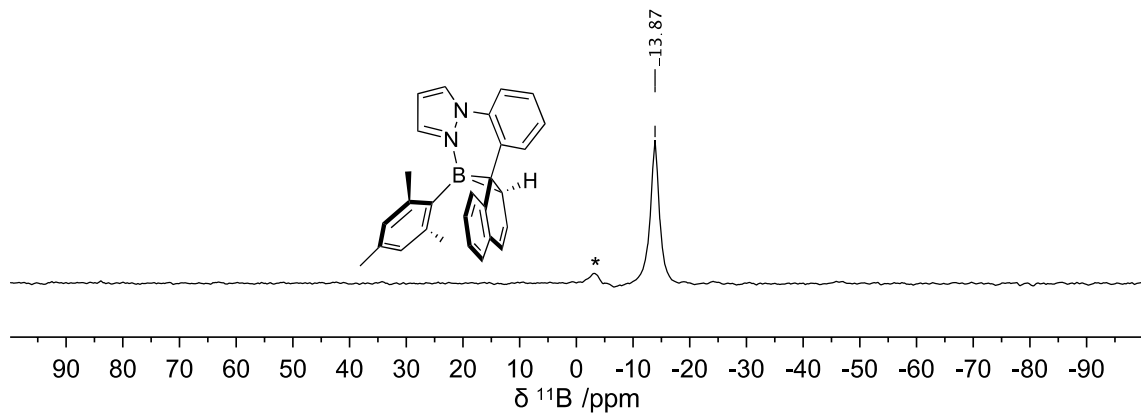
**Figure S76.** Stacked <sup>11</sup>B-NMR spectra showing the conversion of **6** → **6** + **6a** → **6a** under N<sub>2</sub> in C<sub>6</sub>D<sub>6</sub> (300 nm irradiation) with diagnostic chemical shifts highlighted in red (**6a**) or black (unknown impurity).



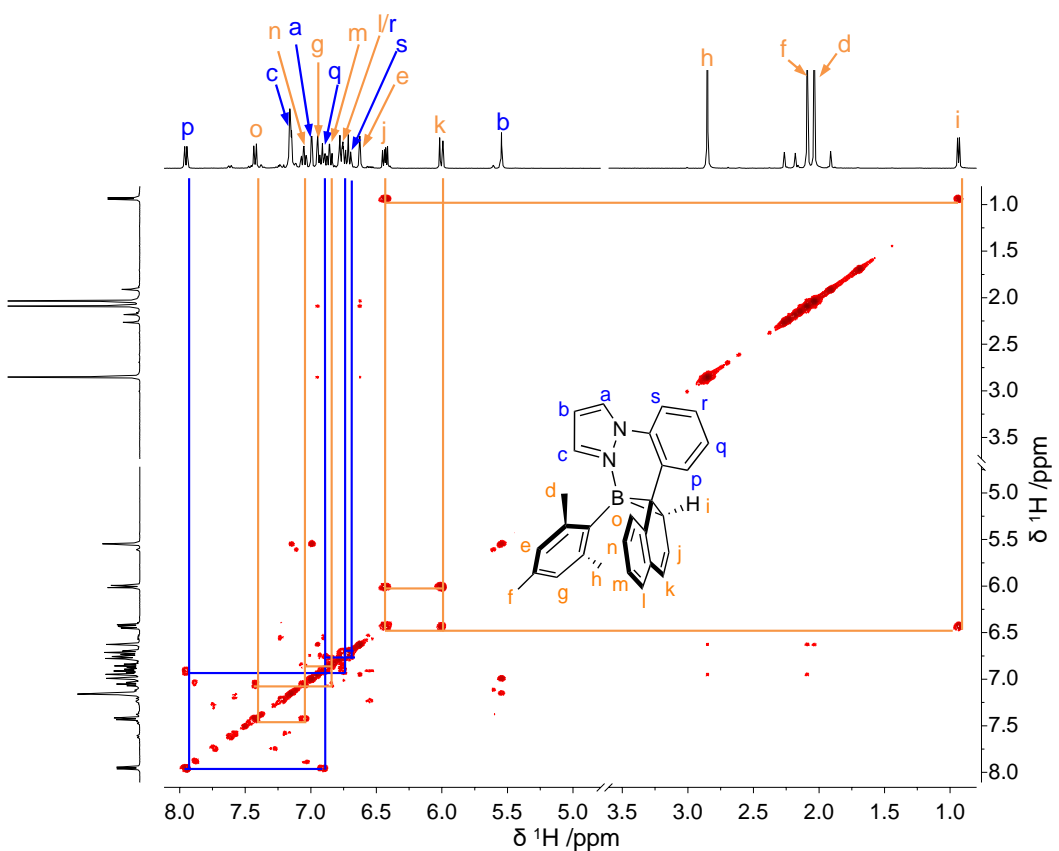
**Figure S77.**  $^1\text{H}$  NMR spectrum of **6a** in  $\text{C}_6\text{D}_6$ . \*Unknown impurities.



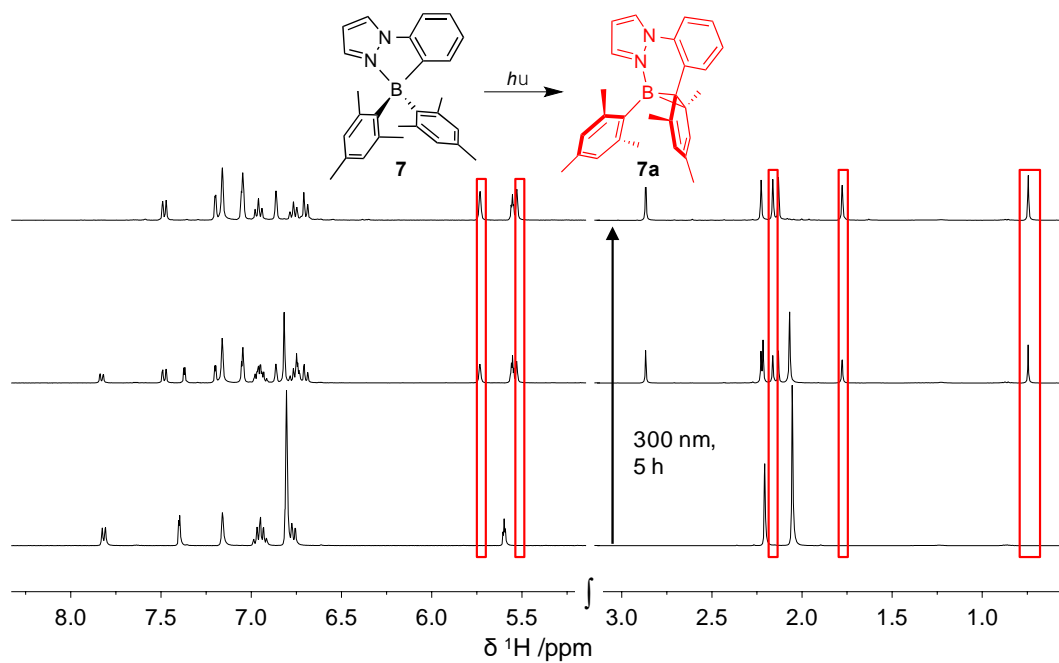
**Figure S78.**  $^{13}\text{C}$  NMR spectrum of **6a** in  $\text{C}_6\text{D}_6$ .



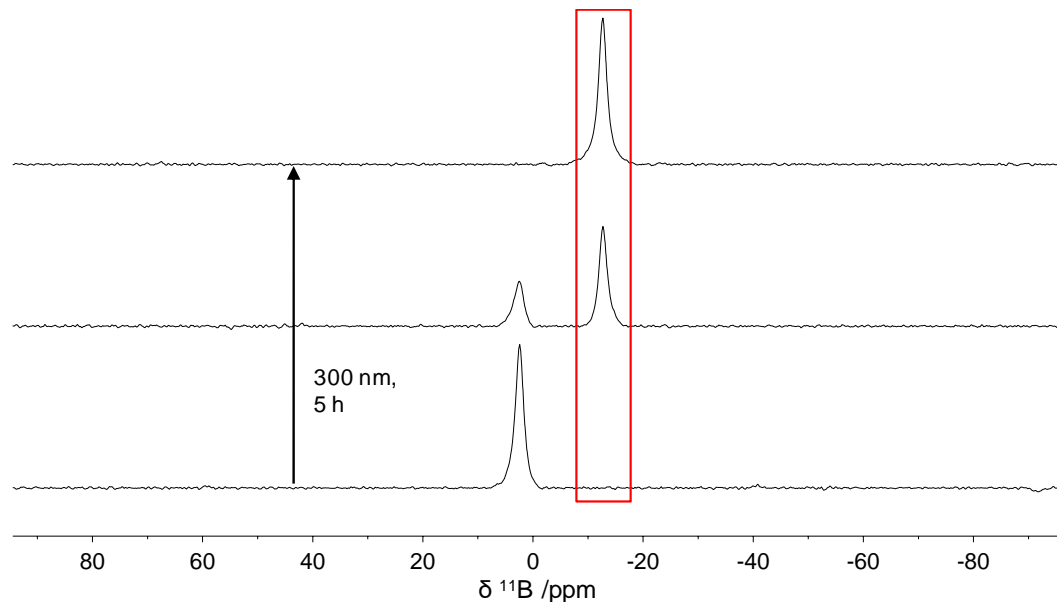
**Figure S79.**  $^{11}\text{B}$  NMR spectrum of **6a** in  $\text{C}_6\text{D}_6$ . \*Unknown impurity.



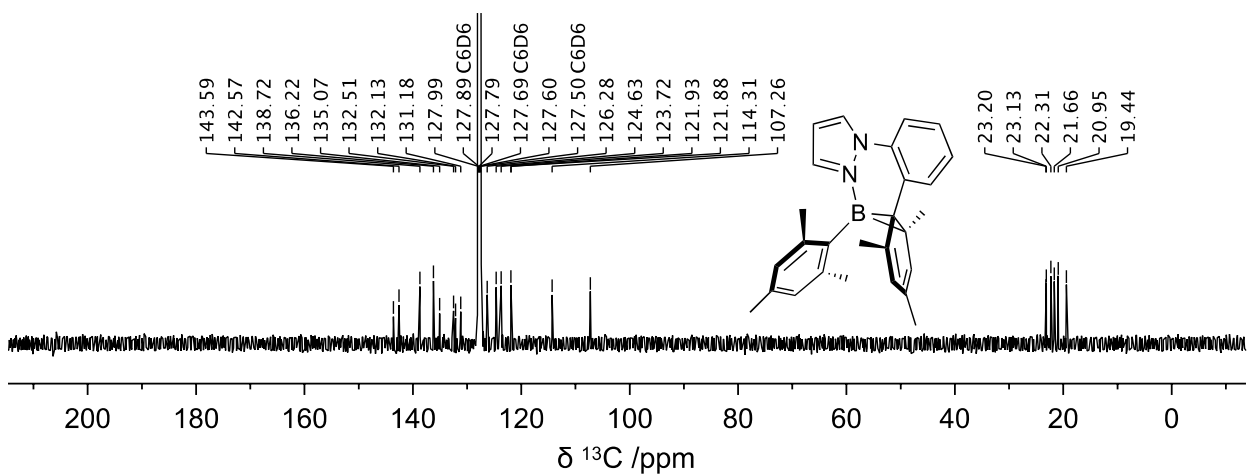
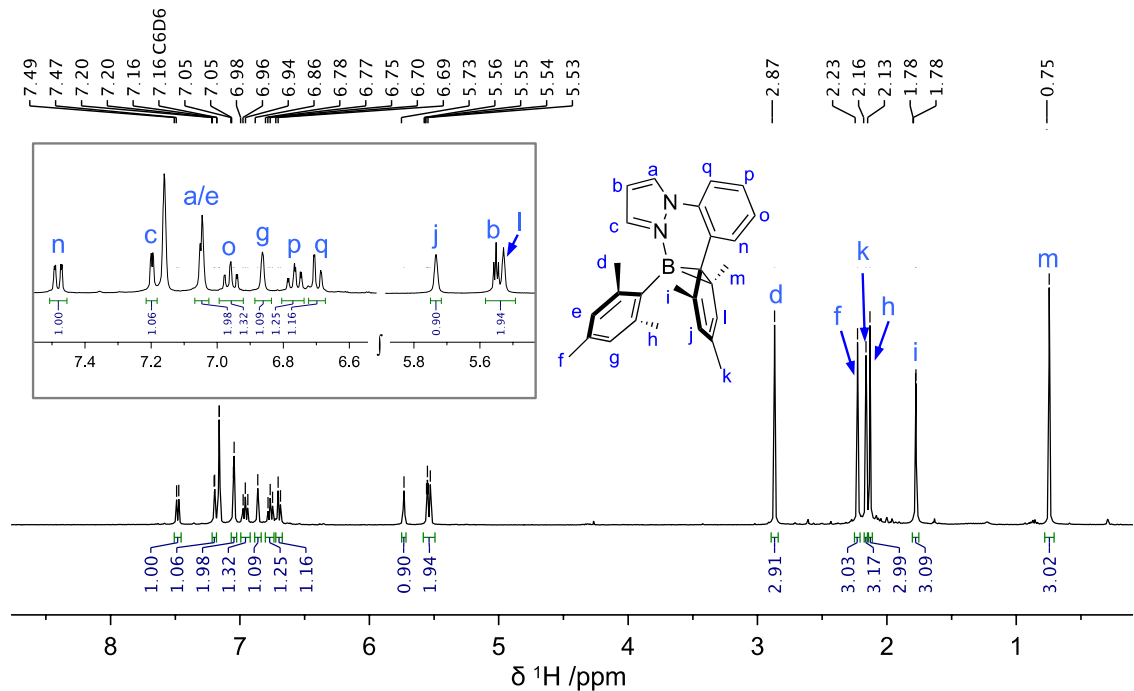
**Figure S80.**  $^1\text{H}$ - $^1\text{H}$  COSY NMR spectrum of **6a** in  $\text{C}_6\text{D}_6$  with diagnostic correlations.



**Figure S81.** Stacked <sup>1</sup>H-NMR spectra showing the conversion of **7** → **7** + **7a** → **7a** under N<sub>2</sub> in C<sub>6</sub>D<sub>6</sub> (300 nm irradiation) with diagnostic chemical shifts highlighted in red (**7a**).



**Figure S82.** Stacked <sup>11</sup>B-NMR spectra showing the conversion of **7** → **7** + **7a** → **7a** under N<sub>2</sub> in C<sub>6</sub>D<sub>6</sub> (300 nm irradiation) with diagnostic chemical shifts highlighted in red (**7a**).



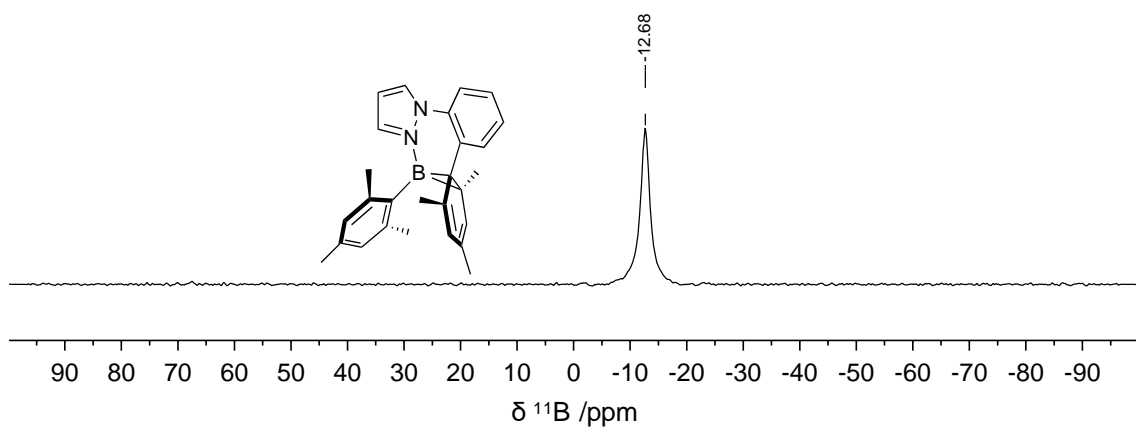


**Figure S85.**  $^{11}\text{B}$  NMR spectrum of **7a** in  $\text{C}_6\text{D}_6$ .

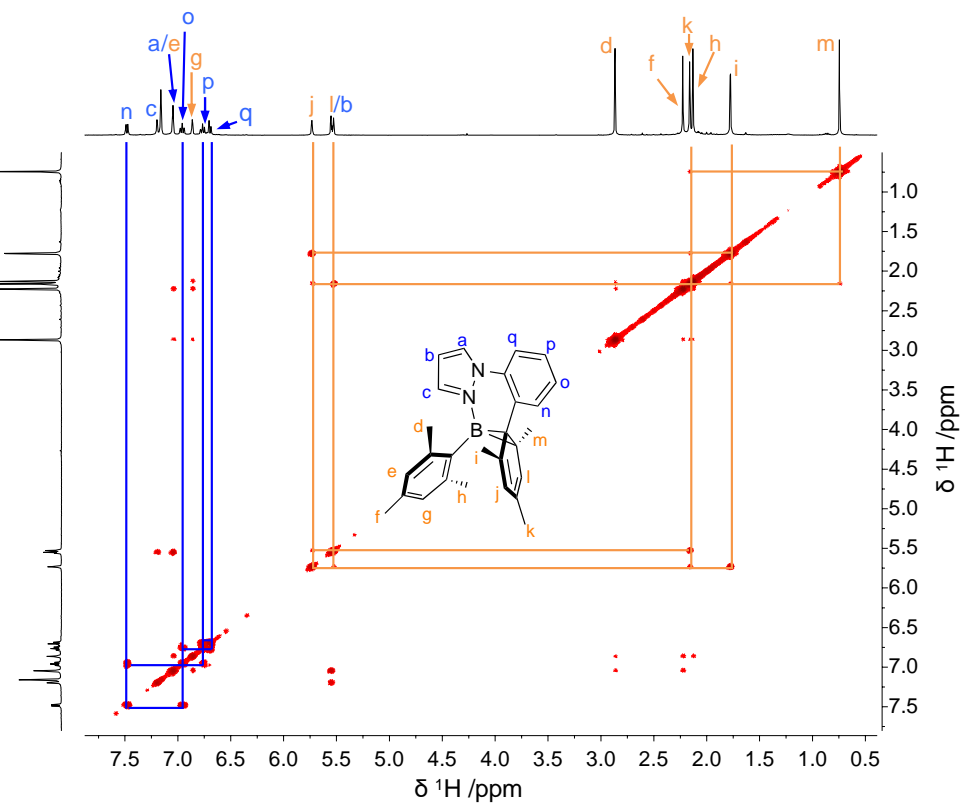


**Figure S86.**  $^1\text{H}$ - $^1\text{H}$  COSY NMR spectrum of **7a** in  $\text{C}_6\text{D}_6$  with diagnostic correlations.

#### S4: Photophysical Properties of **1 – 7**

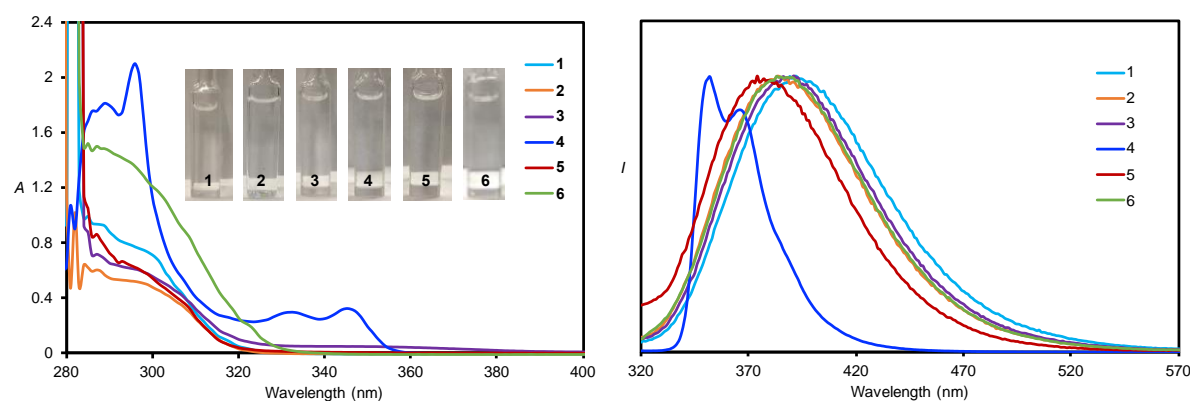


**Figure S87.** UV-Vis (left) and fluorescence (right) spectra of **1 – 6** in toluene at  $10^{-4}$  M. Inset: Photographs showing the colors of **1 – 6**.

**Table S1.** Summary of pertinent photophysical data for **1 – 7**.

	<b>1</b>	<b>2</b>	<b>3</b>	<b>4</b>	<b>5</b>	<b>6</b>	<b>7</b>
$\lambda_{\text{abs}}$ (nm)	300	292	296	296, 333, 347	294	297	305
$\lambda_{\text{em}}$ (nm)	392	384	391	352, 368	374	383	398
$\epsilon$ ( $M^{-1} \text{ cm}^{-1}$ )	7108	5108	6100	20946	6526	13257	3223
$\Phi_{\text{fl}}$	0.19	0.11	0.08	0.33	0.10	0.12	0.12

#### S5: UV/Vis Photoisomerization Data of **1 – 7**

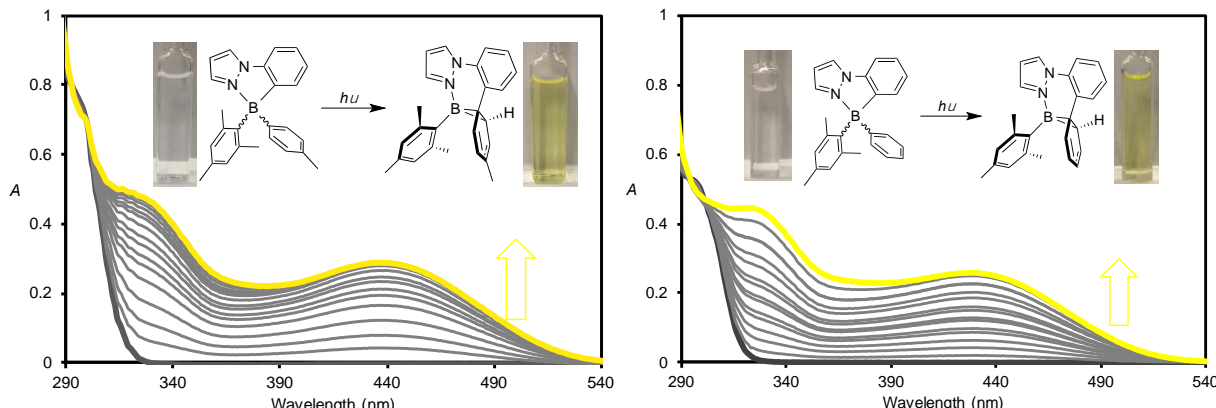


**Figure S88.** Stacked UV-Vis spectra showing the conversion of **1 → 1a** (left) and **2 → 2a** (right) in toluene at  $10^{-4}$  M with 300 nm irradiation. Inset: Photographs showing the solution colors.

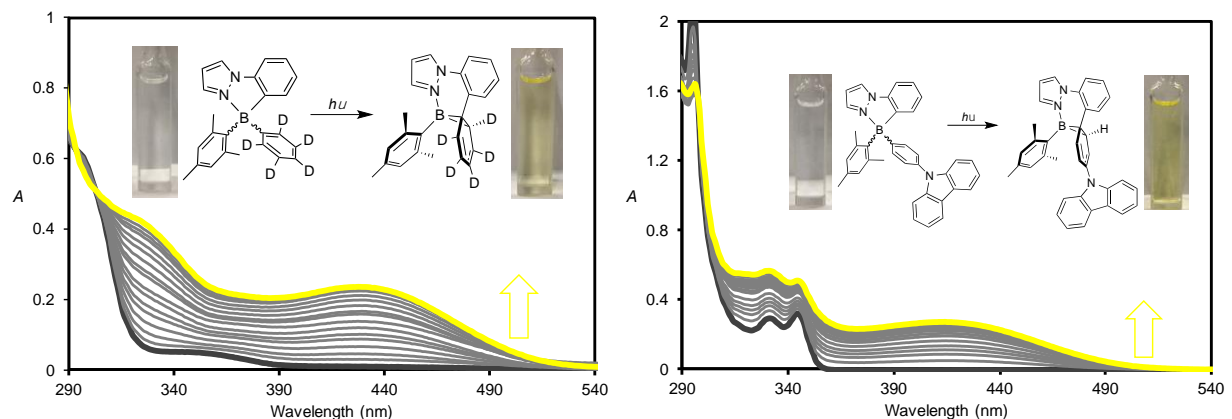


**Figure S89.** Stacked UV-Vis spectra showing the conversion of **3** → **3a** (left) and **4** → **4a** (right) in toluene at  $10^{-4}$  M with 300 nm irradiation. Inset: Photographs showing the solution colors.

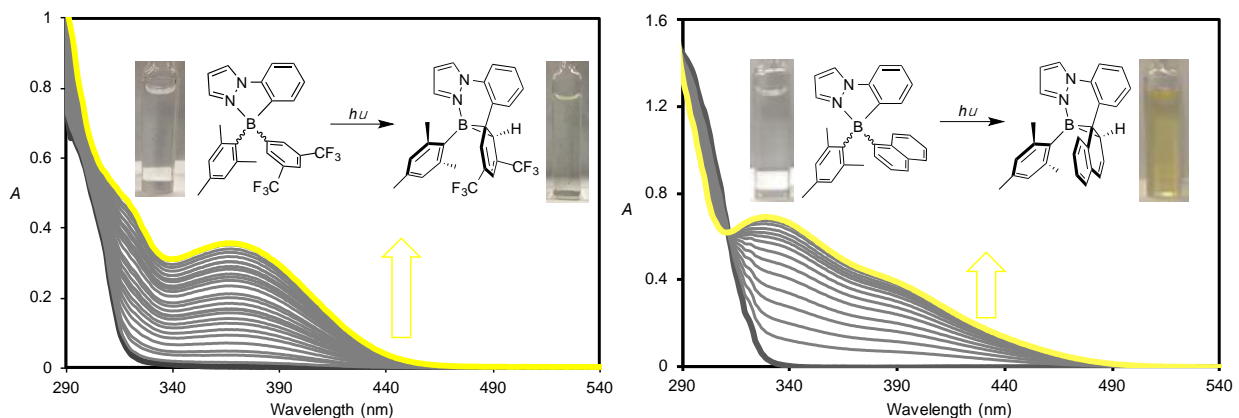


**Figure S90.** Stacked UV-Vis spectra showing the conversion of **5** → **5a** (left) and **6** → **6a** (right) in toluene at  $10^{-4}$  M with 300 nm irradiation. Inset: Photographs showing the solution colors.

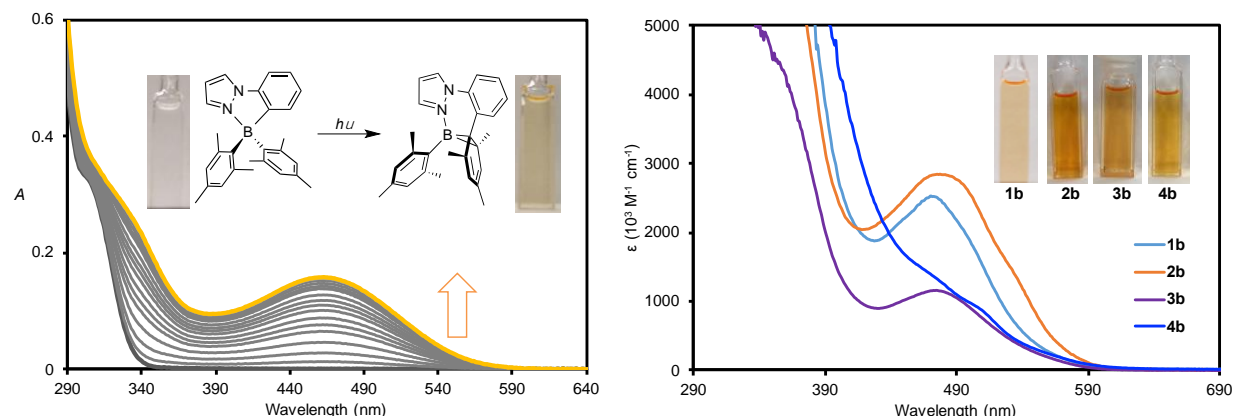


**Figure S91.** Stacked UV-Vis spectra showing the conversion of **7** → **7a** (left) in toluene at  $10^{-4}$  M and UV-Vis spectra of **1b** – **4b** (right). Inset: Photographs showing the solution colors.

**$\Phi_{PI}$  Determination:** In a N<sub>2</sub> filled glovebox, quartz cuvettes were filled with 3.5 mL of 10<sup>-5</sup> M solutions of **5** and **7** in toluene, sealed with a rubber septum, and wrapped with parafilm/Teflon tape. The samples were removed from the glovebox, irradiated with monochromatic 350 nm light, and their UV/Vis spectral absorption change was monitored over time. The rates of formation of **5a** and **7a** were then used to calculate the photoisomerization quantum yield ( $\Phi_{PI}$ ) of **5** and **7** using ppyBMes<sub>2</sub> ( $\Phi_{PI} = 0.88$ ) as a chemical actinometer.<sup>[6]</sup>

**Table S2.** Summary of photophysical data for **1a – 7a** and **1b – 4b**.

	<b>1</b>	<b>2</b>	<b>3</b>	<b>4</b>	<b>5</b>	<b>6</b>	<b>7</b>
“ <b>a</b> ” $\lambda_{abs}$ (nm)	439	435	433	417	373	400	465
$\Phi_{PI}$	-	-	-	-	0.55	-	0.31
“ <b>b</b> ” $\lambda_{abs}$ (nm)	476	485	484	476, 507	-	-	-

**S6. TD-DFT Calculation Data of 1 – 6**

**Table S3.** TD-DFT calculated electronic transitions for **1** along with their corresponding excitation energies and oscillator strengths.

Compound	Spin State	Transition Configuration	Excitation Energy (nm, eV)	Oscillator Strength
<b>1</b>	S <sub>1</sub>	HOMO-4 → LUMO (16%)	267.72 (4.91)	0.0981
		HOMO-1 → LUMO (13%)		
		HOMO → LUMO (60%)		
	S <sub>2</sub>	HOMO-4 → LUMO (13%)	252.40 (5.13)	0.0395
		HOMO-1 → LUMO (47%)		
		HOMO → LUMO (30%)		
	S <sub>3</sub>	HOMO-4 → LUMO (45%)	241.88 (5.17)	0.0673
		HOMO-1 → LUMO (23%)		
		HOMO-2 → LUMO (3%)		
		HOMO-1 → LUMO+1 (3%)		
		HOMO-1 → LUMO+4 (3%)		
		HOMO → LUMO (3%)		
	S <sub>4</sub>	HOMO → LUMO+1 (3%)		
		HOMO-5 → LUMO (10%)	239.96 (5.21)	0.0351
		HOMO-2 → LUMO (26%)		
		HOMO-1 → LUMO (10%)		
		HOMO-4 → LUMO (9%)		
		HOMO-4 → LUMO+1 (3%)		
		HOMO-3 → LUMO (2%)		
		HOMO-2 → LUMO+1 (2%)		
		HOMO-2 → LUMO+2 (7%)		
		HOMO-2 → LUMO+3 (5%)		
		HOMO-1 → LUMO+4		

		(6%)		
		HOMO → LUMO+1 (6%)		
		HOMO → LUMO+3 (2%)		
<b>S<sub>5</sub></b>		HOMO-5 → LUMO (20%)	238.07 (5.21)	0.0170
		HOMO-2 → LUMO+2 (18%)		
		HOMO-2 → LUMO+3 (9%)		
		HOMO-1 → LUMO+4 (5%)		
		HOMO-4 → LUMO+1 (4%)		
		HOMO-3 → LUMO (9%)		
		HOMO-3 → LUMO+1 (2%)		
		HOMO-1 → LUMO+1 (8%)		
		HOMO → LUMO+1 (2%)		
		HOMO → LUMO+2 (4%)		
		HOMO → LUMO+4 (3%)		

**Table S4.** TD-DFT calculated electronic transitions for **1a** along with their corresponding excitation energies and oscillator strengths.

Compound	Spin State	Transition Configuration	Excitation Energy (nm, eV)	Oscillator Strength
<b>1a</b>	S <sub>1</sub>	HOMO → LUMO (96%)	383.39 (3.23)	0.0933
	S <sub>2</sub>	HOMO → LUMO+1 (72%)	318.37 (3.89)	0.0180
		HOMO → LUMO+2 (12%)		
		HOMO → LUMO+3 (5%)		
		HOMO → LUMO+4 (6%)		
	S <sub>3</sub>	HOMO-3 → LUMO (28%)	290.67 (4.27)	0.0653
		HOMO-1 → LUMO (61%)		
		HOMO-4 → LUMO+1 (2%)		

		HOMO → LUMO+1 (3%)		
S <sub>4</sub>		HOMO → LUMO+1 (21%)	274.72 (4.51)	0.0159
		HOMO → LUMO+2 (39%)		
		HOMO → LUMO+3 (12%)		
		HOMO → LUMO+4 (21%)		
		HOMO-3 → LUMO (21%)		
S <sub>5</sub>		HOMO-1 → LUMO (19%)	253.65 (4.89)	0.0100
		HOMO → LUMO+2 (18%)		
		HOMO → LUMO+3 (30%)		
		HOMO-1 → LUMO+2 (2%)		
		HOMO → LUMO+4 (2%)		

**Table S5.** TD-DFT calculated electronic transitions for **1b** along with their corresponding excitation energies and oscillator strengths.

Compound	Spin State	Transition Configuration	Excitation Energy (nm, eV)	Oscillator Strength
<b>1b</b>	S <sub>1</sub>	HOMO → LUMO (97%)	491.45 (2.52)	0.1450
	S <sub>2</sub>	HOMO → LUMO+1 (84%)	358.53 (3.46)	0.1104
		HOMO → LUMO+2 (4%)		
		HOMO → LUMO+3 (7%)		
		HOMO → LUMO+5 (3%)		
	S <sub>3</sub>	HOMO → LUMO+2 (82%)	347.88 (3.56)	0.0246
		HOMO → LUMO+1 (8%)		
		HOMO → LUMO+3 (7%)		
	S <sub>4</sub>	HOMO → LUMO+2 (11%)	323.74 (3.83)	0.1074
		HOMO → LUMO+3 (77%)		
		HOMO → LUMO+1 (5%)		
		HOMO → LUMO+5 (2%)		
	S <sub>5</sub>	HOMO → LUMO+5 (80%)	278.09 (4.46)	0.0009
		HOMO → LUMO+3 (6%)		
		HOMO → LUMO+6 (7%)		

**Table S6.** TD-DFT calculated electronic transitions for **2** along with their corresponding excitation energies and oscillator strengths.

Compound	Spin State	Transition Configuration	Excitation Energy (nm, eV)	Oscillator Strength
<b>2</b>	S <sub>1</sub>	HOMO-4 → LUMO (16%)	263.91 (4.70)	0.1156
		HOMO-2 → LUMO (56%)		
		HOMO-5 → LUMO+1 (2%)		
		HOMO-3 → LUMO (6%)		
		HOMO-1 → LUMO (4%)		
		HOMO → LUMO (8%)		
	S <sub>2</sub>	HOMO → LUMO (83%)	251.84 (4.92)	0.0263
		HOMO-4 → LUMO (4%)		
		HOMO-2 → LUMO (5%)		
	S <sub>3</sub>	HOMO-1 → LUMO (35%)	240.03 (5.17)	0.0108
		HOMO-1 → LUMO+2 (12%)		
		HOMO-5 → LUMO (7%)		
		HOMO-2 → LUMO+1 (4%)		
		HOMO-1 → LUMO+3 (6%)		
		HOMO-1 → LUMO+5 (2%)		
		HOMO → LUMO (2%)		
		HOMO → LUMO+4 (4%)		
		HOMO → LUMO+5 (7%)		
	S <sub>4</sub>	HOMO-4 → LUMO (44%)	238.43 (5.20)	0.0913
		HOMO-2 → LUMO (15%)		
		HOMO-5 → LUMO (6%)		
		HOMO-3 → LUMO (8%)		
		HOMO-1 → LUMO (3%)		

		HOMO-1 → LUMO+2 (3%)		
		HOMO → LUMO+4 (2%)		
		HOMO → LUMO+5 (3%)		
S <sub>5</sub>		HOMO-5 → LUMO (20%)	236.98 (5.23)	0.0137
		HOMO-2 → LUMO+1 (18%)		
		HOMO-4 → LUMO (9%)		
		HOMO-4 → LUMO (5%)		
		HOMO-3 → LUMO (4%)		
		HOMO-2 → LUMO (9%)		
		HOMO-2 → LUMO (2%)		
		HOMO-1 → LUMO (8%)		
		HOMO-1 → LUMO (2%)		
		HOMO → LUMO (4%)		
		HOMO → LUMO (3%)		

**Table S7.** TD-DFT calculated electronic transitions for **2a** along with their corresponding excitation energies and oscillator strengths.

Compound	Spin State	Transition Configuration	Excitation Energy (nm, eV)	Oscillator Strength
2a	S <sub>1</sub>	HOMO → LUMO (96%)	378.46 (3.28)	0.0863
	S <sub>2</sub>	HOMO → LUMO+1 (73%)	319.73 (3.88)	0.0225
		HOMO → LUMO+2 (15%)		
		HOMO → LUMO+3 (6%)		
		HOMO → LUMO+4 (2%)		
	S <sub>3</sub>	HOMO-3 → LUMO (35%)	288.43 (4.30)	0.0649
		HOMO-1 → LUMO (54%)		
		HOMO-4 → LUMO+1 (2%)		
		HOMO → LUMO+1 (3%)		
	S <sub>4</sub>	HOMO → LUMO+1 (20%)	273.10 (4.54)	0.0163
		HOMO → LUMO+2 (50%)		

		HOMO → LUMO+3 (14%)		
		HOMO → LUMO+4 (9%)		
S <sub>5</sub>		HOMO-3 → LUMO (38%)	253.66 (4.89)	0.0086
		HOMO-1 → LUMO (36%)		
		HOMO → LUMO+3 (11%)		
		HOMO-1 → LUMO+2 (2%)		
		HOMO → LUMO+2 (5%)		

**Table S8.** TD-DFT calculated electronic transitions for **2b** along with their corresponding excitation energies and oscillator strengths.

Compound	Spin State	Transition Configuration	Excitation Energy (nm, eV)	Oscillator Strength
2b	S <sub>1</sub>	HOMO → LUMO (97%)	494.79 (2.51)	0.1395
	S <sub>2</sub>	HOMO → LUMO+1 (80%)	363.78 (3.41)	0.1048
		HOMO → LUMO+2 (5%)		
		HOMO → LUMO+3 (9%)		
	S <sub>3</sub>	HOMO → LUMO+1 (11%)	349.20 (3.55)	0.0329
		HOMO → LUMO+2 (80%)		
		HOMO → LUMO+3 (6%)		
	S <sub>4</sub>	HOMO → LUMO+2 (11%)	326.06 (3.80)	0.0972
		HOMO → LUMO+3 (77%)		
		HOMO → LUMO+1 (6%)		
	S <sub>5</sub>	HOMO → LUMO+4 (52%)	279.53 (4.44)	0.0019
		HOMO → LUMO+5 (33%)		
		HOMO → LUMO+3 (5%)		
		HOMO → LUMO+6 (4%)		

**Table S9.** TD-DFT calculated electronic transitions for **4** along with their corresponding excitation energies and oscillator strengths.

Compound	Spin State	Transition Configuration	Excitation Energy (nm, eV)	Oscillator Strength
4	S <sub>1</sub>	HOMO → LUMO+1 (85%)	283.94 (4.37)	0.0657

		HOMO-1 → LUMO+6 (9%)		
S <sub>2</sub>		HOMO-4 → LUMO (46%)	267.31 (4.64)	0.1458
		HOMO → LUMO (38%)		
		HOMO-5 → LUMO (3%)		
		HOMO → LUMO+2 (3%)		
S <sub>3</sub>		HOMO-1 → LUMO+1 (75%)	256.33 (4.84)	0.1194
		HOMO → LUMO+6 (16%)		
		HOMO → LUMO+12 (2%)		
S <sub>4</sub>		HOMO-5 → LUMO (13%)	253.51 (4.89)	0.0522
		HOMO-2 → LUMO (55%)		
		HOMO → LUMO (10%)		
		HOMO-4 → LUMO (8%)		
		HOMO → LUMO+2 (2%)		
S <sub>5</sub>		HOMO-2 → LUMO (25%)	249.56 (4.97)	0.1315
		HOMO → LUMO+2 (25%)		
		HOMO-5 → LUMO (5%)		
		HOMO-4 → LUMO (5%)		
		HOMO-4 → LUMO+2 (6%)		
		HOMO → LUMO (4%)		
		HOMO → LUMO+4 (8%)		
		HOMO → LUMO+5 (7%)		

**Table S10.** TD-DFT calculated electronic transitions for **4a** along with their corresponding excitation energies and oscillator strengths.

Compound	Spin State	Transition Configuration	Excitation Energy (nm, eV)	Oscillator Strength
<b>4a</b>	S <sub>1</sub>	HOMO-1 → LUMO (12%)	365.33 (3.39)	0.1167
		HOMO → LUMO (84%)		
	S <sub>2</sub>	HOMO → LUMO+1 (65%)	322.03 (3.85)	0.0189
		HOMO → LUMO+3 (19%)		

		HOMO-1 → LUMO+1 (8%)		
		HOMO → LUMO+4 (2%)		
<b>S<sub>3</sub></b>		HOMO-5 → LUMO (25%)	284.48 (4.35(8))	0.0969
		HOMO-3 → LUMO (24%)		
		HOMO-1 → LUMO+2 (23%)		
		HOMO → LUMO+2 (12%)		
		HOMO-2 → LUMO+7 (3%)		
		HOMO-1 → LUMO (5%)		
<b>S<sub>4</sub></b>		HOMO-5 → LUMO (16%)	284.07 (4.36)	0.0349
		HOMO-3 → LUMO (16%)		
		HOMO-1 → LUMO+2 (35%)		
		HOMO → LUMO+2 (18%)		
		HOMO-2 → LUMO+7 (5%)		
		HOMO → LUMO (3%)		
<b>S<sub>5</sub></b>		HOMO → LUMO+1 (15%)	269.97 (4.59)	0.0158
		HOMO → LUMO+3 (59%)		
		HOMO-1 → LUMO+1 (9%)		
		HOMO-1 → LUMO+3 (4%)		
		HOMO → LUMO+4 (5%)		

**Table S11.** TD-DFT calculated electronic transitions for **4b** along with their corresponding excitation energies and oscillator strengths.

Compound	Spin State	Transition Configuration	Excitation Energy (nm, eV)	Oscillator Strength
<b>4b</b>	S <sub>1</sub>	HOMO → LUMO (96%)	483.27 (2.57)	0.2036
	S <sub>2</sub>	HOMO → LUMO+1 (80%)	362.35 (3.42)	0.1310
		HOMO → LUMO+3 (4%)		

		HOMO → LUMO+4 (9%)		
		HOMO → LUMO+5 (2%)		
S <sub>3</sub>		HOMO → LUMO+3 (84%)	338.86 (3.66)	0.0416
		HOMO → LUMO+1 (8%)		
		HOMO → LUMO+4 (4%)		
S <sub>4</sub>		HOMO → LUMO+4 (81%)	318.18 (3.90)	0.0750
		HOMO → LUMO+1 (7%)		
		HOMO → LUMO+3 (8%)		
S <sub>5</sub>		HOMO-1 → LUMO (75%)	292.44 (4.24)	0.0941
		HOMO-1 → LUMO+1 (8%)		
		HOMO-1 → LUMO+4 (4%)		
		HOMO-1 → LUMO+5 (3%)		

**Table S12.** TD-DFT calculated electronic transitions for **5** along with their corresponding excitation energies and oscillator strengths.

Compound	Spin State	Transition Configuration	Excitation Energy (nm, eV)	Oscillator Strength
<b>5</b>	S <sub>1</sub>	HOMO-2 → LUMO (81%)	259.24 (4.78)	0.1367
		HOMO-3 → LUMO (3%)		
		HOMO-3 → LUMO+2 (3%)		
	S <sub>2</sub>	HOMO → LUMO (88%)	251.95 (4.92)	0.0227
	S <sub>3</sub>	HOMO-2 → LUMO+1 (10%)	241.24 (5.14)	0.0203
		HOMO-1 → LUMO (40%)		
		HOMO-1 → LUMO+4 (11%)		
		HOMO-4 → LUMO (5%)		
		HOMO-3 → LUMO (5%)		
		HOMO → LUMO+5 (7%)		

		HOMO → LUMO+6 (2%)		
S <sub>4</sub>		HOMO-2 → LUMO+1 (25%)	238.97 (5.19)	0.0243
		HOMO-1 → LUMO+4 (12%)		
		HOMO-5 → LUMO+2 (6%)		
		HOMO-5 → LUMO+3 (3%)		
		HOMO-4 → LUMO (4%)		
		HOMO-3 → LUMO (5%)		
		HOMO-3 → LUMO+1 (7%)		
		HOMO-3 → LUMO+2 (5%)		
		HOMO-1 → LUMO (5%)		
		HOMO-1 → LUMO+3 (2%)		
		HOMO → LUMO+5 (9%)		
		HOMO → LUMO+6 (2%)		
S <sub>5</sub>		HOMO-4 → LUMO (12%)	237.15 (5.23)	0.0244
		HOMO-3 → LUMO (10%)		
		HOMO-3 → LUMO+1 (16%)		
		HOMO-2 → LUMO+2 (11%)		
		HOMO-5 → LUMO+2 (5%)		
		HOMO-5 → LUMO+3 (3%)		
		HOMO-2 → LUMO+3 (4%)		
		HOMO-1 → LUMO (6%)		
		HOMO-1 → LUMO+4 (7%)		

		HOMO → LUMO+1 (2%)		
		HOMO → LUMO+5 (6%)		

**Table S13.** TD-DFT calculated electronic transitions for **5a** along with their corresponding excitation energies and oscillator strengths.

Compound	Spin State	Transition Configuration	Excitation Energy (nm, eV)	Oscillator Strength
<b>5a</b>	S <sub>1</sub>	HOMO → LUMO (78%)	339.04 (3.66)	0.0924
		HOMO → LUMO+1 (18%)		
	S <sub>2</sub>	HOMO → LUMO (18%)	321.83 (3.85)	0.0285
		HOMO → LUMO+1 (68%)		
		HOMO → LUMO+2 (12%)		
	S <sub>3</sub>	HOMO-3 → LUMO (42%)	281.06 (4.41)	0.0647
		HOMO-1 → LUMO (48%)		
		HOMO-4 → LUMO+1 (2%)		
	S <sub>4</sub>	HOMO-3 → LUMO (44%)	256.35 (4.84)	0.0339
		HOMO-1 → LUMO (42%)		
		HOMO-1 → LUMO+3 (3%)		
	S <sub>5</sub>	HOMO-3 → LUMO+1 (11%)	255.57 (4.85)	0.0377
		HOMO → LUMO+2 (63%)		
		HOMO-1 → LUMO+1 (7%)		
		HOMO → LUMO+1 (9%)		

**Table S14.** TD-DFT calculated electronic transitions for **6** along with their corresponding excitation energies and oscillator strengths.

Compound	Spin State	Transition Configuration	Excitation Energy (nm, eV)	Oscillator Strength
<b>6</b>	S <sub>1</sub>	HOMO → LUMO (75%)	282.26 (4.39)	0.1134
		HOMO → LUMO+1 (14%)		
		HOMO-4 → LUMO (7%)		

		HOMO-3 → LUMO+1 (32%)		
S <sub>2</sub>		HOMO → LUMO+2 (13%)	269.49 (4.60)	0.0094
		HOMO → LUMO+3 (28%)		
		HOMO-3 → LUMO+2 (3%)		
		HOMO-2 → LUMO+1 (2%)		
		HOMO → LUMO+1 (6%)		
		HOMO → LUMO+4 (9%)		
S <sub>3</sub>		HOMO → LUMO (11%)	267.50 (4.63)	0.0945
		HOMO → LUMO+1 (70%)		
		HOMO-3 → LUMO+1 (3%)		
		HOMO-3 → LUMO+3 (3%)		
		HOMO → LUMO+2 (8%)		
S <sub>4</sub>		HOMO-4 → LUMO (39%)	255.08 (4.86)	0.0710
		HOMO-1 → LUMO (46%)		
		HOMO → LUMO (4%)		
S <sub>5</sub>		HOMO-4 → LUMO (37%)	249.08 (4.98)	0.0584
		HOMO-1 → LUMO (44%)		
		HOMO → LUMO (3%)		

**Table S15.** TD-DFT calculated electronic transitions for **6a** along with their corresponding excitation energies and oscillator strengths.

Compound	Spin State	Transition Configuration	Excitation Energy (nm, eV)	Oscillator Strength
<b>6a</b>	S <sub>1</sub>	HOMO → LUMO (93%)	358.61 (3.46)	0.0922
	S <sub>2</sub>	HOMO-1 → LUMO (10%)	306.40 (4.05)	0.0200
		HOMO → LUMO+1 (60%)		
		HOMO → LUMO+2 (18%)		
		HOMO → LUMO+3 (4%)		

	S <sub>3</sub>	HOMO-1 → LUMO (69%)	295.15 (4.20)	0.0967
		HOMO → LUMO+1 (12%)		
		HOMO-4 → LUMO (7%)		
		HOMO-3 → LUMO (3%)		
		HOMO → LUMO+3 (2%)		
	S <sub>4</sub>	HOMO → LUMO+1 (14%)	275.10 (4.51)	0.0640
		HOMO → LUMO+2 (68%)		
		HOMO-1 → LUMO+2 (3%)		
		HOMO → LUMO+5 (2%)		
		HOMO → LUMO+6 (2%)		
	S <sub>5</sub>	HOMO-1 → LUMO+1 (30%)	261.68 (4.74)	0.0349
		HOMO → LUMO+3 (33%)		
		HOMO-3 → LUMO+1 (4%)		
		HOMO-1 → LUMO+2 (4%)		
		HOMO → LUMO+1 (5%)		
		HOMO → LUMO+5 (5%)		
		HOMO → LUMO+6 (7%)		

**Table S16.** TD-DFT calculated electronic transitions for **7** along with their corresponding excitation energies and oscillator strengths.

Compound	Spin State	Transition Configuration	Excitation Energy (nm, eV)	Oscillator Strength
<b>7</b>	S <sub>1</sub>	HOMO-4 → LUMO (11%)	274.85 (4.51)	0.0703
		HOMO → LUMO (77%)		
		HOMO-2 → LUMO (3%)		
	S <sub>2</sub>	HOMO-2 → LUMO (13%)	258.17 (4.80)	0.0322
		HOMO-1 → LUMO (70%)		
		HOMO-4 → LUMO (4%)		

		HOMO → LUMO (5%)		
S <sub>3</sub>		HOMO-4 → LUMO (53%)	247.78 (5.00)	0.0882
		HOMO-1 → LUMO (16%)		
		HOMO → LUMO (10%)		
		HOMO-2 → LUMO (9%)		
S <sub>4</sub>		HOMO-4 → LUMO (12%)	244.61 (5.07)	0.0164
		HOMO-2 → LUMO (29%)		
		HOMO-5 → LUMO (4%)		
		HOMO-4 → LUMO+1 (4%)		
		HOMO-3 → LUMO+2 (3%)		
		HOMO-2 → LUMO+1 (7%)		
		HOMO-2 → LUMO+3 (4%)		
		HOMO-1 → LUMO (2%)		
		HOMO-1 → LUMO+5 (4%)		
		HOMO → LUMO+1 (8%)		
		HOMO → LUMO+4 (4%)		
		HOMO → LUMO+5 (3%)		
S <sub>5</sub>		HOMO-3 → LUMO (21%)	241.00 (5.14)	0.0036
		HOMO-1 → LUMO+3 (14%)		
		HOMO-3 → LUMO+1 (4%)		
		HOMO-3 → LUMO+2 (6%)		
		HOMO-3 → LUMO+5 (4%)		
		HOMO-2 → LUMO+2 (7%)		
		HOMO-2 → LUMO+6		

		(5%)		
		HOMO → LUMO+1 (5%)		
		HOMO → LUMO+4 (7%)		
		HOMO → LUMO+5 (7%)		

**Table S17.** TD-DFT calculated electronic transitions for **7a** along with their corresponding excitation energies and oscillator strengths.

Compound	Spin State	Transition Configuration	Excitation Energy (nm, eV)	Oscillator Strength
<b>7a</b>	S <sub>1</sub>	HOMO → LUMO (94%)	404.75 (3.06)	0.0658
		HOMO → LUMO+1 (2%)		
	S <sub>2</sub>	HOMO → LUMO+1 (79%)	330.18 (3.76)	0.0199
		HOMO → LUMO+2 (9%)		
		HOMO → LUMO+4 (6%)		
	S <sub>3</sub>	HOMO-3 → LUMO (28%)	292.00 (4.25)	0.0512
		HOMO-1 → LUMO (57%)		
		HOMO → LUMO+1 (3%)		
		HOMO → LUMO+2 (5%)		
	S <sub>4</sub>	HOMO → LUMO+1 (13%)	282.63 (4.39)	0.0319
		HOMO → LUMO+2 (44%)		
		HOMO → LUMO+4 (26%)		
		HOMO-1 → LUMO (4%)		
		HOMO → LUMO+5 (7%)		
	S <sub>5</sub>	HOMO → LUMO+3 (69%)	256.43 (4.83)	0.0046
		HOMO-3 → LUMO (8%)		
		HOMO-1 → LUMO (5%)		
		HOMO → LUMO+2 (5%)		
		HOMO → LUMO+4 (3%)		
		HOMO → LUMO+5 (3%)		

**Table S18.** Primary orbitals which contribute to the calculated transitions of **1** (iso = 0.03). Most H atoms have been omitted for clarity.

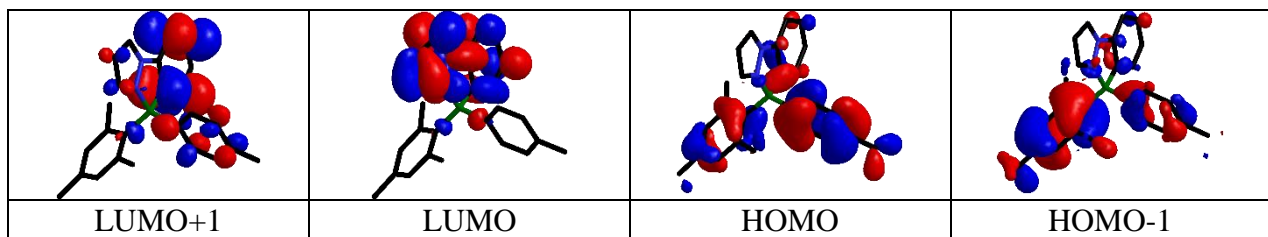


**Table S19.** Primary orbitals which contribute to the calculated transitions of **1a** (iso = 0.03). Most H atoms have been omitted for clarity.

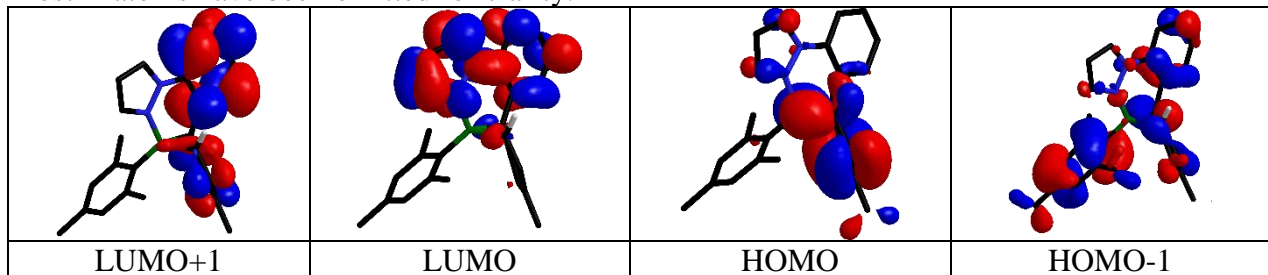


**Table S20.** Primary orbitals which contribute to the calculated transitions of **1b** (iso = 0.03). Most H atoms have been omitted for clarity.

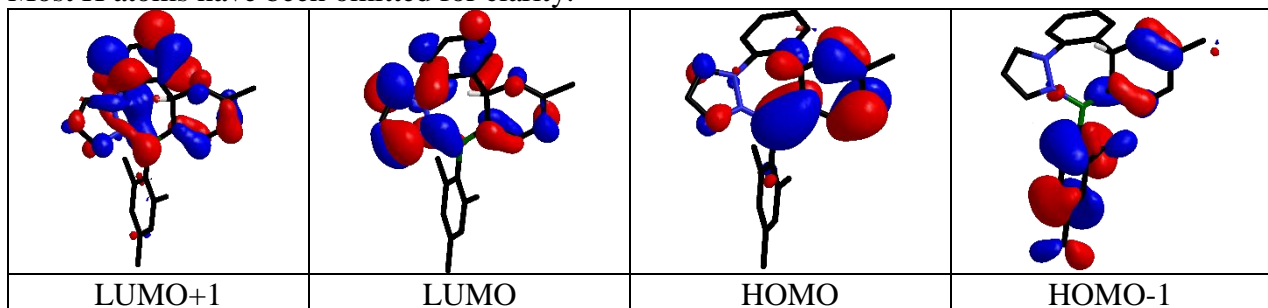


**Table S21.** Primary orbitals which contribute to the calculated transitions of **2** (iso = 0.03). Most H atoms have been omitted for clarity.

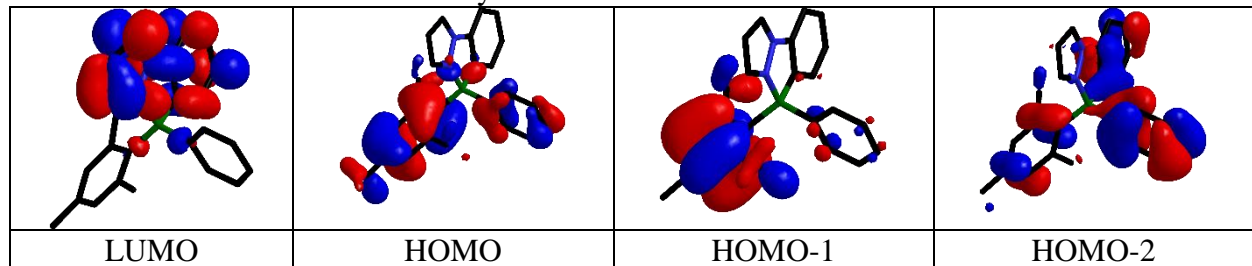


**Table S22.** Primary orbitals which contribute to the calculated transitions of **2a** (iso = 0.03). Most H atoms have been omitted for clarity.

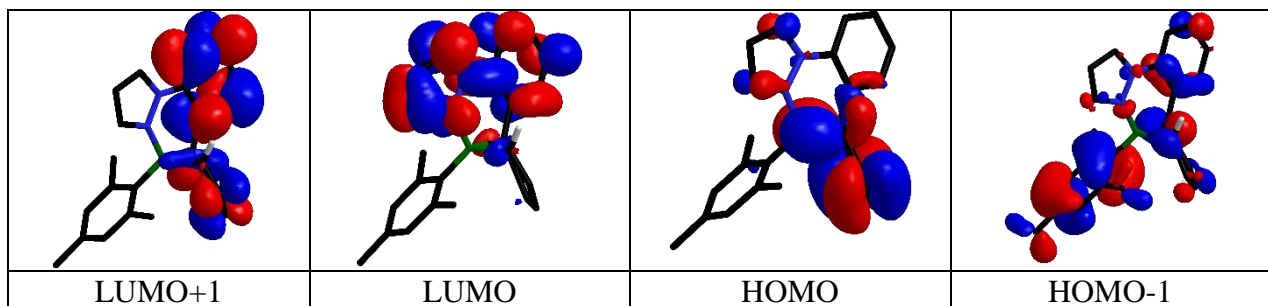


**Table S23.** Primary orbitals which contribute to the calculated transitions of **2b** (iso = 0.03). Most H atoms have been omitted for clarity.

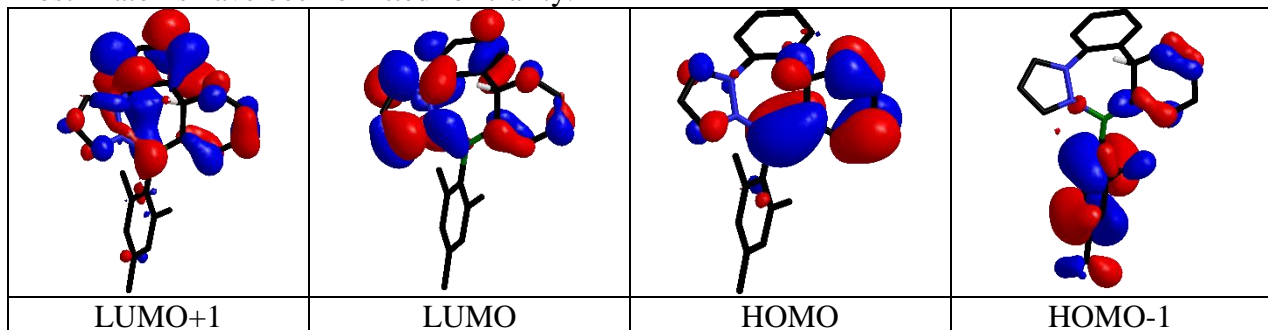


**Table S24.** Primary orbitals which contribute to the calculated transitions of **4** (iso = 0.03). Most H atoms have been omitted for clarity.

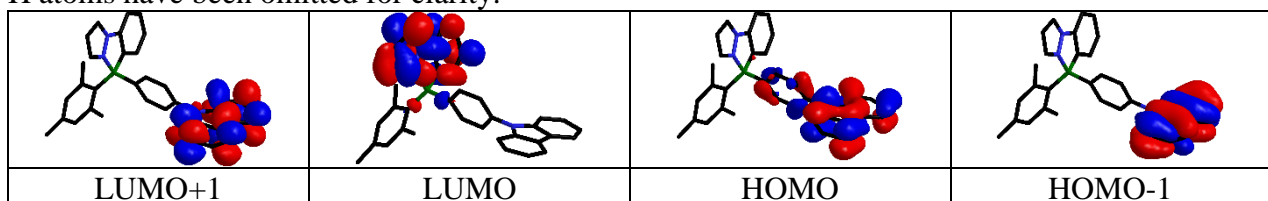


**Table S25.** Primary orbitals which contribute to the calculated transitions of **4a** (iso = 0.03). Most H atoms have been omitted for clarity.

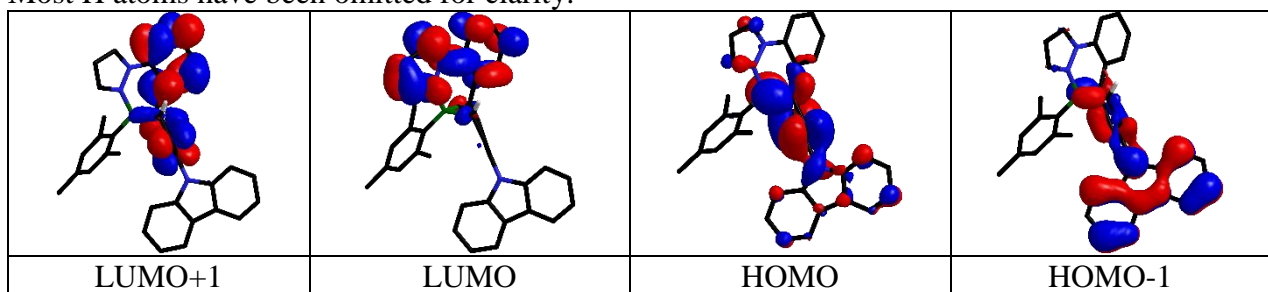


**Table S26.** Primary orbitals which contribute to the calculated transitions of **4b** (iso = 0.03). Most H atoms have been omitted for clarity.

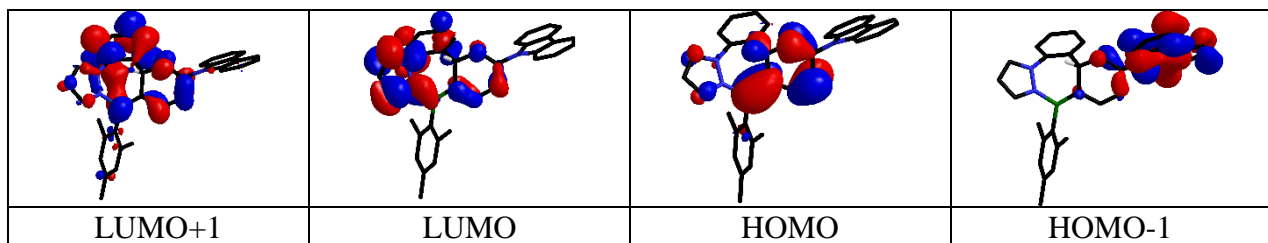


**Table S27.** Primary orbitals which contribute to the calculated transitions of **5** (iso = 0.03). Most H atoms have been omitted for clarity.

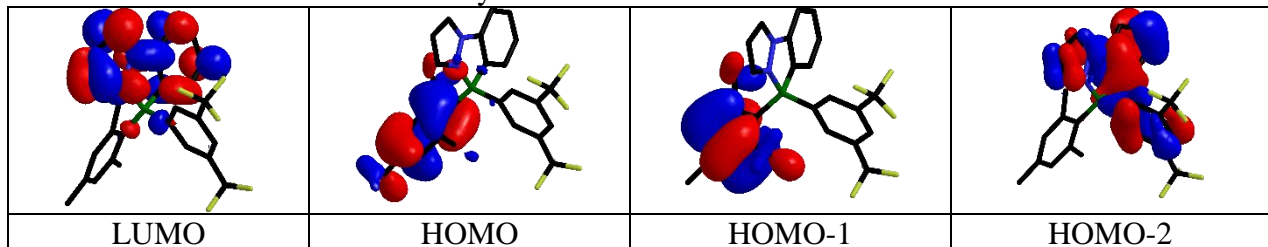


**Table S28.** Primary orbitals which contribute to the calculated transitions of **5a** (iso = 0.03). Most H atoms have been omitted for clarity.

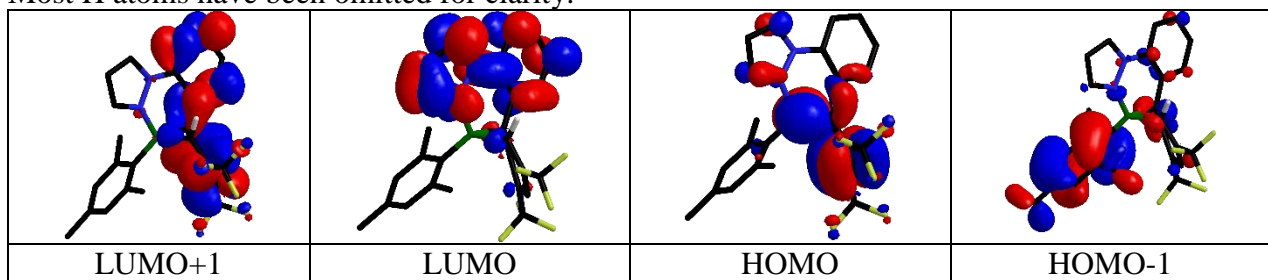


**Table S29.** Primary orbitals which contribute to the calculated transitions of **6** (iso = 0.03). Most H atoms have been omitted for clarity.

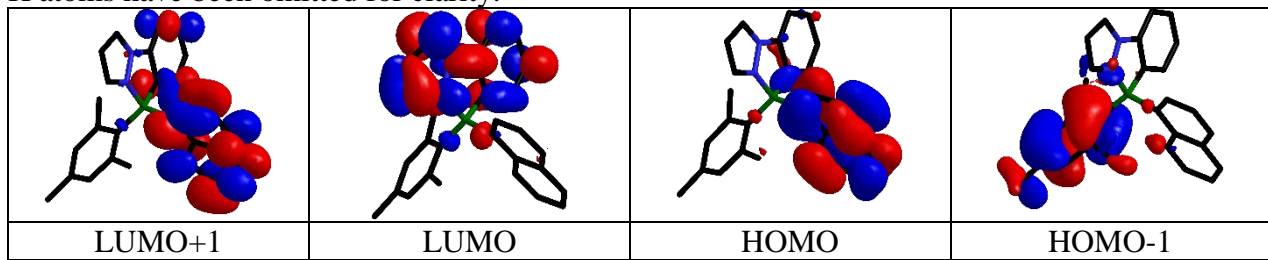


**Table S30.** Primary orbitals which contribute to the calculated transitions of **6a** (iso = 0.03). Most H atoms have been omitted for clarity.

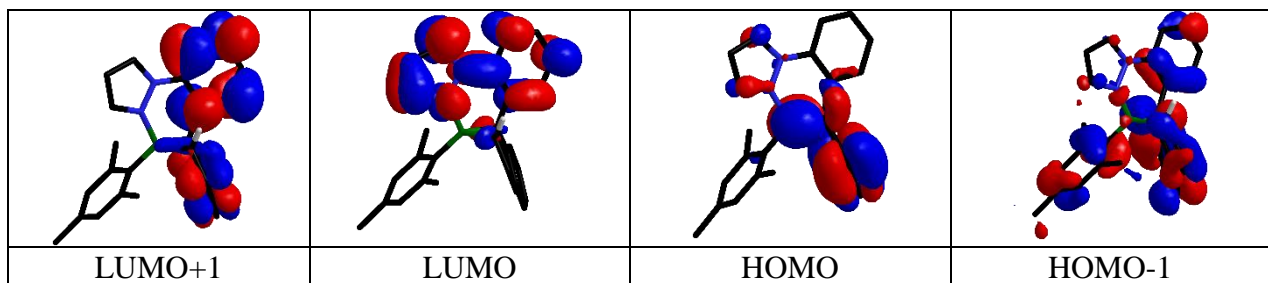


**Table S31.** Primary orbitals which contribute to the calculated transitions of **7** ( $\text{iso} = 0.03$ ). Most H atoms have been omitted for clarity.

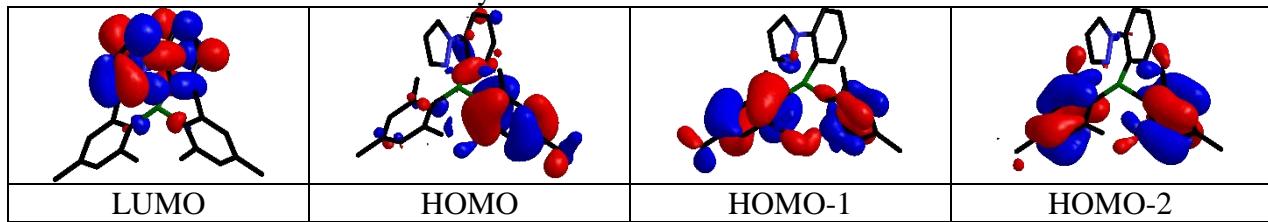


**Table S32.** Primary orbitals which contribute to the calculated transitions of **7a** ( $\text{iso} = 0.03$ ). Most H atoms have been omitted for clarity.

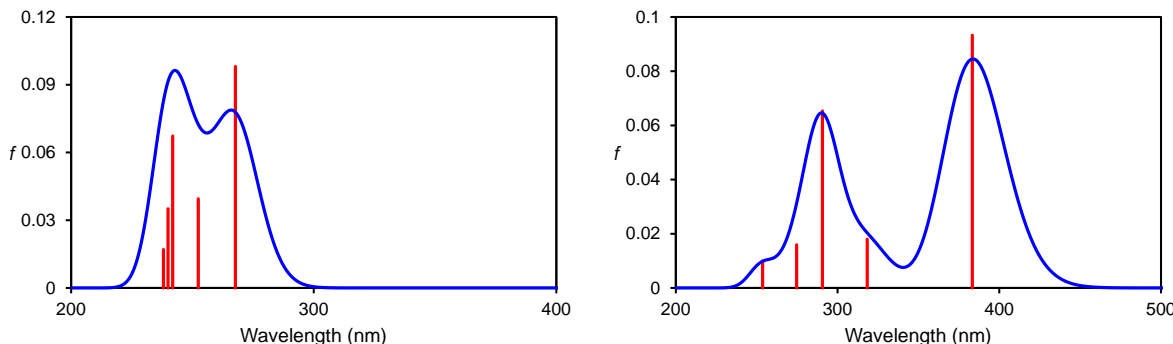
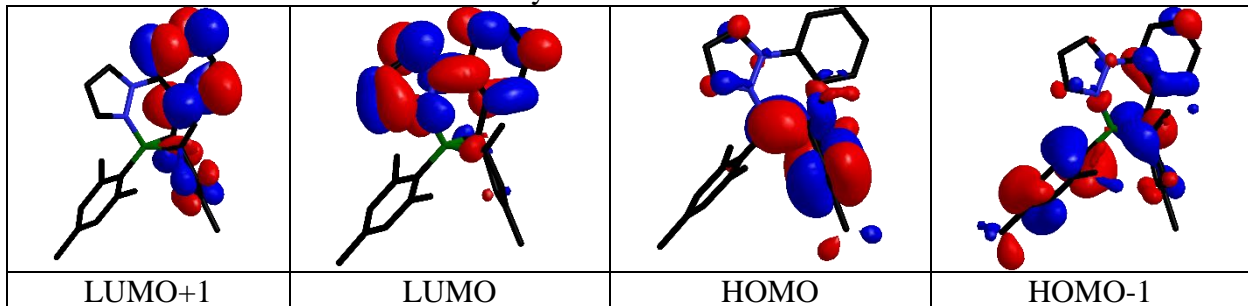


**Figure S92.** Predicted UV/Vis spectra of **1** (left) and **1a** (right) for their first five excited states.<sup>[10]</sup>

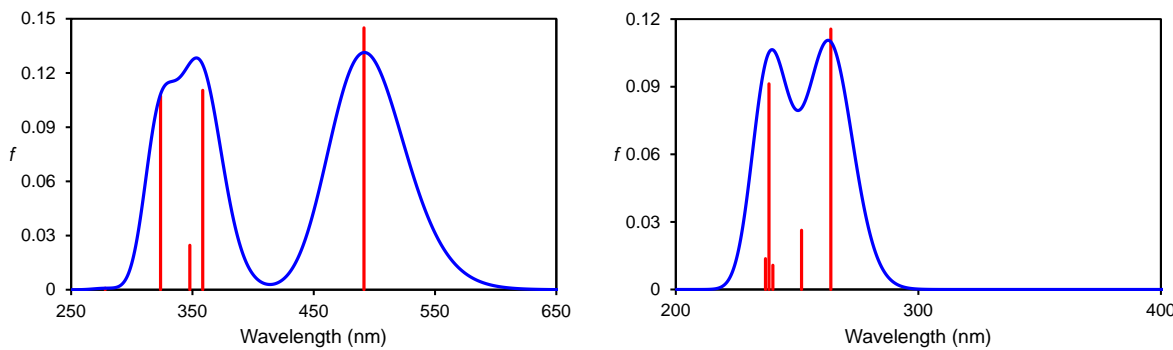


**Figure S93.** Predicted UV/Vis spectra of **1b** (left) and **2** (right) for their first five excited states.<sup>[10]</sup>

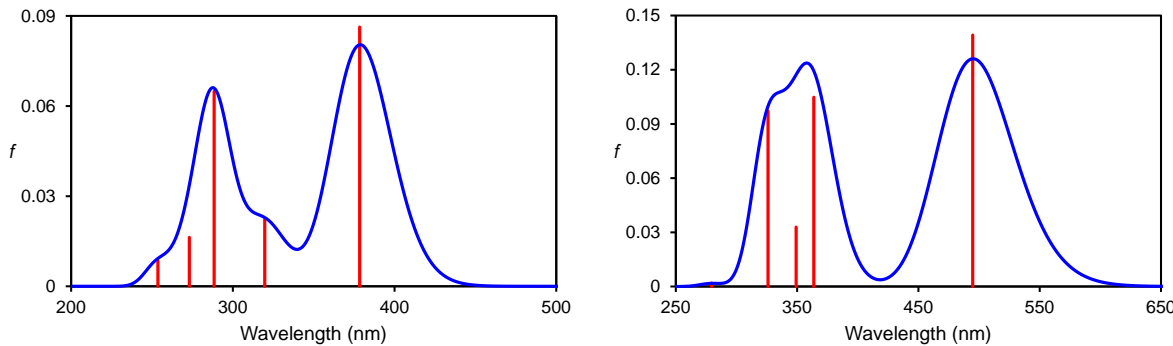


**Figure S94.** Predicted UV/Vis spectra of **2a** (left) and **2b** (right) for their first five excited states.<sup>[10]</sup>

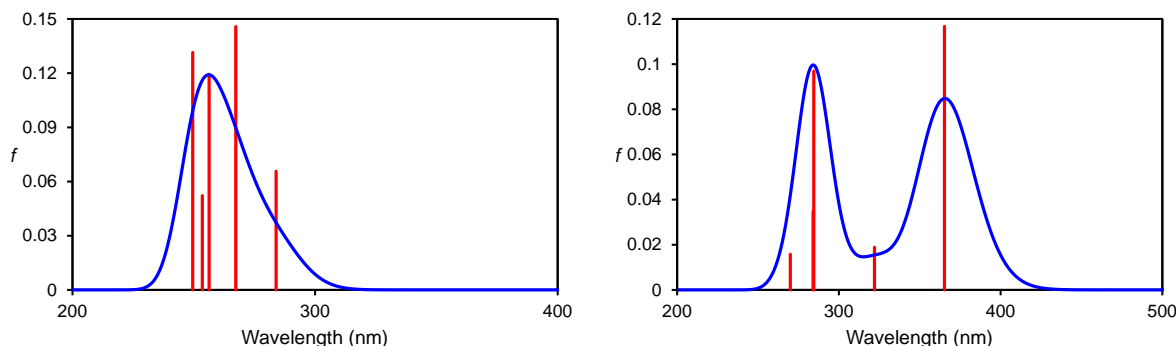


**Figure S95.** Predicted UV/Vis spectra of **4** (left) and **4a** (right) for their first five excited states.<sup>[10]</sup>

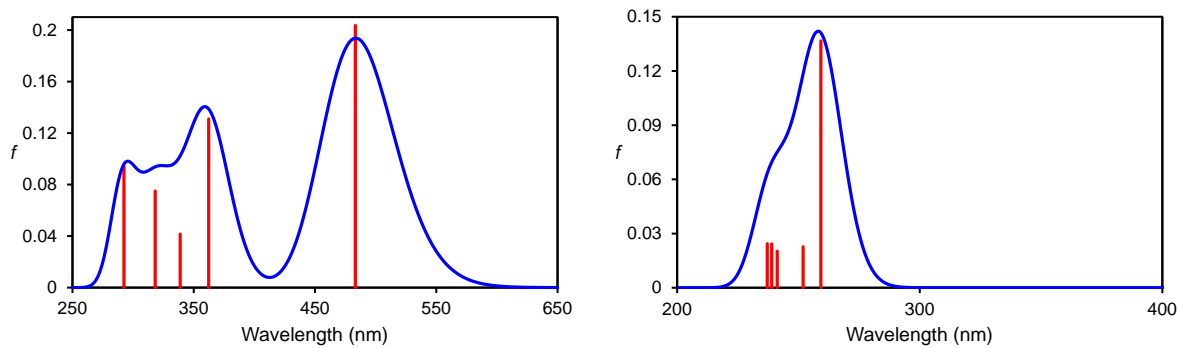


**Figure S96.** Predicted UV/Vis spectra of **4b** (left) and **5** (right) for their first five excited states.<sup>[10]</sup>

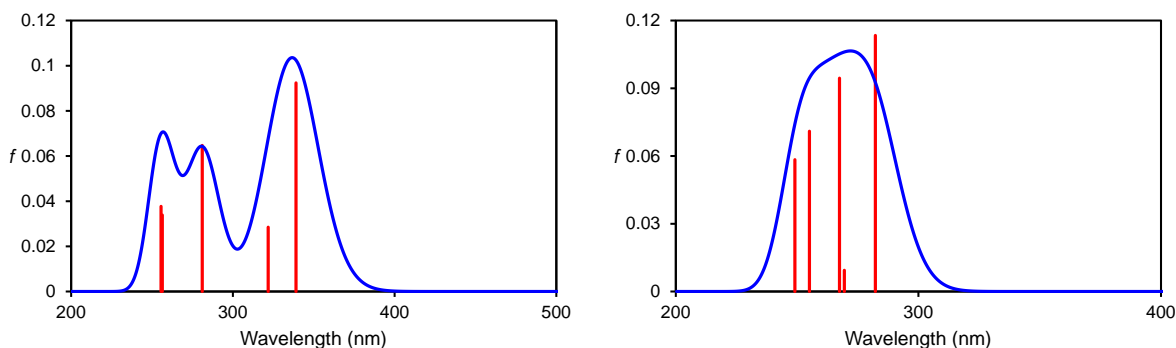


**Figure S97.** Predicted UV/Vis spectra of **5a** (left) and **6** (right) for their first five excited states.<sup>[10]</sup>

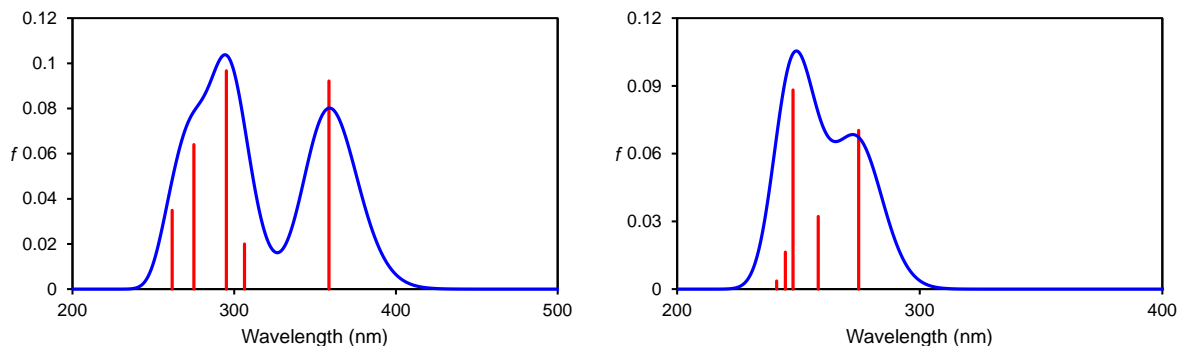


**Figure S98.** Predicted UV/Vis spectra of **6a** (left) and **7** (right) for their first five excited states.<sup>[10]</sup>

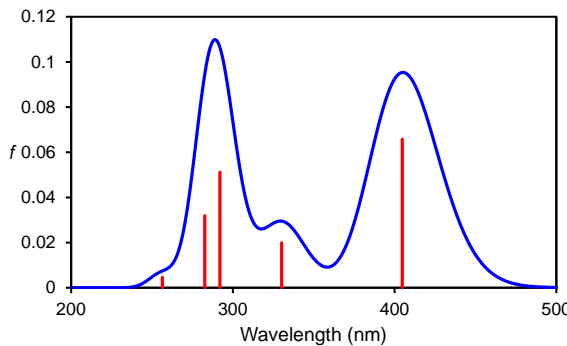


**Figure S99.** Predicted UV/Vis spectra of **7a** for its first five excited states.<sup>[10]</sup>

## S7. X-Ray Crystal Structure Data of **4** and **6**

Colourless crystals of **4** and off-white crystals of **6** were grown by layering CH<sub>2</sub>Cl<sub>2</sub> solutions of each with hexanes. Single crystals were mounted on a sample holder and diffraction data were collected on a Bruker D8-Venture diffractometer with Mo K<sub>α</sub> radiation at 180 K. Data were processed using the Bruker APEX III software and SHELXTL software package (SHELXTL-2014/7)<sup>[11]</sup> and corrected for absorption effects. All non-hydrogen atoms were refined anisotropically. The crystal data of **4** and **6** have been deposited at the Cambridge Crystallographic Data Center (CCDC No. 1858646, 1858647).

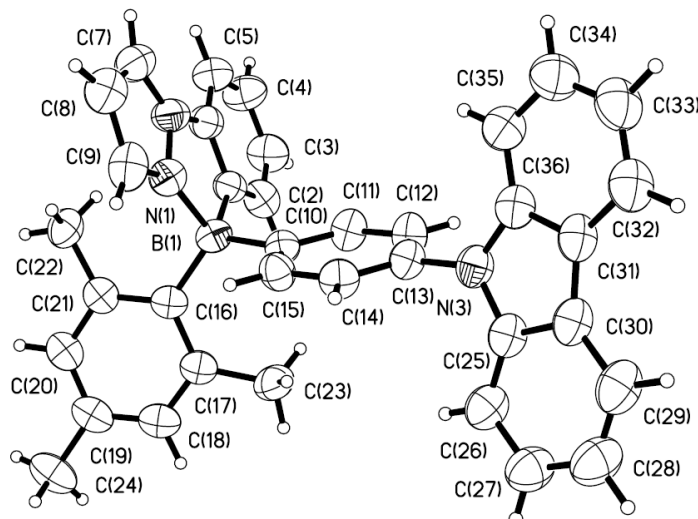


**Figure S100.** The crystal structure of **4** with labeling schemes.

**Table S33.** Crystal Data and Structural Refinement for **4**.

Identification code

**4**

Empirical formula

C<sub>36</sub>H<sub>30</sub>B<sub>1</sub>N<sub>3</sub>

Formula weight	515.44
Temperature	180(2) K
Wavelength	0.71073 Å
Crystal system	Triclinic
Space group	P-1
Unit cell dimensions	$a = 10.6235(9)$ Å $\alpha = 72.283(3)^\circ$ . $b = 12.3400(13)$ Å $\beta = 72.107(3)^\circ$ . $c = 12.5242(13)$ Å $\gamma = 64.832(3)^\circ$ .
Volume	1385.1(2) Å <sup>3</sup>
Z	2
Density (calculated)	1.236 Mg/m <sup>3</sup>
Absorption coefficient	0.072 mm <sup>-1</sup>
F(000)	544
Crystal size	0.150 x 0.100 x 0.080 mm <sup>3</sup>
Theta range for data collection	2.165 to 27.235°.
Index ranges	-13<=h<=13, -15<=k<=15, -16<=l<=16
Reflections collected	47718
Independent reflections	6154 [R(int) = 0.1716]
Completeness to theta = 25.242°	99.9 %
Absorption correction	Semi-empirical from equivalents
Max. and min. transmission	0.745 and 0.545
Refinement method	Full-matrix least-squares on F <sup>2</sup>
Data / restraints / parameters	6154 / 0 / 365
Goodness-of-fit on F <sup>2</sup>	1.065
Final R indices [I>2sigma(I)]	R1 = 0.0747, wR2 = 0.1844
R indices (all data)	R1 = 0.1776, wR2 = 0.2710
Extinction coefficient	0.024(4)
Largest diff. peak and hole	0.710 and -0.285 e.Å <sup>-3</sup>

**Table S34.** Atomic coordinates ( $\times 10^4$ ) and equivalent isotropic displacement parameters ( $\text{\AA}^2 \times 10^3$ ) for **4**. U(eq) is defined as one third of the trace of the orthogonalized  $U^{ij}$  tensor.

	x	y	z	U(eq)
B(1)	3049(4)	5222(4)	3092(3)	45(1)
C(1)	4611(4)	5063(3)	2308(3)	44(1)
N(1)	3148(3)	5996(3)	3891(2)	50(1)
C(2)	5342(4)	4547(4)	1329(3)	56(1)
N(2)	4466(3)	6050(3)	3627(3)	54(1)
C(3)	6683(4)	4515(4)	766(4)	67(1)
N(3)	2993(3)	730(3)	6465(2)	51(1)
C(4)	7342(5)	4992(4)	1182(4)	71(1)
C(5)	6670(4)	5516(4)	2157(3)	60(1)
C(6)	5336(4)	5527(3)	2679(3)	50(1)
C(7)	4574(5)	6625(4)	4341(3)	58(1)
C(8)	3299(5)	6961(4)	5084(4)	67(1)
C(9)	2402(5)	6545(4)	4776(3)	64(1)
C(10)	3010(4)	3963(3)	3981(3)	44(1)
C(11)	4073(4)	2834(3)	3868(3)	51(1)
C(12)	4083(4)	1777(3)	4665(3)	54(1)
C(13)	3001(4)	1817(3)	5629(3)	47(1)
C(14)	1918(4)	2917(3)	5780(3)	50(1)
C(15)	1936(4)	3969(3)	4966(3)	49(1)
C(16)	1802(3)	6003(3)	2360(3)	45(1)
C(17)	1070(4)	5438(3)	2072(3)	48(1)
C(18)	14(4)	6136(4)	1437(3)	54(1)
C(19)	-382(4)	7385(4)	1060(3)	55(1)
C(20)	382(4)	7931(4)	1280(3)	54(1)
C(21)	1468(4)	7271(3)	1899(3)	47(1)
C(22)	2284(4)	7973(3)	1987(3)	56(1)
C(23)	1415(5)	4071(4)	2354(4)	63(1)
C(24)	-1569(4)	8108(5)	413(4)	73(1)
C(25)	2022(4)	176(3)	6665(3)	51(1)
C(26)	1009(4)	441(4)	6057(3)	61(1)
C(27)	177(5)	-257(4)	6432(4)	70(1)
C(28)	358(5)	-1210(5)	7386(4)	76(1)
C(29)	1362(5)	-1470(4)	7999(4)	69(1)
C(30)	2223(4)	-769(3)	7638(3)	54(1)
C(31)	3347(4)	-776(3)	8050(3)	53(1)

C(32)	4011(5)	-1480(4)	8970(3)	64(1)
C(33)	5083(5)	-1245(4)	9122(4)	74(1)
C(34)	5537(5)	-324(4)	8366(4)	72(1)
C(35)	4905(4)	384(4)	7450(4)	61(1)
C(36)	3806(4)	156(3)	7300(3)	51(1)

**Table S35.** Bond lengths [Å] and angles [°] for **4**.

B(1)-C(1)	1.611(5)
B(1)-C(10)	1.621(5)
B(1)-C(16)	1.627(5)
B(1)-N(1)	1.630(5)
C(1)-C(6)	1.377(5)
C(1)-C(2)	1.407(5)
N(1)-C(9)	1.332(5)
N(1)-N(2)	1.362(4)
C(2)-C(3)	1.370(5)
N(2)-C(7)	1.354(5)
N(2)-C(6)	1.402(5)
C(3)-C(4)	1.368(6)
N(3)-C(36)	1.388(5)
N(3)-C(25)	1.389(5)
N(3)-C(13)	1.430(4)
C(4)-C(5)	1.404(6)
C(5)-C(6)	1.362(5)
C(7)-C(8)	1.362(6)
C(8)-C(9)	1.443(6)
C(10)-C(11)	1.386(5)
C(10)-C(15)	1.399(5)
C(11)-C(12)	1.378(5)
C(12)-C(13)	1.384(5)
C(13)-C(14)	1.378(5)
C(14)-C(15)	1.389(5)
C(16)-C(17)	1.417(5)
C(16)-C(21)	1.417(5)
C(17)-C(18)	1.394(5)
C(17)-C(23)	1.516(5)
C(18)-C(19)	1.379(5)
C(19)-C(20)	1.380(5)
C(19)-C(24)	1.508(5)

C(20)-C(21)	1.399(5)
C(21)-C(22)	1.507(5)
C(25)-C(26)	1.378(5)
C(25)-C(30)	1.405(5)
C(26)-C(27)	1.374(6)
C(27)-C(28)	1.394(6)
C(28)-C(29)	1.375(6)
C(29)-C(30)	1.404(5)
C(30)-C(31)	1.435(5)
C(31)-C(32)	1.397(5)
C(31)-C(36)	1.407(5)
C(32)-C(33)	1.366(6)
C(33)-C(34)	1.396(6)
C(34)-C(35)	1.376(6)
C(35)-C(36)	1.387(5)

C(1)-B(1)-C(10)	111.8(3)
C(1)-B(1)-C(16)	112.4(3)
C(10)-B(1)-C(16)	119.2(3)
C(1)-B(1)-N(1)	94.3(3)
C(10)-B(1)-N(1)	102.8(3)
C(16)-B(1)-N(1)	113.1(3)
C(6)-C(1)-C(2)	115.6(3)
C(6)-C(1)-B(1)	112.7(3)
C(2)-C(1)-B(1)	131.7(3)
C(9)-N(1)-N(2)	107.2(3)
C(9)-N(1)-B(1)	141.6(3)
N(2)-N(1)-B(1)	111.0(3)
C(3)-C(2)-C(1)	122.8(4)
C(7)-N(2)-N(1)	110.9(3)
C(7)-N(2)-C(6)	136.9(3)
N(1)-N(2)-C(6)	112.2(3)
C(4)-C(3)-C(2)	118.5(4)
C(36)-N(3)-C(25)	108.8(3)
C(36)-N(3)-C(13)	126.1(3)
C(25)-N(3)-C(13)	124.6(3)
C(3)-C(4)-C(5)	121.4(4)
C(6)-C(5)-C(4)	117.5(4)
C(5)-C(6)-C(1)	124.1(4)
C(5)-C(6)-N(2)	126.3(3)

C(1)-C(6)-N(2)	109.5(3)
N(2)-C(7)-C(8)	107.6(4)
C(7)-C(8)-C(9)	105.9(4)
N(1)-C(9)-C(8)	108.4(4)
C(11)-C(10)-C(15)	115.6(3)
C(11)-C(10)-B(1)	123.0(3)
C(15)-C(10)-B(1)	121.2(3)
C(12)-C(11)-C(10)	122.8(3)
C(11)-C(12)-C(13)	120.0(3)
C(14)-C(13)-C(12)	119.5(3)
C(14)-C(13)-N(3)	119.7(3)
C(12)-C(13)-N(3)	120.8(3)
C(13)-C(14)-C(15)	119.3(3)
C(14)-C(15)-C(10)	122.8(3)
C(17)-C(16)-C(21)	116.3(3)
C(17)-C(16)-B(1)	121.9(3)
C(21)-C(16)-B(1)	121.7(3)
C(18)-C(17)-C(16)	120.3(3)
C(18)-C(17)-C(23)	115.7(3)
C(16)-C(17)-C(23)	123.9(3)
C(19)-C(18)-C(17)	123.3(4)
C(18)-C(19)-C(20)	116.7(3)
C(18)-C(19)-C(24)	121.3(4)
C(20)-C(19)-C(24)	121.9(4)
C(19)-C(20)-C(21)	122.3(4)
C(20)-C(21)-C(16)	120.9(3)
C(20)-C(21)-C(22)	116.1(3)
C(16)-C(21)-C(22)	123.0(3)
C(26)-C(25)-N(3)	129.1(3)
C(26)-C(25)-C(30)	122.4(4)
N(3)-C(25)-C(30)	108.5(3)
C(27)-C(26)-C(25)	117.7(4)
C(26)-C(27)-C(28)	121.4(4)
C(29)-C(28)-C(27)	120.9(4)
C(28)-C(29)-C(30)	118.9(4)
C(29)-C(30)-C(25)	118.6(4)
C(29)-C(30)-C(31)	134.2(4)
C(25)-C(30)-C(31)	107.2(3)
C(32)-C(31)-C(36)	119.0(4)
C(32)-C(31)-C(30)	134.2(4)

C(36)-C(31)-C(30)	106.9(3)
C(33)-C(32)-C(31)	119.3(4)
C(32)-C(33)-C(34)	121.2(4)
C(35)-C(34)-C(33)	120.9(4)
C(34)-C(35)-C(36)	118.1(4)
C(35)-C(36)-N(3)	129.8(4)
C(35)-C(36)-C(31)	121.6(4)
N(3)-C(36)-C(31)	108.6(3)

Symmetry transformations used to generate equivalent atoms:

**Table S36.** Anisotropic displacement parameters ( $\text{\AA}^2 \times 10^3$ ) for **4**. The anisotropic displacement factor exponent takes the form:  $-2\pi^2 [ h^2 a^{*2} U_{11} + \dots + 2 h k a^{*} b^{*} U_{12} ]$

	U <sub>11</sub>	U <sub>22</sub>	U <sub>33</sub>	U <sub>23</sub>	U <sub>13</sub>	U <sub>12</sub>
B(1)	48(2)	52(2)	40(2)	-11(2)	-6(2)	-24(2)
C(1)	42(2)	46(2)	44(2)	-1(2)	-11(2)	-19(2)
N(1)	55(2)	52(2)	44(2)	-6(1)	-9(1)	-23(2)
C(2)	51(2)	59(2)	47(2)	-1(2)	-3(2)	-21(2)
N(2)	56(2)	57(2)	55(2)	-3(2)	-19(2)	-28(2)
C(3)	57(2)	83(3)	58(3)	-23(2)	0(2)	-25(2)
N(3)	59(2)	47(2)	44(2)	-4(1)	-7(1)	-22(2)
C(4)	72(3)	91(3)	64(3)	-27(3)	-10(2)	-38(3)
C(5)	57(2)	71(3)	61(3)	-14(2)	-12(2)	-30(2)
C(6)	50(2)	49(2)	51(2)	-2(2)	-14(2)	-22(2)
C(7)	68(3)	60(3)	57(2)	-7(2)	-17(2)	-32(2)
C(8)	74(3)	65(3)	60(3)	-11(2)	-11(2)	-27(2)
C(9)	82(3)	55(3)	48(2)	-11(2)	-8(2)	-22(2)
C(10)	45(2)	46(2)	41(2)	-10(2)	-8(2)	-17(2)
C(11)	57(2)	50(2)	40(2)	-14(2)	5(2)	-21(2)
C(12)	61(2)	46(2)	43(2)	-12(2)	2(2)	-16(2)
C(13)	53(2)	44(2)	42(2)	-9(2)	-6(2)	-20(2)
C(14)	46(2)	55(2)	44(2)	-10(2)	0(2)	-21(2)
C(15)	43(2)	47(2)	49(2)	-9(2)	-6(2)	-14(2)
C(16)	42(2)	55(2)	36(2)	-9(2)	-3(1)	-21(2)
C(17)	44(2)	57(2)	42(2)	-10(2)	-5(2)	-21(2)
C(18)	46(2)	75(3)	43(2)	-15(2)	-3(2)	-25(2)
C(19)	44(2)	74(3)	39(2)	-10(2)	-6(2)	-16(2)
C(20)	53(2)	58(2)	41(2)	-8(2)	-9(2)	-14(2)

C(21)	47(2)	52(2)	37(2)	-7(2)	-3(2)	-18(2)
C(22)	70(3)	49(2)	49(2)	-2(2)	-12(2)	-28(2)
C(23)	73(3)	64(3)	68(3)	-11(2)	-26(2)	-34(2)
C(24)	52(2)	98(4)	54(3)	-10(2)	-14(2)	-14(2)
C(25)	59(2)	49(2)	41(2)	-8(2)	-4(2)	-22(2)
C(26)	72(3)	63(3)	49(2)	-8(2)	-9(2)	-33(2)
C(27)	79(3)	79(3)	62(3)	-7(2)	-16(2)	-42(3)
C(28)	88(3)	86(3)	66(3)	-5(3)	-9(3)	-53(3)
C(29)	92(3)	67(3)	48(2)	-3(2)	-5(2)	-42(3)
C(30)	67(2)	49(2)	42(2)	-9(2)	-3(2)	-25(2)
C(31)	69(3)	47(2)	40(2)	-8(2)	-9(2)	-20(2)
C(32)	86(3)	60(3)	41(2)	-8(2)	-14(2)	-24(2)
C(33)	97(4)	68(3)	56(3)	-7(2)	-30(2)	-23(3)
C(34)	81(3)	76(3)	65(3)	-13(3)	-24(2)	-27(3)
C(35)	65(3)	61(3)	58(3)	-12(2)	-12(2)	-25(2)
C(36)	62(2)	50(2)	40(2)	-12(2)	-8(2)	-20(2)

---

**Table S37.** Hydrogen coordinates ( $\times 10^4$ ) and isotropic displacement parameters ( $\text{\AA}^2 \times 10^3$ ) for **4**.

	x	y	z	U(eq)
H(2)	4888	4207	1046	68
H(3)	7143	4169	101	80
H(4)	8275	4968	804	85
H(5)	7128	5851	2442	73
H(7)	5390	6768	4326	70
H(8)	3051	7383	5682	80
H(9)	1444	6646	5141	77
H(11)	4826	2786	3213	61
H(12)	4833	1022	4554	65
H(14)	1165	2956	6435	60
H(15)	1189	4724	5083	58
H(18)	-456	5732	1254	65
H(20)	164	8784	1003	64
H(22A)	2039	8768	1461	84
H(22B)	3306	7510	1785	84
H(22C)	2039	8095	2774	84
H(23A)	1123	3804	3182	95

H(23B)	2441	3647	2114	95
H(23C)	905	3877	1949	95
H(24A)	-1541	7628	-96	110
H(24B)	-1453	8873	-43	110
H(24C)	-2484	8292	957	110
H(26)	889	1084	5400	73
H(27)	-537	-85	6032	84
H(28)	-220	-1687	7617	92
H(29)	1472	-2114	8655	82
H(32)	3721	-2115	9485	77
H(33)	5529	-1716	9753	89
H(34)	6291	-184	8486	87
H(35)	5213	1010	6935	73

---

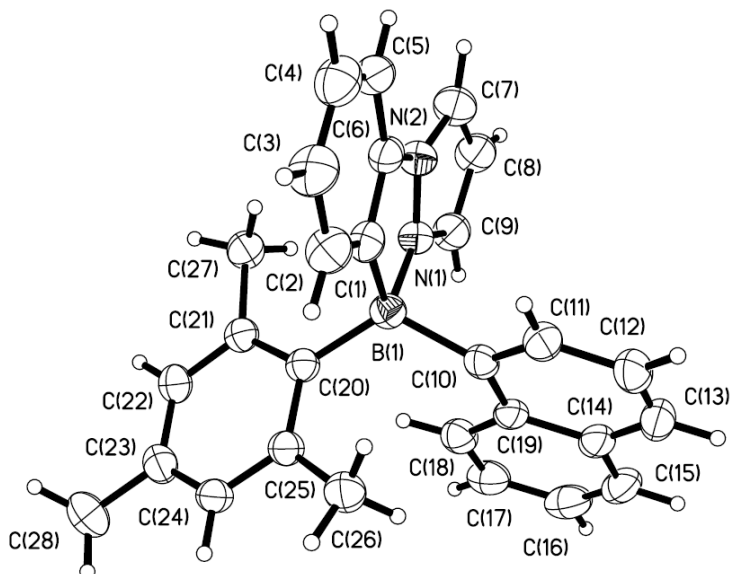


**Figure S101.** The crystal structure of **6** with labeling schemes.

**Table S38.** Crystal Data and Structural Refinement for **6**.

Identification code	<b>6</b>
Empirical formula	C <sub>28</sub> H <sub>25</sub> B N <sub>2</sub>
Formula weight	400.31
Temperature	180(2) K
Wavelength	0.71073 Å
Crystal system	Monoclinic
Space group	P <sub>2</sub> 1/c
Unit cell dimensions	a = 8.2022(5) Å      α = 90°.

	$b = 12.6631(10) \text{ \AA}$	$\beta = 100.564(3)^\circ$ .
	$c = 20.9039(15) \text{ \AA}$	$\gamma = 90^\circ$ .
Volume	$2134.4(3) \text{ \AA}^3$	
Z	4	
Density (calculated)	$1.246 \text{ Mg/m}^3$	
Absorption coefficient	$0.072 \text{ mm}^{-1}$	
F(000)	848	
Crystal size	$0.120 \times 0.120 \times 0.080 \text{ mm}^3$	
Theta range for data collection	$1.889 \text{ to } 27.186^\circ$	
Index ranges	$-10 \leq h \leq 10, -16 \leq k \leq 16, -26 \leq l \leq 26$	
Reflections collected	43856	
Independent reflections	4751 [ $R(\text{int}) = 0.1358$ ]	
Completeness to theta = $25.242^\circ$	99.9 %	
Absorption correction	Semi-empirical from equivalents	
Max. and min. transmission	0.745 and 0.641	
Refinement method	Full-matrix least-squares on $F^2$	
Data / restraints / parameters	4751 / 0 / 284	
Goodness-of-fit on $F^2$	1.069	
Final R indices [ $I > 2\sigma(I)$ ]	$R_1 = 0.0565, wR_2 = 0.1311$	
R indices (all data)	$R_1 = 0.1352, wR_2 = 0.1836$	
Extinction coefficient	0.0112(17)	
Largest diff. peak and hole	0.387 and -0.266 e. $\text{\AA}^{-3}$	

**Table S39.** Atomic coordinates ( $\times 10^4$ ) and equivalent isotropic displacement parameters ( $\text{\AA}^2 \times 10^3$ ) for **6**. U(eq) is defined as one third of the trace of the orthogonalized  $U^{ij}$  tensor.

	x	y	z	U(eq)
B(1)	7126(3)	2699(2)	5579(1)	31(1)
C(1)	6229(3)	2800(2)	4825(1)	35(1)
N(1)	8730(3)	2029(2)	5421(1)	34(1)
C(2)	4713(3)	3203(2)	4524(1)	44(1)
N(2)	8687(3)	1939(2)	4774(1)	37(1)
C(3)	4227(4)	3175(3)	3857(1)	49(1)
C(4)	5257(4)	2733(2)	3468(2)	50(1)
C(5)	6765(4)	2294(2)	3741(1)	44(1)
C(6)	7200(3)	2345(2)	4411(1)	36(1)
C(7)	10152(3)	1567(2)	4656(2)	47(1)
C(8)	11159(3)	1419(2)	5247(2)	47(1)
C(9)	10241(3)	1717(2)	5709(1)	41(1)
C(10)	8104(3)	3763(2)	5885(1)	32(1)
C(11)	8208(3)	4618(2)	5488(1)	38(1)
C(12)	9266(4)	5482(2)	5680(2)	47(1)
C(13)	10252(3)	5493(2)	6278(2)	48(1)
C(14)	10203(3)	4653(2)	6717(1)	40(1)
C(15)	11240(3)	4648(3)	7341(2)	49(1)
C(16)	11226(4)	3832(3)	7760(2)	52(1)
C(17)	10148(3)	2984(3)	7579(1)	45(1)
C(18)	9121(3)	2963(2)	6985(1)	38(1)
C(19)	9114(3)	3788(2)	6528(1)	33(1)
C(20)	5946(3)	2072(2)	5998(1)	29(1)
C(21)	5836(3)	958(2)	6036(1)	31(1)
C(22)	4823(3)	484(2)	6414(1)	35(1)
C(23)	3838(3)	1057(2)	6760(1)	37(1)
C(24)	3858(3)	2141(2)	6694(1)	35(1)
C(25)	4868(3)	2656(2)	6321(1)	32(1)
C(26)	4719(3)	3847(2)	6279(1)	43(1)
C(27)	6761(3)	231(2)	5655(1)	41(1)
C(28)	2751(4)	517(3)	7168(2)	53(1)

**Table S40.** Bond lengths [ $\text{\AA}$ ] and angles [ $^\circ$ ] for **6**.

B(1)-C(1)	1.618(4)
B(1)-C(20)	1.626(4)
B(1)-C(10)	1.638(4)
B(1)-N(1)	1.648(3)
C(1)-C(2)	1.383(4)
C(1)-C(6)	1.402(4)
N(1)-C(9)	1.335(3)
N(1)-N(2)	1.351(3)
C(2)-C(3)	1.380(4)
N(2)-C(7)	1.355(3)
N(2)-C(6)	1.410(3)
C(3)-C(4)	1.392(4)
C(4)-C(5)	1.381(4)
C(5)-C(6)	1.382(4)
C(7)-C(8)	1.368(4)
C(8)-C(9)	1.382(4)
C(10)-C(11)	1.377(4)
C(10)-C(19)	1.444(4)
C(11)-C(12)	1.408(4)
C(12)-C(13)	1.359(4)
C(13)-C(14)	1.410(4)
C(14)-C(15)	1.420(4)
C(14)-C(19)	1.422(3)
C(15)-C(16)	1.356(4)
C(16)-C(17)	1.398(4)
C(17)-C(18)	1.366(4)
C(18)-C(19)	1.416(4)
C(20)-C(25)	1.416(3)
C(20)-C(21)	1.417(3)
C(21)-C(22)	1.384(3)
C(21)-C(27)	1.510(3)
C(22)-C(23)	1.384(4)
C(23)-C(24)	1.381(4)
C(23)-C(28)	1.506(4)
C(24)-C(25)	1.398(3)
C(25)-C(26)	1.514(4)
C(1)-B(1)-C(20)	110.7(2)
C(1)-B(1)-C(10)	114.8(2)
C(20)-B(1)-C(10)	119.2(2)

C(1)-B(1)-N(1)	94.78(19)
C(20)-B(1)-N(1)	115.6(2)
C(10)-B(1)-N(1)	98.65(18)
C(2)-C(1)-C(6)	115.9(2)
C(2)-C(1)-B(1)	133.0(2)
C(6)-C(1)-B(1)	111.1(2)
C(9)-N(1)-N(2)	106.2(2)
C(9)-N(1)-B(1)	140.4(2)
N(2)-N(1)-B(1)	111.61(19)
C(3)-C(2)-C(1)	121.2(3)
N(1)-N(2)-C(7)	110.5(2)
N(1)-N(2)-C(6)	111.7(2)
C(7)-N(2)-C(6)	137.5(2)
C(2)-C(3)-C(4)	120.5(3)
C(5)-C(4)-C(3)	120.9(3)
C(4)-C(5)-C(6)	116.4(3)
C(5)-C(6)-C(1)	125.0(3)
C(5)-C(6)-N(2)	124.4(2)
C(1)-C(6)-N(2)	110.5(2)
N(2)-C(7)-C(8)	107.0(3)
C(7)-C(8)-C(9)	106.1(2)
N(1)-C(9)-C(8)	110.2(3)
C(11)-C(10)-C(19)	117.1(2)
C(11)-C(10)-B(1)	119.4(2)
C(19)-C(10)-B(1)	122.6(2)
C(10)-C(11)-C(12)	122.8(3)
C(13)-C(12)-C(11)	120.2(3)
C(12)-C(13)-C(14)	120.5(3)
C(13)-C(14)-C(15)	121.1(3)
C(13)-C(14)-C(19)	119.5(3)
C(15)-C(14)-C(19)	119.4(3)
C(16)-C(15)-C(14)	121.5(3)
C(15)-C(16)-C(17)	119.3(3)
C(18)-C(17)-C(16)	121.0(3)
C(17)-C(18)-C(19)	121.6(3)
C(18)-C(19)-C(14)	117.2(2)
C(18)-C(19)-C(10)	122.9(2)
C(14)-C(19)-C(10)	119.9(2)
C(25)-C(20)-C(21)	116.2(2)
C(25)-C(20)-B(1)	119.2(2)

C(21)-C(20)-B(1)	124.5(2)
C(22)-C(21)-C(20)	121.0(2)
C(22)-C(21)-C(27)	116.6(2)
C(20)-C(21)-C(27)	122.3(2)
C(23)-C(22)-C(21)	122.6(2)
C(24)-C(23)-C(22)	116.8(2)
C(24)-C(23)-C(28)	121.8(2)
C(22)-C(23)-C(28)	121.4(3)
C(23)-C(24)-C(25)	122.6(2)
C(24)-C(25)-C(20)	120.5(2)
C(24)-C(25)-C(26)	116.6(2)
C(20)-C(25)-C(26)	122.8(2)

---

**Table S41.** Anisotropic displacement parameters ( $\text{\AA}^2 \times 10^3$ ) for **6**. The anisotropic displacement factor exponent takes the form:  $-2\pi^2 [ h^2 a^*{}^2 U^{11} + \dots + 2 h k a^* b^* U^{12} ]$

	U <sup>11</sup>	U <sup>22</sup>	U <sup>33</sup>	U <sup>23</sup>	U <sup>13</sup>	U <sup>12</sup>
B(1)	30(1)	31(2)	33(2)	-1(1)	6(1)	3(1)
C(1)	37(1)	30(2)	38(2)	1(1)	4(1)	-4(1)
N(1)	35(1)	35(1)	34(1)	-5(1)	10(1)	-2(1)
C(2)	43(2)	46(2)	42(2)	0(1)	2(1)	2(1)
N(2)	39(1)	38(1)	37(1)	-4(1)	12(1)	0(1)
C(3)	46(2)	57(2)	39(2)	4(1)	-6(1)	2(1)
C(4)	52(2)	48(2)	45(2)	2(1)	-1(1)	-4(1)
C(5)	54(2)	41(2)	37(2)	-6(1)	11(1)	-9(1)
C(6)	45(2)	32(2)	31(1)	-2(1)	8(1)	-9(1)
C(7)	40(2)	46(2)	57(2)	-7(2)	16(1)	7(1)
C(8)	33(1)	48(2)	60(2)	-13(2)	11(1)	6(1)
C(9)	31(1)	44(2)	49(2)	-7(1)	7(1)	3(1)
C(10)	31(1)	30(1)	38(2)	-1(1)	12(1)	2(1)
C(11)	41(2)	33(2)	44(2)	-3(1)	12(1)	0(1)
C(12)	52(2)	33(2)	60(2)	0(1)	24(2)	-3(1)
C(13)	42(2)	36(2)	70(2)	-14(2)	22(2)	-9(1)
C(14)	31(1)	41(2)	49(2)	-16(1)	13(1)	-3(1)
C(15)	34(2)	56(2)	56(2)	-27(2)	7(1)	-5(1)
C(16)	39(2)	71(2)	45(2)	-22(2)	3(1)	7(2)
C(17)	40(2)	59(2)	35(2)	-5(1)	6(1)	6(1)
C(18)	32(1)	43(2)	38(2)	-3(1)	8(1)	2(1)

C(19)	28(1)	35(2)	37(2)	-10(1)	10(1)	0(1)
C(20)	27(1)	31(1)	28(1)	-2(1)	3(1)	1(1)
C(21)	27(1)	33(2)	31(1)	-1(1)	2(1)	2(1)
C(22)	33(1)	33(2)	38(2)	4(1)	6(1)	-2(1)
C(23)	33(1)	44(2)	35(2)	3(1)	6(1)	-4(1)
C(24)	31(1)	43(2)	32(1)	-7(1)	7(1)	0(1)
C(25)	28(1)	37(2)	31(1)	-4(1)	5(1)	0(1)
C(26)	41(2)	36(2)	55(2)	-4(1)	17(1)	2(1)
C(27)	44(2)	29(2)	51(2)	-3(1)	14(1)	2(1)
C(28)	51(2)	59(2)	54(2)	11(2)	21(2)	-3(2)

---

**Table S42.** Hydrogen coordinates ( $\times 10^4$ ) and isotropic displacement parameters ( $\text{\AA}^2 \times 10^3$ ) for **6**.

	x	y	z	U(eq)
H(2)	3994	3505	4783	53
H(3)	3181	3458	3661	59
H(4)	4917	2734	3008	60
H(5)	7467	1974	3482	53
H(7)	10427	1435	4242	56
H(8)	12267	1163	5325	56
H(9)	10628	1702	6166	49
H(11)	7539	4625	5066	46
H(12)	9291	6058	5391	56
H(13)	10979	6072	6402	58
H(15)	11960	5229	7467	59
H(16)	11941	3837	8172	63
H(17)	10130	2415	7873	54
H(18)	8394	2380	6877	45
H(22)	4802	-265	6437	42
H(24)	3157	2554	6909	43
H(26A)	3673	4067	6402	65
H(26B)	4738	4074	5832	65
H(26C)	5650	4170	6575	65
H(27A)	7946	243	5846	61
H(27B)	6603	467	5202	61
H(27C)	6336	-490	5672	61

H(28A)	2171	1051	7382	80
H(28B)	3437	78	7499	80
H(28C)	1937	72	6889	80

---

## S8: References:

- 1) Das, A.; Ghosh, I.; König, B. *Chem. Commun.* **2016**, *52*, 8695–8698.
- 2) Wang, L.; Ji, E.; Liu, N.; Dai, B. *Synthesis*. **2016**, *48*, 737–750.
- 3) Frisch, M. J.; Trucks, G. W.; Schlegel, H. B.; Scuseria, G. E.; Robb, M. A.; Cheeseman, J. R.; Scalmani, G.; Barone, V.; Mennucci, B.; Petersson, G. A. H.; Nakatsuji, M.; Caricato, X.; Li, H. P. F.; Hratchian, A.; Izmaylov, J.; Bloino, G.; Zheng, J. L.; Sonnenberg, M.; Hada, M.; Ehara, K.; Toyota, R.; Fukuda, J.; Hasegawa, M.; Ishida, T.; Nakajima, Y.; Honda, O.; Kitao, H.; Nakai, T.; Vreven, J. A.; Montgomery Jr., J. E.; Peralta, F.; Ogliaro, M.; Bearpark, J. J.; Heyd, E.; Brothers, K. N.; Kudin, V. N.; Staroverov, T.; Keith, R.; Kobayashi, J.; Normand, K.; Raghavachari, A.; Rendell, J. C.; Burant, S. S.; Iyengar, J.; Tomasi, M.; Cossi, N.; Rega, J. M.; Millam, M.; Klene, J. E.; Knox, J. B.; Cross, V.; Bakken, C.; Adamo, J.; Jaramillo, R.; Gomperts, R. E.; Stratmann, O.; Yazyev, A. J.; Austin, R.; Cammi, C.; Pomelli, J. W.; Ochterski, R. L.; Martin, K.; Morokuma, V. G.; Zakrzewski, G. A.; Voth, P.; Salvador, J. J.; Dannenberg, S.; Dapprich, A. D.; Daniels, O.; Farkas, J. B.; Foresman, J. V.; Ortiz, J.; Cioslowski, J.; Fox, D. J. Gaussian 09 Revision C.01, 2010.
- 4) (a) Lee, C.; Yang, W.; Parr, R. G. *Phys. Rev. B*, **1988**, *37*, 785-789. (b) Becke, A. D. *J. Chem. Phys.*, **1993**, *98*, 1372-1377. (c) A. D. Becke, *J. Chem. Phys.*, **1993**, *98*, 5648-5652.
- 5) (a) Schaefer, A.; Horn, H.; Ahlrichs, R. *J. Chem. Phys.* **1992**, *97*, 2571-2577. (b) Schaefer, A.; Huber, C.; Ahlrichs, R. *J. Chem. Phys.* **1994**, *100*, 5829-5835.
- 6) Mellerup, S. K.; Li, C.; Peng, T.; Wang, S. *Angew. Chem. Int. Ed.* **2017**, *56*, 6093–6097.
- 7) Mellerup, S. K.; Li, C.; Radtke, J.; Wang, X.; Li, Q-S.; Wang, S. *Angew. Chem.* **2018**, *130*, 1–6.
- 8) Leazer Jr., J. L.; Cvetovich, R.; Tsay, F. -R.; Dolling, U.; Vickery, T.; Bachert, D. *J. Org. Chem.* **2003**, *68*, 3695–3698.

- 9) Dorkó, E.; Varga, E.; Gáti, T.; Holczbauer, T.; Pápai, I.; Mehdi, H.; Soós, T. *Synlett.* **2014**, 25, 1525–1528.
- 10) Data used in creating the predicted UV/Vis spectra generated by GaussSum V2.2: O’Boyle, N. M.; Tenderholt, A. L.; Langner, K. M. *J. Comp. Chem.* **2008**, 29, 839–845.
- 11) SHELXTL, version 6.14; Bruker AXS: Madison, WI, 2000–2003.